The University Of Sheffield.

Modulation Classification Based on Deep Learning

Yilin Sun

A thesis submitted in partial fulfilment of the requirements for the degree of

Doctor of Philosophy

The University of Sheffield

Faculty of Engineering

Department of Electronic and Electrical Engineering

Submission Date

February 2023

Declaration

I, the author, confirm that this Thesis is my own work. I am aware of the University's Guidance on the Use of Unfair Means (www.sheffield.ac.uk/ssid/unfair-means). This study has not previously been presented for an award at this, or any other, university.

Please ensure that any publications arising from the thesis are acknowledged in this section.

Acknowledgements

I would like to express my deepest gratitude to my thesis advisor, Edward A Ball, for his unwavering support, encouragement and guidance throughout the entire research process.

I am also grateful to my family, for their love and support throughout this journey.

I would like to extend my gratitude to my friends, Bingxue Wu, Yichao He and Yiyun Liu, for their companionship and support in the UK.

Thank you all for your support and encouragement throughout this process.

Abstract

This study aims to improve the efficiency and accuracy of Automatic Modulation Classification (AMC) within the wireless communication systems by developing and comparing different models. AMC is critical technology for identifying modulation types of received signals, which can optimise data transmission speed and reliability. AMC becomes indispensable in increasingly complex, multi-user and adaptive systems where dynamic modulation is prevalent. The motivation for this study is to investigate different models to enhance AMC techniques and contribute to the development of 5G and the emerging 6G networks.

This study utilises Deep Learning (DL) as an underlying technology and investigates the key methodologies, focusing on improving the accuracy, detecting a wider signal to noise ratios (SNR) range, and covering higher frequency bands. Initially, the research draws inspiration from image classification techniques to develop the AMC using constellation images (CI). Secondly, taking into account the advantages of graphic characters and statistical features, the Graphic Representation of Features (GRF) is introduced. The models are tested across a range of SNR values from -10 dB to 20 dB. After initially working on the 2GHz spectrum, higher frequency bands at 28 GHz and 70 GHz are also explored. Different AMC models are compared to identify the most effective approach for improving the accuracy of Modulation Classification across a wider SNR range and higher frequency bands.

The primary finding of this study is that the AMC model with GRF provides outstanding detection accuracy compared to the AMC model with CI and previous studies, especially in lower SNR levels and higher frequency bands. All these methods harness the power of Artificial Intelligence (AI). The most innovative contribution of this research is the application of image classification techniques in AMC. Particularly for the AMC with GRF, the model leverages both graphic characters and statistical features. Although the best accuracies are achieved at the lower carrier frequencies, the applicability of the developed models is verified in millimetre wave bands. Future research in AMC, focusing on more

complex signal environmental conditions, can get benefit from this work, such as multiple interferences and higher frequency bands.

CONTENTS

List of Abbreviations

5G	5th generation
6G	6th generation
8PSK	8-Phase Shift Keying
ADMP	Average Data-Maximum Phase
AI	Artificial Intelligence
ALRT	Average Likelihood Ratio Test
AM	Amplitude modulation
AMC	Automatic Modulation Classification
AM-SC	Amplitude modulation suppressed carrier transmission
AWGN	Additive white Gaussian noise
BPN	Back-Propagation Network
BPSK	Binary Phase Shift Keying
CI	Constellation images
CNN	Convolutional Neural Network
CPN	Counter Propagation Network
CW	Continuous wave modulation
D2D	Device-to-device
DBNs	Deep Belief Networks

DFT	Discrete Fourier Transform
DL	Deep Learning
DNN	Deep Neural Network
DSA	Dynamic Spectrum Access
FM	Frequency Modulation
GLRT	Generalized Likelihood Ratio Test
GRF	Graphic Representation of Features
I/Q	In-phase and Quadrature Components
JPEMC	Joint Power Estimation and Modulation Classification
LLF	Log-likelihood
MD	Minimum distance
ML	Machine Learning
mmW	Millimetre Wave
OQPSK	Offset quadrature phase-shift keying
Ph&D-GLRT	Phase and Data GLRT
PSD	Power Spectral Density
QAM	Quadrature Amplitude Modulation
QPSK	Quadrature Phase Shift Keying
ReLU	Rectified Linear Unit
RF	Radio Frequency

RFs	Random Forests
RNN	Residual Neural Network
SDR	Software Defined Radio
SNR	Signal to Noise Ratio
SVM	Support Vector Machines

List of Figures

List of Publications

[1] Sun, Y., & Ball, E. A. (2022). Deep learning applied to automatic modulation classification at 28 GHz. In *Intelligent Systems and Applications: Proceedings of the 2022 Intelligent Systems Conference (IntelliSys) Volume 1* Vol. 1 (pp. 403-414). Amsterdam, The Netherlands: Springer International Publishing. doi:10.1007/978-3-031-16072-1_30

[2] Sun, Y., & Ball, E. (2022). Automatic modulation classification using techniques from image classification. *IET Communications*, *16*(11), 1303-1314. doi:10.1049/cmu2.12335

[3] Sun, Y., & Ball, E. (2021). Automatic modulation classification based on machine learning. In *Advances in Automation, Mechanical and Design Engineering: SAMDE 2021* (pp. 53-67). Beijing, China: Springer Cham. doi:10.1007/978-3-031-09909-0_5

Chapter 1 Introduction

Amidst the ongoing revolution of the communication systems, the 5G networks have achieved the progress through dense small cell deployments, millimetre wave (mmW) communications and device-to-device (D2D) communications. The next research step of the revolution is building a highly efficient, intelligent system for 6G networks, aiming to provide ultra-reliable and low-latency communications. The spectrum resource is invaluable for the communication and vital for developing the next generation wireless networks. To fulfil this purpose, Artificial Intelligence (AI) is integrated to provide novel and comprehensive solutions for the 6G wireless communication systems.

Automatic Modulation Classification (AMC) determines the modulation type of a received signal in communication systems. In 6G, AMC plays an important role in enabling the efficient utilisation of the spectrum and support for various communication scenarios, such as massive IoT and tactile internet. It is also crucial for supporting advanced communication technologies, such as non-orthogonal multiple access and mmW communications. By accurately identifying the modulation type, AMC can enable the receiver to optimise its signal processing, increase the transmission capacity and enhance the overall system performance. With the advantages of AMC, it is worthwhile focusing on AMC techniques.

1.1 Background

1.1.1 Communication system

As the radio digital communication system develops, enhancing spectrum efficiency becomes increasingly urgent. To address this need, Dynamic Spectrum Access (DSA) is a promising starting point for the proposed spectrum sensing and signal classification. In this context, modulation classification performs a significant role and is widely employed in a variety of applications, such as software defined radio systems and radar communication in the military. There is a high demand for radio frequency (RF) bands [1].

In conditions of heightened demand for RF bands, the AMC technology can meet high-quality requirements by optimising signal demodulation, information extraction, and interference detection without limitations imposed by complex environments and various emitters. As 6G is expected to support a wide range of communication requirements, AMC can be used to classify the modulation type of incoming signals and dynamically adjust the network configuration to optimise performance [2]. This can lead to more efficient use of network resources and improved network performance. At the same time, AMC enables the system to adapt to changing conditions and provide secure communication in challenging environments [3]. In the 6G communication system, the AMC system can be employed in mobile phones to improve the performance of the modulation and demodulation by themselves. AMC technology also can be utilised for spectrum monitoring interference detection in an efficient way [4], [5], which allows cognitive radio users to adapt their own transmissions dynamically to avoid interfering [6]. This can help to improve the overall spectrum efficiency of the network and enable more efficient use of the available radio spectrum.

Radio spectrum is a limited and precious resource for the communication system. The millimetre wave (mmW) band has gained significant attention recently as a promising solution for next-generation wireless communication systems, including 5G and 6G. The mmW spectrum, ranging from 30 GHz to 300 GHz, offers a vast amount of bandwidth and high data rates, making it ideal for supporting high-bandwidth applications such as virtual reality and augmented reality. In this study, the AMC systems are tested at 2GHz, which frequency is in the current communication range. Subsequently, systems under 28 GHz and 70 GHz are also considered, falling within the operating frequency in 5G and 6G.

To illustrate the experimental process, the project comprises two main components. The first involves dataset preparation. Input data is generated through two different methods: MATLAB simulation, where modulation is performed mathematically based on constellations, and direct hardware generation using a signal generator.

The second part involves "feature analysis." Initially, the MATLAB-simulated data is evaluated, followed by testing the signal data obtained from the signal generator. Multiple features are extracted from the modulated data. Some of these features alone may not directly distinguish between different modulation types. If there are future requirements to enhance

the neural network based on the effective features, additional features should be considered and re-evaluated. The objective of this study is to identify features that can enhance the efficiency of the classification system across a wider SNR range.

In hardware experiments, a phase lock is typically necessary within the constellation for a clear observation through symbol display. In such cases, conducting experiments with realistic hardware is essential, regardless of the precision of the software system. This allows for the detection of results even without phase or frequency lock.

1.1.2 AMC technology

Automatic Modulation Classification (AMC) plays a critical role in wireless communication and signal processing. The fundamental purpose of AMC is to identify the modulation scheme employed in each received signal. Modulation is the process of altering one or multiple properties of a carrier signal, such as its amplitude, frequency or phase, to encode information. It, exists in various forms, including Amplitude Modulation (AM), Frequency Modulation (FM), Phase Shift Keying (PSK), Quadrature Amplitude Modulation (QAM) and others.

In conventional communication architectures, the modulation scheme is generally pre-defined and known to both the transmitter and the receiver. However, the increasing complexity of modern communication environments has given rise to scenarios in which the receiver may lack a priori knowledge of the modulation type of incoming signals. Such situations are commonly encountered in adaptive, cognitive or non-cooperative communication systems. Under these circumstances, AMC emerges as an indispensable tool for accurately determining the modulation scheme in use, thereby facilitating the correct decoding of the received signal.

The significance of AMC extends to multiple aspects of wireless communication. Firstly, it adds a layer of adaptability, especially salient in cognitive and software-defined radios, enabling the receiver to adjust dynamically to various modulation schemes. Secondly, AMC aids in the interoperability between diverse systems employing different or multiple communication standards. Thirdly, AMC proves to be invaluable in spectrum monitoring, offering essential capabilities for identifying the modulation types active across a range of

frequencies, a critical requirement for regulatory and surveillance applications. Lastly, in secure or military environments where the modulation scheme may be intentionally altered to thwart unauthorised access or jamming, AMC is crucial for maintaining secure and reliable communication channels.

For the state, various methodologies can be employed to implement AMC, ranging from classical statistical approaches to contemporary machine learning and deep learning techniques. The overarching challenge is to design an AMC system that is accurate as well as being efficient and robust, even under challenging conditions such as low SNR. Consequently, AMC continues to be an active area of research, driven by the escalating demands for flexibility, efficiency and security in modern communication systems.

The motivation for enhancing Automatic Modulation Classification (AMC) in this thesis is rooted in the growing complexities of 5G and emerging 6G wireless communication networks. In these advanced systems, multiple users often interact dynamically, and adaptive modulation schemes are increasingly common to optimise data throughput and reliability. Whilst the modulation type is traditionally pre-determined between a transmitter and receiver, in modern adaptive systems, being able to identify the modulation type of an incoming signal becomes crucial quickly and accurately.

1.2 Objectives and Contributions

In this work, AMC models are proposed based on DL technology. The overall target is to detect the modulation types with higher accuracy in wider SNR range, especially in low SNR and higher frequency bands in mmW, which brings the scenarios closer to the development of actual wireless communication systems. At the same time, the algorithms should be less complex. The contributions are achieved by the objectives in the following paragraphs.

The AMC model should explore the SNR area which is not provided in the earlier studies. This study begins on AMC with CI, which provides a basic novel solution of AMC with inspiration from image classification. The hybrid model is indicated based on the AMC with CI, which improves the accuracy by 23% at -10 dB SNR. The AMC with GRF is proposed to reduce the complexity according to the hybrid model, which slightly decreases the accuracy at a low SNR, whilst still being 20% more than the AMC with CI at -10 dB SNR.

The AMC model should explore the mmW bands which will be a benefit for 6G communications, whilst not provided in the previous works. In this research, the model was tested in different frequency bands (2 GHz, 28 GHz and 70 GHz). The contribution not only involves testing the model in these bands, but also includes the testing of simulated data. First, simulated data is tested, followed by the evaluation of lab-collected data, which is then compared to the simulated data. Due to limitations in the lab hardware, the lab-collected data is also processed by introducing noise, allowing the AMC models to function across different SNR levels rather than several fixed levels. The complexity of the AMC model should also be reduced. In this study, the AMC models are all based on DL. Different transfer learning structures are tested and compared to a CNN network. Transfer learning as pretrained networks do not require the adjustment of many parameters during the build-up session. Compared to the basic CNN model provided in this study, transfer learning provides higher accuracy despite the similar time in running the test.

The biggest contribution and novelty of this study is proposing the model AMC with GRF. This model provides a good use of the graphic features and statistical characteristics of the modulated signals. With the advantages of both, the models provide results across the -10 to 20 dB SNR under 2 GHz, 28 GHz and 73 GHz bands.

The following are my first three authored publications related to this thesis, which is guided and supervised by Edward A Ball.

Automatic modulation classification based on machine learning, which proposes the model AMC with CI and hybrid model. This study is related to Chapter 3.

Automatic modulation classification using techniques from image classification, which proposes the model AMC with GRF and compares it to the model AMC with CI. This study is related to Chapter 4.

Deep learning applied to automatic modulation classification at 28 GHz, which tests the AMC models at 28 GHz and compares them to the model performance at 2GHz. This study is related to part of Chapter 5.

1.3 Thesis Outline and Organisation

This study focuses on Automatic Modulation Classification (AMC) with Deep Learning (DL), which optimises the accuracy of the procedure when receiving digital modulated signals in wider SNR ranges and higher frequency bands.

Chapter 1 indicates a basic introduction of the research background, and introduces the AMC technology, the motivation and contribution of this work.

Chapter 2 provides the previous studies of AMC technology and AI techniques.

Chapter 3 introduces the model AMC with constellation images. The model is based on DL networks and tested with the signals from -10 dB to 20 dB SNR. Four different structed DL networks are introduced and compared. After that, the hybrid model is introduced, tested and compared.

Chapter 4 proposes the model AMC with Graphic Representation of Features (GRF), which uses statistical features and graphic characteristics of the signals. This system is tested and compared to the other models.

In Chapter 5, the signals from mmW are tested by the AMC models, the results are then analysed and compared.

Chapter 6 gives conclusions from this study, provides the contributions and gives future research directions.

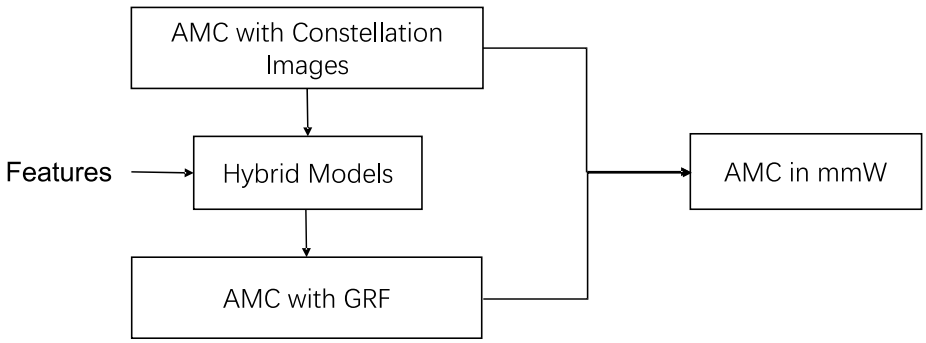

Figure 1 Research structure of thesis

Figure 1 presents the general flow chart of the research progress of this thesis. Inspired from the image classification, Constellation Images are used as the dataset to classify different modulation types in Chapter 3. Statistical features are employed as a supplement, and a hybrid model is indicated. To improve the accuracy of the AMC models, AMC with GRF is developed from the Hybrid model. The AMC models are tested within mmW bands to predict the performance in 6G.

Chapter 2 Literature Review

In this chapter, the previous studies and some background knowledge are provided. The 6G communication system and AI application in 6G are introduced. The digital modulations employed in this study are proposed in this chapter. After that, different kinds of modulation recognition are introduced and compared. Likelihood-based algorithms and feature-based recognition are the two general categories for the classifiers, which are also known as Statistical Algorithms and Pattern Algorithms. The innovative advantages are proposed and the shortcomings are also introduced. The technique of image classification is introduced at the end, which has inspired this research study.

2.1 6G Technology

The drawbacks and limitations of the developing 5G cellular system are driving the revolution for 6G wireless communications. The general requirement of the communication system defines the targets of the 6G system. With the trends and challenges of the 6G, AI also serves as a pervasive technology for improving and guaranteeing the performance.

2.1.1 6G Background

For the development of 6G towards higher frequency ranges, wider bandwidths and massive antenna arrays, businesses are aiming to build the intelligent communication systems. The detailed key targets of 6G networks are expected to be: Ultra-high data rate and ultra-low latency communication [7], high energy efficiency for resource-constrained devices, ubiquitous global network coverage [8], and trusted and intelligent connectivity [9]. The key performance indicators of 5G and 6G are compared in Table 1 [10].

Table 1 Key performance indicators for 5G and 6G

	5G	6G
Rate requirements	1 Gb/s	1 Tb/s
Downlink data rate	20 Gb/s	1 Tb/s
Uplink data rate	10 Gb/s	1 Tb/s
Latency	1 ms	0.1 ms
Operating Frequency	3- 300 Hz	Up to 1 THz

There are seven trends [11] which are expected in the ongoing development for these technologies: 'More Bits, More Spectrum, More Reliability', 'From Areal to Volumetric Spectral and Energy Efficiency', 'Emergence of Smart Surfaces and Environments', 'Massive Availability of Small Data', 'From Self-Organising Networks to Self-Sustaining Networks', 'Convergence of Communications, Computing, Control, Localisation and Sensing' and 'End of the Smartphone Era'.

On the road towards 6G, the more intelligent techniques and processing efforts should be introduced as significant progress compared to 5G, which is the reason the AI is considered as a fundamental technique rather than an optimisation tool [12].

2.1.2 AI Technologies Involved in Wireless Communications

For the purpose of the impact of the next generation of wireless communication, it can leverage the artificial intelligence which has penetrated into diverse subjects. Modern AI systems are typically based on ML [13]. With these data-driven algorithms, building truly intelligent communication systems is a reachable and highly efficient objective.

The two main functions can be concluded to be [14]: Intelligent and analytics, with the capability of parsing the large amounts of data collected from the devices; it is a revolution to

analyse and predict the information and statements of wireless communication systems in order to make network-wide operational decisions. The second function is presented as self-organising network control and optimisation, in which the system can automatically control the operations and optimise the resources based on self-learned skills.

At the Physical Layer, ML is involved with channel coding [15], [16], synchronisation [17], positioning [18] and channel estimations [19]. At the Medium Access Control Layer, the Federated Learning for orientation and mobility prediction in virtual reality networks [20], predictive resource allocation in machine-type communications [21], [22], predictive power management and asymmetric traffic accommodation are presented in literatures. At the Application Layer, ML is utilised for the network performance management automation [23], ML-Aided unmanned aerial vehicles control [24], [25], opportunistic data transfer in vehicular networks and software development. ML is also an ongoing trend being applied to the security of wireless networks, which is considering attack [26] and defence [27].

The AI techniques empower new opportunities and challenges for wireless communications developing towards 6G.

2.2 AMC Technology

This section introduces the state of the art of AMC technology. The main objective is improving the accuracy of classification especially in areas with low SNR. In real-world communication environments, signals often encounter various sources of noise, interference and fading. As a result, the received signal may have a low SNR, especially in dense urban areas or challenging terrains. Exploring the low SNR regime helps in designing more robust communication systems. If a system can perform well under low SNR conditions, it is likely to be more resilient under various challenging scenarios. In defence scenarios, signals are often intentionally transmitted at low power to avoid detection, leading to low SNR at the receiver. Reliable AMC in such conditions is crucial for intelligence and electronic warfare operations.

There are different target standards of AMC in different scenarios. For the mission-critical applications, such as defence and aerospace, the accuracy needs to be extremely high, often

approaching 99% or more, even in areas with low SNR. For the general consumer applications, an accuracy of 90-95% is acceptable. However, as technologies evolve and user expectations rise, this threshold might increase. In academic research, achieving state-of-the-art performance often means pushing the accuracy as high as possible on benchmark datasets. In conclusion, the need for AMC at low SNRs is driven by the challenges and requirements of modern communication systems. The acceptable accuracy level varies based on the specific application and its associated demands. In this work, the objective is to improve the accuracy of the AMC system, especially at low SNRs.

2.2.1 Statistical Algorithms for Detecting Modulation Type

One traditional approach of AMC is likelihood-based, which applies the statistical method and mathematic models. In this branch, the target is estimated as a multiple hypothesis testing problem, making the decision between a variety of modulation types. This kind of recognition employs a significant part in the early years. Although this study focuses on the pattern recognised approach, the advantages from the decision theoretic approach could be used as a lesson.

Maximum-likelihood decision theory is used as a critical method in a report [28]. PSK and QAM are distinguished by setting two statistical models, coherent maximum-likelihood classification and noncoherent pseudo maximum likelihood classification. The benchmark of this study is error rate, which means the number of wrongly detected symbols over all detected symbols. The error rate is less than 10% when the signal is higher than 9 dB and 12 dB for the coherent model and the noncoherent model, respectively. The coherent model has a better ability for distinguishing PSK and QAM including high order type, such as QAM64. However, it needs to calculate different parameters required from a variety of methods every time. The only parameter, carrier phase, that is not necessary for the noncoherent model, performs at 3dB worse according to the coherent model. Each type of modulation has its own probability of error for both models. The limitation of this study is that some parameters cannot be obtained during the pre-processing when the SNR is lower than 10 dB. At the same time, the low SNR area should be explored with other models.

Based on the Likelihood algorithm, three classifiers were provided and compared in [29], a square-law classifier, a phase-based classifier (weighting on the phase histogram) and a quasi-log-likelihood ratio (qLLR) rule. The benchmark of this study is the probability of correct classification. The qLLR rule shows the best classification results, which achieves 54% at -10 dB SNR. The other two classifiers perform worse than the qLLR rule. The statistical methods show the advantage in the low SNR area. However, these classifiers can only work for MPSK. For the other modulations, the whole system should be rebuilt.

For further research, three kinds of likelihood techniques are discussed, the Average Likelihood Ratio Test (ALRT) [28] [30] on which previous studies are based, the Generalised Likelihood Ratio Test (GLRT) and a hybrid of the two. The two innovative approaches, the Phase and Data GLRT (Ph&D-GLRT), developed from GLRT and the Average Data-Maximum Phase (ADMP) based on the mix of ALRT and GLRT, are proposed. The critical limitation of the GLRT technique is the failure for high SNR. When the different modulations transmit at the same time, they produce the same symbol and the same value of log-likelihood functionals (LLF) because of the maximisation in LLF. The hybrid one solves this problem by averaging the data symbols before maximising. The final results only show the classifications between modulation pairs instead of detecting in the general spectrum with the accuracy increased to 90% after 3dB SNR between 16QAM and 16PSK [31]. However, the idea of two mixed algorithms could be a novel point to develop the situation.

Overall, for the likelihood-based algorithms, some of them show the advantage in a low SNR area. However, there are still limitations; the models can only be used to classify the fixed modulation types. The parameters and models will need to be recalculated and rebuilt for the other modulation types, which increases the complexity of the work, yet in the practical systems, the modulation types are not known in advance for some scenarios. In this way, the AMC techniques should be developed for these advanced systems.

2.2.2 Pattern Algorithms for Modulation Type Detection

There are some limitations of the likelihood-based models. The probability of error is high, even over 0dB SNR, which is the limitation of the detected modulation types. After that, the

feature-based approaches have more potential for a good use of the characters of signals to be applied in the system and can reach a high accuracy of classification, as will be shown below. In these algorithms, the classification is generally divided into two parts: features extraction and modulation classification, which usually employ a neural network to optimise their capability. During the recognition process, the statistical classifier and the neural network classifier are the two main approaches.

1) Statistical Classifier

In the early work, pattern recognition is proposed with the neural network. Amplitude variance, phase variance, frequency variance and amplitude skewness are illustrated as the good characters to classify the types amongst Amplitude modulation (AM), suppressed carrier transmission (AM-SC), Frequency modulation (FM), Continuous wave modulation (CW) and Quadrature phase shift keying (QPSK) [32]. In these cases, these features can help to divide the types of modulation into small groups for the complex training data set. Only the AM-SC and QPSK are distinguished exactly at the end in the simple dataset. It is obvious from this research that the variances are helpful, which help to distinguish the QPSK modulation from others.

In this paper [32], kinds of neural network pattern classifiers and maximum-likelihood pattern classifiers are compared. The Back-Propagation Network (BPN) from the neural network classifiers and the maximum-likelihood classifier have a better capability compared to the Counter Propagation Network (CPN) from the neural network classifiers and the minimum distance (MD) classifier. However, the overtraining occurs for the fixed data set in BPN, where the accuracy decreases from 95.6% to 91.2% at 24dB SNR. As actually happened to this SNR level, the accuracy must decrease a lot around 10dB SNR and must be less than 95% at least. In this way, these features should be considered, and other classifiers should be compared in further experiments.

Besides the features introduced previously, the high order cumulants also play a critical role in the AMC algorithm. Cumulants are proposed to represent the moments in an alternative way and the moments can measure the functions quantitively [33]. Cumulants are derived from the cumulant-generating function, which is the natural logarithm of the moment-generating function of a random variable. One of the most useful properties of

cumulants is the additivity for independent random variables. The baseband signal can be written as $r(t) = s(t) + n(t)$, where $s(t)$ is the transmitted signal, $n(t)$ is Gaussian noise and $r(t)$ is the received signal. Generally, the transmitted signal and the Gaussian noise are independent in the channel. The m-th order cumulants can be written by (1).

$$Cum_m(r) = Cum_m(s+n)$$
$$= Cum_m(s) + Cum_m(n) \quad (1)$$

Also, the second-order cumulant, fourth-order cumulant and sixth-order cumulant are:

$$Cum_2(r) = E[r^2] - (E[r])^2 \quad (2)$$

$$Cum_4(r) = E[r^4] - 4E[r^3]E[r] + 6E[r^2](E[r])^2 - 3(E[r])^4 \quad (3)$$

$$Cum_6(r) = E[r^6] - 6E\left[r^5\right]E[r] + 15E[r^4](E[r])^2 - 30E[r^3](E[r])^3 + 30E[r^2]\,(E[r])^4 - 6(E[r])^6 \quad (4)$$

E[·] denotes the expectation operator. These cumulants are used in signal processing, especially for AMC. As the Gaussian noise is a Gaussian distributed random variable, the cumulants of order higher than two are zero. In this way, high order cumulants are statistical measures which can capture the non-Gaussian characteristics of the signals. The signals can be processed without the interference of the Gaussian noise, which improves the performance of AMC in a low SNR area.

When the higher order cumulants of the received signals are calculated, the part of the Gaussian noise is zero and the signals are now independent. After extracting the features, the Support Vector Machines (SVM) is applied in the recognition process. The exact value ranges to distinguish the digital modulation types are illustrated in the paper, which should be considered in following study. The high order cumulants will be applied in this study [33], although the values could change because of the different representations of signals. The accuracy stretches to 96% at around 10 dB SNR for 200 samples. When the number of samples increase, the accuracy also improves. However, the probability of correct classification is between 50% to 70% at around 0dB SNR, which still needs to be improved.

The eighth order cumulant is also employed [34]. In this case, more types of digital modulation are recognised, such as BPSK, QPSK, Offset quadrature phase-shift keying (OQPSK), 8PSK, 16PSK, 4PAM, 8QAM, 16QAM, 32QAM and 64QAM. This system also applies the decision tree as the recognition part. The frequency offset is added to avoid the degradation of the AMC system, which improves the performance efficiently. The accuracy of this system can reach 70% at 10dB SNR for 500 samples and increase to 91% for 3000 samples. However, the timing error is ignored which may lead to a failure in the real application.

According to the timing error, the cyclic cumulants are utilised. Whilst the research also works on the high order cumulants [35][36], the analysed signal model is actually circular which is the function with the Fourier components. Cyclic cumulants work similar to the system in [32], yet perform better, especially for less input training data needed. In this model [36], the average probability of correct classification nearly reaches 88% for detecting QPSK and QAM16 at 5dB. There is the limitation, where classification only works between specific modulation pairs. The classification performances are not considered in lower SNR areas.

Compared to the previous classifiers, the binary hierarchical polynomial classifiers are also proposed. The high order cumulants are extracted as the main features to classify M-PSK and M-QAM modulations. This could achieve the 100% correct classification at 20dB by 512 symbols [37]. After evaluating the performance of the other classifiers, a hierarchical polynomial classifier works better than SVM with the probability of correct classification, i.e. 96.49% compared to 91.23% at 10dB SNR. However, when the SNR decreases to 0dB, the probability of correct classification stays at around 65%, which is the challenge for optimising the system.

2) Neural Network Classifier

Machine learning has evolved to a popular technology associated with a wide range of tasks. To achieve automatic modulation recognition and demodulation, the distinction is necessary[38]. There are 32 expert features extracted as the learning features to develop the Convolutional Neural Network (CNN) from 8-time lags [39].

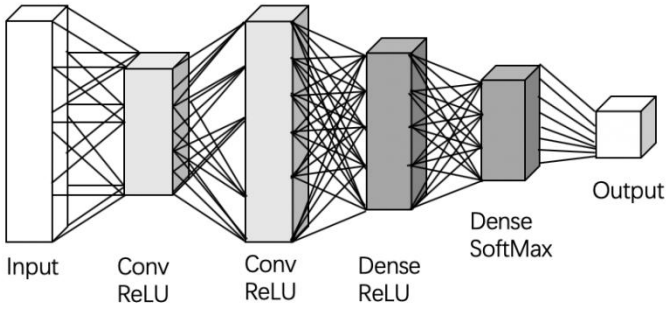

Figure 2 Structure of CNN

As Figure 2 shows, there are two convolutional layers and two dense fully connected layers. The characters of the signals can be captured by the two convolutional layers and the feature map can be produced by these two layers. After that, the features can be learnt by the two sequential layers. Finally, the results of the classification are output. The networks classify both digital modulations and analogue modulations. The running time is less than the SVM classifiers, which implements better performance at 0 dB SNR. The overall accuracy of 87.4 % is achieved from -20 dB to 20 dB SNR, and also achieves around 80% at 0 dB SNR. It has the potential to develop in the range and amounts of modulation types of detection. However, there is a lack of investigation about the other kinds of filters, layers and structures, which should be in the comprehensive experiments. In this case, the misrecognition between 8PSK and QPSK still occurs at 18 dB SNR, although the classification accuracy of other modulations is nearly at 100 %. From -10 dB to -5 dB SNR, the accuracy decreases dramatically, which is around 20 % at -10 dB. The accuracy should be improved at low SNRs.

To eliminate the complexity of the system, the pre-processing such as high order cumulants capture can be removed. The deep learning classifier is trained in one end-to-end part, which also devotes itself to the radio traffic sequence recognition and protocol recognition [40]. Two convolutional layers are set at first, followed by two fully connected layers. A couple of kernels consist of each whole layer, whose function is convolution. After convoluting by the kernels, the features are passed to the sequential layers like pooling layers and fully

connected layers, where the kernels are the feature detectors. The results of recognition are finally obtained. The format of input data also influences the classification results. The received signals, which are represented in Amplitude/phase format work as the input of the AMC system, can get better detection accuracy than the signals represented in I/Q format and frequency domain data when the SNR is higher than 4 dB. It is shown that CNN with I/Q representing can achieve higher accuracy under 4dB SNR, such as 76% at 0dB SNR. It is nevertheless true that the data captured from the signal generator in the next section is still in an I/Q format, which requires the pre-processing of the format conversion. In another study, the raw I/Q data normalised to unit variance works as the input directly [41]. The results demonstrate the excellence of the residual neural network (RNN) compared to the CNN, which achieve the similar accuracy of the previous system [40]. Thus, the architectures of the system and parameters of the training part all influence the recognition results.

A Deep Neural Network (DNN) based approach is proposed by 21 statistical features, including high order cumulants and deviation of the input signals. Features like kurtosis and skewness are also employed in the system, which is utilised in the earlier studies. It is significant that this learning structure [42] reaches nearly 100% accuracy at -5 dB SNR compared to the 70% accuracy of the conventional artificial neural network. In this case, the features and structure of the neural network should be evaluated in the following experiments. Overall, the challenge for these models is to define the detailed parameters and layers to elevate the accuracy of AMC models.

2.2.3 Other Types of Classification

As the CNN architecture is famous as its ability to process images, to recognise the modulation types, the images of constellation are used as the input training data set with the labels of the names of modulations [43]. This is because constellation diagrams are clear to observe the characters of each digital modulation type and they make a good use of the capability of CNN and achieve the accuracy around 75% at 0 dB SNR. This model only explores the -4 dB ~14 dB SNR areas. The challenge of this study is that the data conversion procedure from complex samples to images indeed incurs information loss due to the limited

resolution of images. The data enhanced conversion which can keep more original information should be considered.

There is also a method to distinguish BPSK linear frequency modulation, Costas codes, Frank codes and poly-codes (T1, T2, T3 and T4). Different from the constellation recognition, the image of waveform detection is proposed [44]. However, it is hard to capture the waveforms from the real world and recognise each type from a mixture of signals and noise, which is only useful to analyse single classification. Particularly during the low SNR, it is not easy to attach the labels on the raw data, which will be a difficult problem in the following chapters, with little potential to develop this technique further.

2.3 Image Classification

Image classification is a central problem in the field of computer vision and has gained significant attention in recent years with the advancements in artificial intelligence (AI) and deep learning algorithms. The objective of image classification is to assign a semantic label or class to an image based on its visual content. This task has numerous real-world applications, such as object recognition in autonomous vehicles, face recognition in security systems and image categorisation in image retrieval systems.

Convolutional Neural Networks (CNNs) have emerged as the state-of-the-art method for image classification. The AlexNet architecture is proposed [45]. It demonstrates its superior performance on the ImageNet dataset. This study establishes the efficacy of deep CNNs in image classification tasks.

Subsequently, the Very Deep Convolutional Networks are introduced [46], known as VGG, which demonstrate the importance of increasing the depth of CNNs for improved performance. Their study shows that very deep networks could outperform shallower networks in image classification tasks. Recently, transfer learning has emerged as a promising approach for improving the performance of image classification systems [47]. Transfer learning allows pre-trained CNN models to be fine-tuned for a target task, reducing the need for large amounts of annotated data and avoiding overfitting.

Other approaches, such as Support Vector Machines (SVMs), Random Forests (RFs) and Deep Belief Networks (DBNs), have also been applied to image classification with different performance, strengths and weaknesses.

In this situation, image classification with AI has made substantial progress with deep learning approaches, particularly CNNs, demonstrating exceptional performance. Transfer learning has also proved to be a powerful technique for improving the performance of image classification systems, which is employed in this work.

2.4 Summary

This chapter introduces the general 6G developing trends and the AI techniques involved with wireless networks, which provides a background knowledge of the communication system. The main part of this chapter is the state of art of AMC technology. Different AMC models are introduced, and the results are compared under the same SNR levels. The challenges are also indicated. Finally, the image classification techniques are introduced which are involved in the following chapters.

Compared to the pattern algorithms, the performance of statistical algorithms is worse. The pattern algorithms have a good use of the characteristics of the signals. The AI models of pattern algorithms provide significant improvement. Whilst the other types of AMC models demonstrate innovated ways of classifying the signals, the models come with some other limitations.

For the AMC models mentioned in this chapter, the main challenges can be concluded as:

1. Limited classification SNR range and limited modulation types. The models are not generally applicable.
2. To achieve the higher possibility of correct classification, adjusting the detailed parameters and layers of CNN is complex.
3. Part of the original information or the characteristics are lost.

There are also detailed challenges based on the specific models mentioned earlier. However, the overall target is to improve the performance of the classification, especially at low SNR areas; at the same time, the models should be applied to more scenarios.

After analysis of the extant literature, the feature-based approaches indicate better performance with a higher possibility of correct classification, and they have more potential area to improve. Some of the papers use the high-order cumulants and some of them utilise variances. According to the papers which use high-order cumulants, each work has different features and different kinds of classifier. It is also shown that cumulants, variances and other features are token advantages with DNN. In this way, the features are also considered in the following chapters.

According to the papers using statistical classifiers, their value of features to classify the modulation types are fixed, and the only way to elevate the accuracy is to increase the samples, although overtraining happens. Amongst the studies, CNN is a significant classifier with very good capability. Different papers propose different accuracy compared to RNN and DNN with different input variables and different neural network structures. In this case, different kinds of neural network are built and compared in the following chapters.

Based on the different structures mentioned previously, there is not an experiment to compare them with all the features. For the features used in the pattern recognition, high order cumulants and other kinds of basic parameters such as variances should be analysed together to strengthen the classification system. Different network structures, filters and input variables are investigated in this work.

Chapter 3 AMC with Constellation Images

This chapter indicates the method of AMC with constellation images, which is inspired by AI techniques and takes advantage of image classification. The constellation images are captured from -10dB to 20 dB to provide enough training data. Four different DL networks structures are introduced and compared. Based on this, the hybrid model is also developed and compared to the model only using the constellation images.

3.1 Introduction

As the situation of precious spectrum resources and the high occupation, Dynamic Spectrum Access (DSA) is involved in mitigating the crowded circumstances. In this situation, AMC devotes itself to the efficiency of signal classification. In previous studies, people indicated many techniques with which to be associated, and these can mainly be divided into statistical algorithms and pattern algorithms. At the same time, AI technology improves the accuracy of detection and reduces the complexity of calculation. With inspiration from this biomorphic technique, this chapter introduces the AMC with Constellation Images (CI). To improve the classification performance, the hybrid model is introduced.

In [48], there is only simulated data, yet in the journal paper [49], there is simulated data from MATLAB and collected data from Ettus. The Ettus E310 is a software-defined radio (SDR) platform developed by Ettus Research, which seamlessly integrates an RF frontend with baseband processing and I/O functionalities with an operational frequency range spanning from 70 MHz to 6 GHz.

The statistical algorithms from existing studies requires some calculation of the different features [28], which only considers classification from 6 dB SNR, and the probability of correct classification is less than 80% at 10dB. The high-order-cumulants and SVM model

are introduced with 50% around 0 dB SNR [33], which improve the classification results. The limitation of low accuracy and limited classify modulation types are the motivation for this study. After the traditional methods, CNN is approved with less running time than SVM [39], which shows the outstanding performance. In this way, the AI techniques are involved in this part.

The innovative contribution of this chapter is the model of AMC with CI, which uses the constellation image to classify the modulation types with transfer learning. The hybrid model also improves the results based on AMC with CI, which also includes the statistical features into the model.

This chapter is organised as follows: in section 3.2, the signal models and modulated data collected in different ways are introduced and compared. The data simulated with MATLAB in different SNR levels with phase lock are provided to show the ideal modulated signals. After that, the SDR equipment is built up in the lab for the signal collection system. The data collected in the lab without phase lock is also introduced and compared with MATLAB simulated data. In section 3.3, four kinds of deep learning structures are introduced for image classification. A hybrid model is also developed based on deep learning. In section 3.4, the results of AMC with CI are analysed.

3.2 Signal Models

In this section, the model of the signals and system are introduced as the background features. All the models involved are all based on this model. Constellations and statistical features are all collected and calculated according to the system model. After that, AMC with CI, hybrid model and AMC with GRF are utilising the features for the consequent DL models.

As the original transmitted signal is defined with $s(t)$ which passes through the additive white Gaussian noise (AWGN) channel in baseband, the noise is defined with $n(t)$ and $r(t)$ represents the received signal. The system can be described by (5).

$$r(t) = s(t) + n(t) \tag{5}$$

The time is represented by t, which provides a method of indexing or referencing the value of a signal at different moments. $s(t)$ is the original signal which transmits through the additive white Gaussian noise (AWGN) channel, and $n(t)$ represents the noise applied to the signals. Here, the original signal and the received signal are indicated, and the data is collected with the in-phase and quadrature components *(I/Q)*.

With the demand of features calculation and analysis, the raw data should be represented by convention using in-phase and quadrature components in (6).

$$a[i] = a_I[i] + j * a_Q[i] \tag{6}$$

$a[i]$ represents the *i*-th sample of a discrete complex signal. $a_I[i]$ represents the i-th sample of the in-phase component of the signal. $a_Q[i]$ represents the *i*-th sample of the quadrature components of the signal. Hence, the signals are composed of a real part and an imaginary part, representing the characters of their constellation diagrams. All the statistical features and constellations are calculated and captured by this model. Furthermore, the data captured by the lab test hardware is also read as I/Q data [41].

The four kinds of modulated signals investigated and applied in this study are: BPSK, QPSK, 8PSK and QAM16. There are 100 symbols which are utilised, and then sampled at the rate of 50 samples per symbol.

SNR is also an important metric to describe the noise and represent the signals in the real world, here defined by (7).

$$SNR = \frac{power\ of\ signal}{power\ of\ noise} = 20log_{10}\left\{\frac{\sqrt{\frac{1}{N}\sum |a[i]|^2}}{std(|noise|)}\right\} \tag{7}$$

In this study, signals are considered from -10 dB to 20 dB SNR. Note that the focus of previous studies was on the classification above 10 dB SNR [50]. The SNR value less than 0 dB is important and should also be tested, to improve the performance in distinguishing between modulation types. The models have been developed from -10 dB to 20 dB SNR to provide a comprehensive dataset.

At the same time, the system is without phase lock or frequency lock. Phase lock refers to the condition where the phase difference between two oscillating signals remains constant over time. Frequency lock refers to the condition where two oscillating signals maintain the same frequency. In communication systems, the accurate reception, demodulation and decoding of a signal often require the receiver to be synchronised with the transmitter in terms of frequency and phase. However, in this work, the classification models can work without them.

Signal model is building at the start of this work, for simulating signals, measuring and testing some properties of the signals. It is employed in the simulation in MATLAB first, and then tests the signals collected from the lab. For the signals collected from the lab, it is obvious to see that there is Gaussian Noise coming with the signals, and also Thermal Noise coming through the channel.

Thermal noise is created by the thermal agitation of the electrons in the various elements that build up the receiver [51]. Normally, the thermal noise is well-approximated by a Gaussian distribution. However, in the digital systems, the analogue-to-digital conversion process introduces quantisation noise, which may interact with thermal noise in complex ways. The Noise as an internal noise cannot be eliminated. For the measurement of the practical signals, the SNR level is calculated by the voltage amplitudes of the received signals, (8), (9), (10).

$$SNR = 20 * log_{10}(\frac{V_s}{V_n}) \tag{8}$$

$$V = \sqrt{I^2 + Q^2} \tag{9}$$

$$V_s = \frac{1}{n}\sum_{i=1}^{n} V_i \tag{10}$$

V_s is the voltage of signal, V_n is the voltage of noise. The amplitude of the complex signal V can be calculated by the in-phase component of signal, I and the quadrature component of signal, Q. The V_s can be calculated by (10). V_i represents the magnitude of the i-th sample of signal and n is the total number of samples.

3.3 Constellations of Collected Data

As the technique indicated in this chapter is AMC with CI, the Constellation images are the main data involved in this chapter. Constellations can reflect the signals which are modulated by digital modulations in a complex plane as scatter diagrams. Signals with different modulation types have different constellation images. In this case, AMC with CI takes good use of this point based on the physical characteristics of the constellation images. For the deep learning following, the building of the dataset is the first and vital step. In this section, the constellations are introduced in detail and under different conditions. Four kinds of modulation type are considered, BPSK, QPSK, 8PSK and QAM16. The constellation images are collected in two main paths. The first group of data is simulated by MATLAB. After that, the hardware system is built to test the signals without phase-lock going through the wire. The simulation data will also be tested later as contrasts.

3.3.1 Simulated Data

Before testing the signal data in practice, the simulation is considered. According to the theory of each digital modulation type, modulated signals are simulated by MATLAB. The constellation images are observed and collected at the same time. In this section, the constellation images at different SNR levels are compared, and their physical characteristics are observed. After these, constellation images under proper conditions are utilised as training and testing datasets for the CNN, which is a part of the AMC algorithm. To find out the proper conditions, constellation images under different conditions are shown as follows.

First of all, the sample rate is considered. To build up the dataset of constellation images for the CNN, it is essential to produce clear images to be classified. The sample rate is the first variable to be confirmed for the constellation generation. There are 100 symbols utilised for the MATLAB simulation. To consider the influence of the sample rate, the number of symbols is fixed for this section.

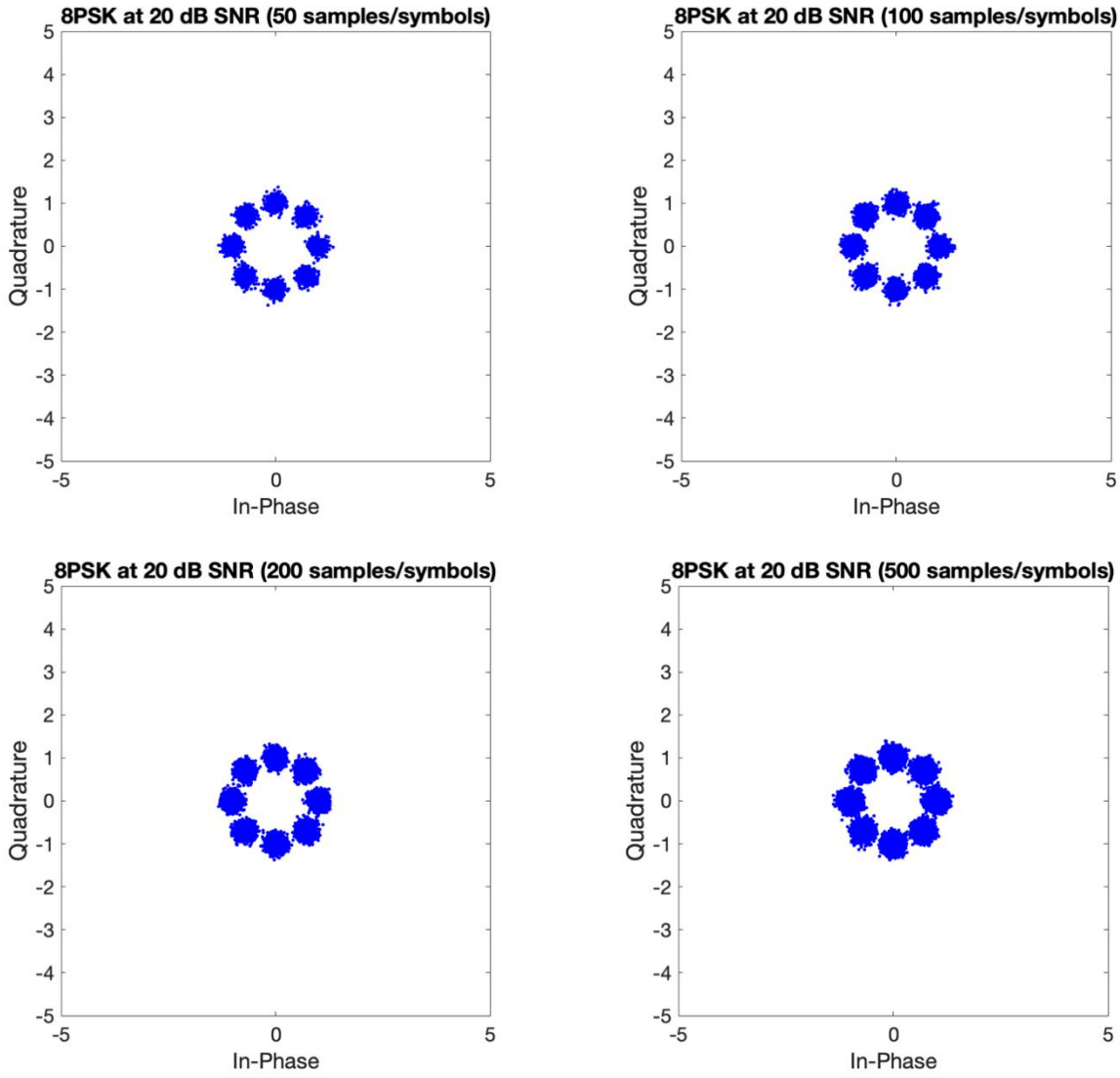

Figure 3 Constellations of 8PSK at 20 dB SNR with different sample rates

Figure 3 indicates the constellation images of 8PSK at 20 dB SNR, yet with different sample rates. The sample rates are 50, 100, 200 and 500 samples per symbol. It can be observed that the constellation image is clearer with 50 samples per symbol, which is also easier for CNN to classify. There are narrower gaps between the groups of dots with 200 samples per symbol. This difference is not obvious nor is it convincing enough. Consequently, the constellation images at 10 dB SNR are applied.

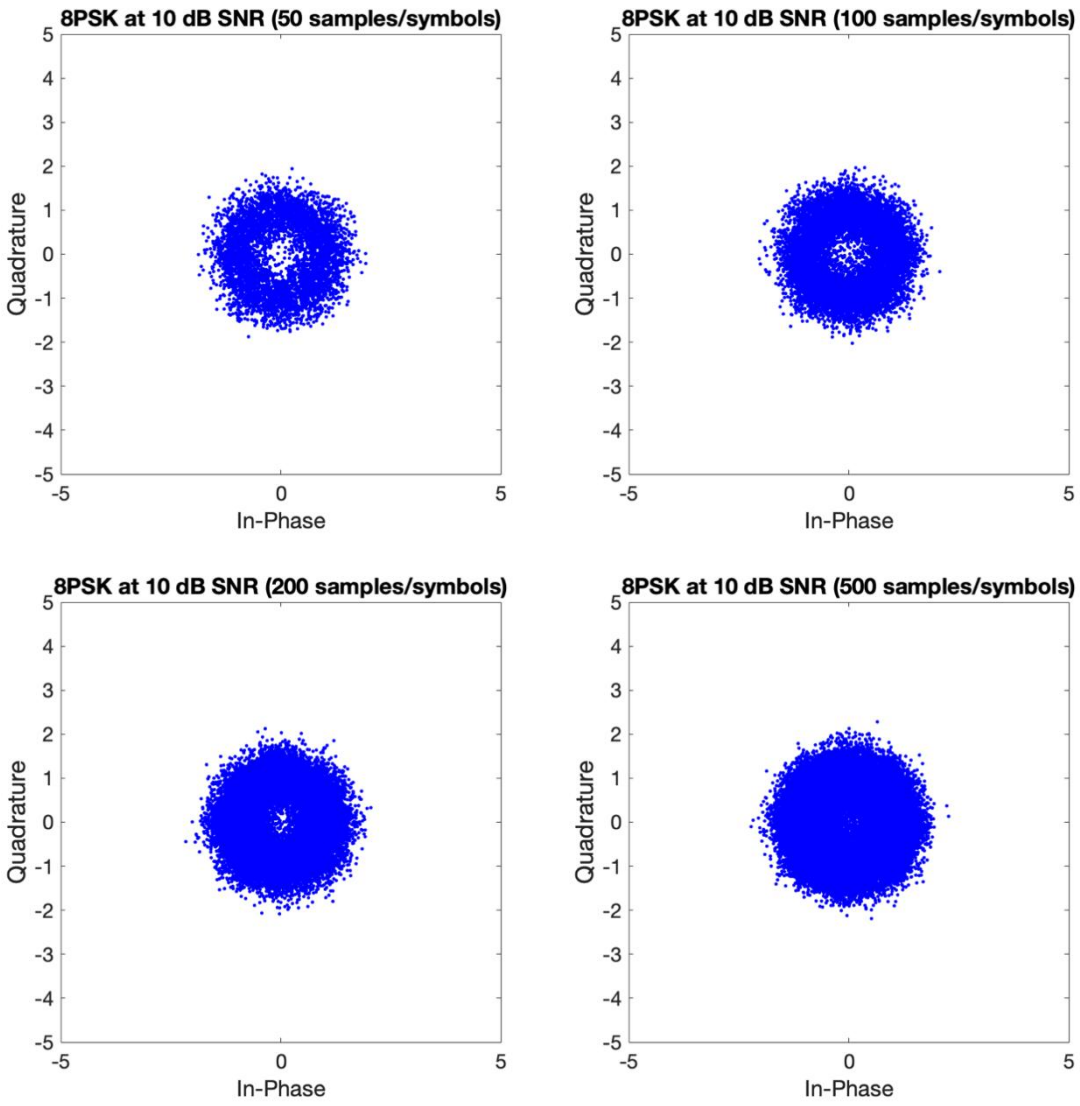

Figure 4 Constellations of 8PSK at 10 dB SNR with different sample rates

Constellation images of 8PSK with the same sample rates at 10 dB SNR are shown in Figure 4. It is obvious that the constellation image with 50 samples per symbol has clear characteristics. Also, the distribution shape is more similar to the constellation image at a higher SNR level compared to the other three. However, the sampled symbols cannot be lower than 100 symbols for this case. This is because there are too few sample dots to sketch the constellation images which can be classified easily by the CNN later.

Overall, the sample rate is set at 50 samples per symbol with 100 symbols for the rest of the simulation in this section. This sample rate is for data collection not for simulating the real AMC system. After setting the sample rate, the constellation images at different levels are provided and compared as follows: BPSK, QPSK, 8PSK and QAM16 are simulated from -10 dB to 20 dB SNR.

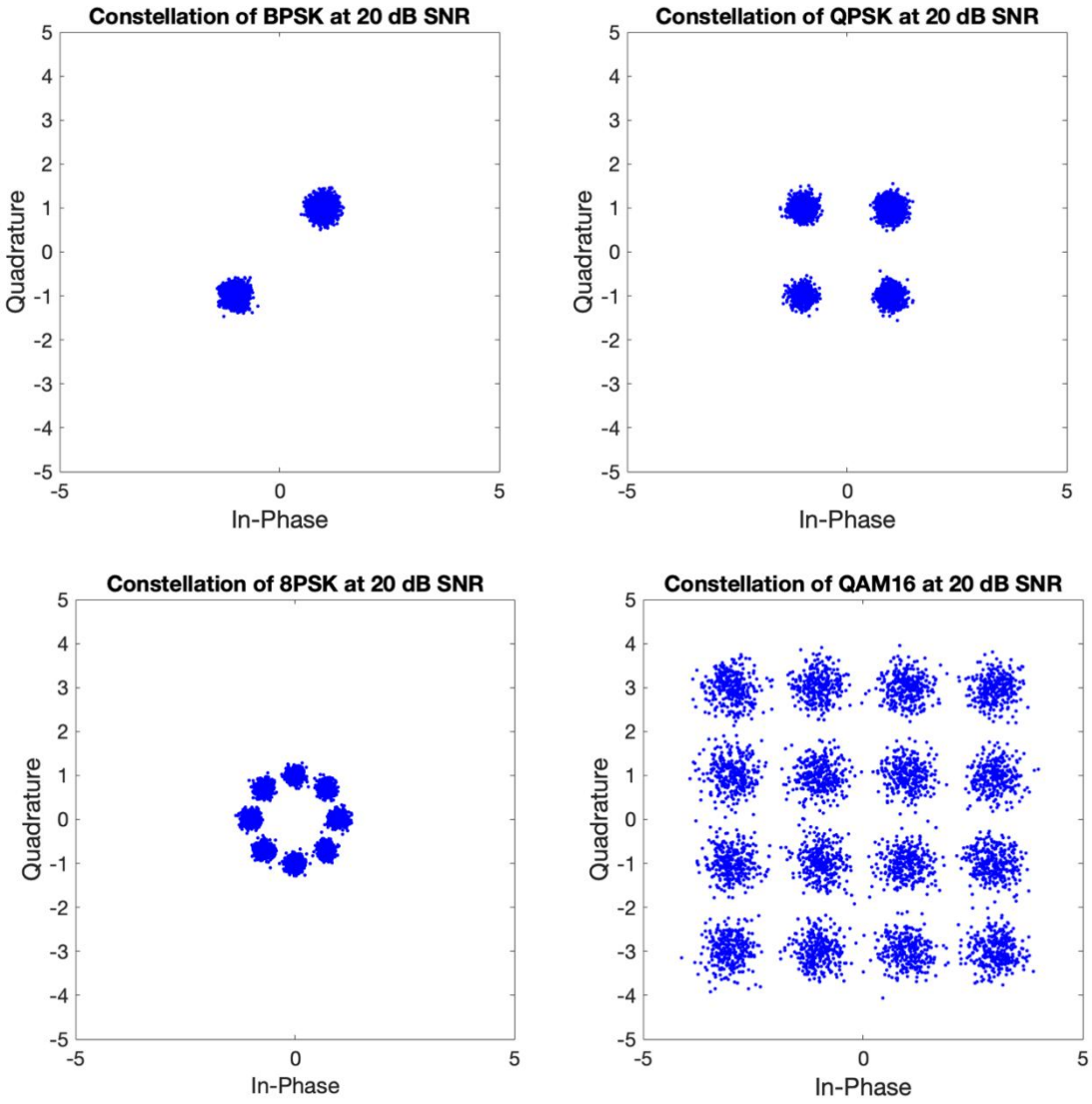

Figure 5 Constellations of BPSK, QPSK, 8PSK and QAM16 at 20 dB SNR

For the Deep Learning model and the first part of the hybrid model, the main principle is image classification. To be applied by Deep Learning, the data of modulated signals are transferred to the constellation images. Figure 5 shows the constellations as examples of the four modulations at 20 dB SNR.

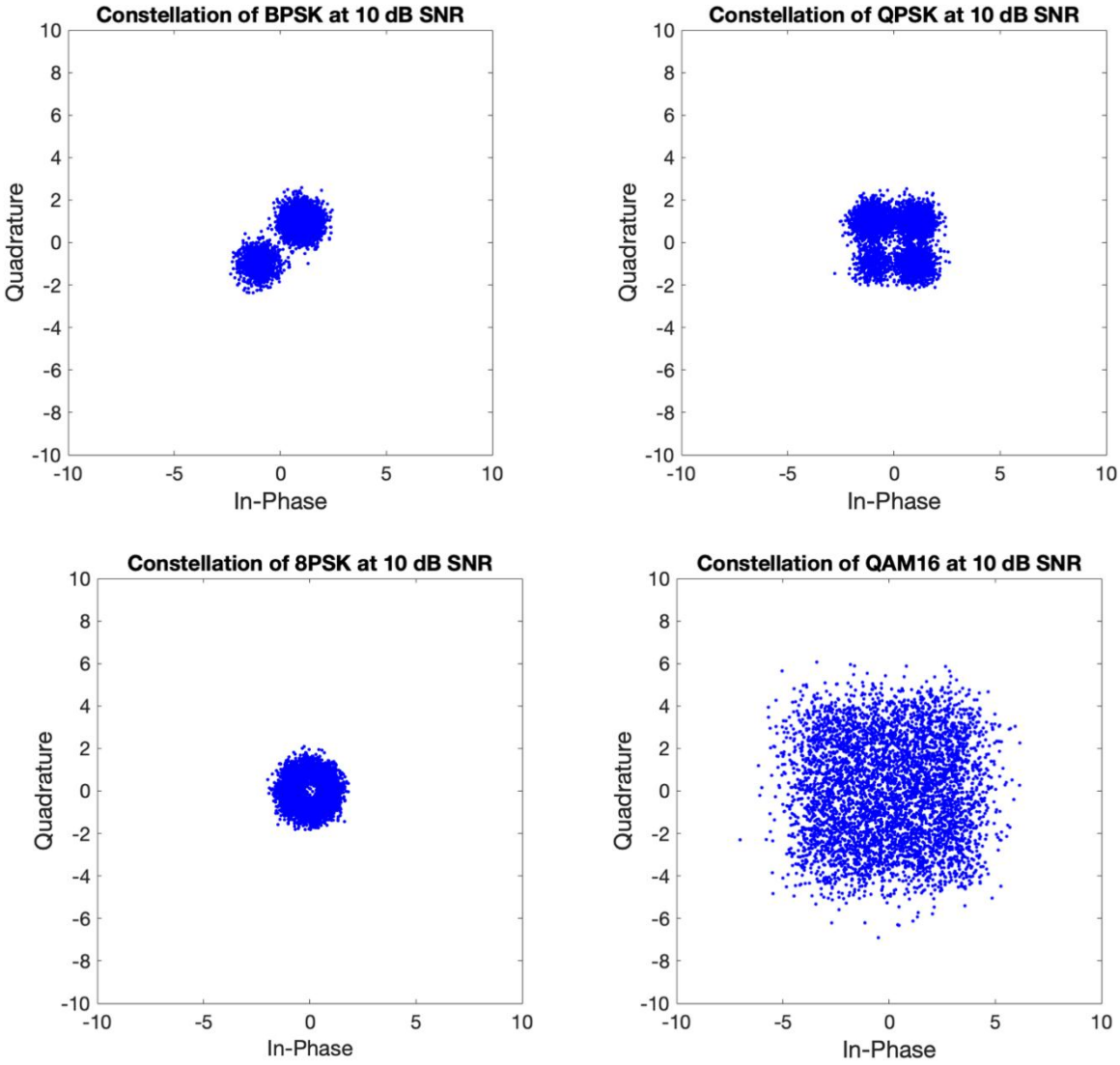

Figure 6 Constellations of BPSK, QPSK, 8PSK and QAM16 at 10 dB SNR

Figure 6 indicates the four modulation types at 10 dB SNR. The constellation images still can be detected clearly by the eyes because of the specific shapes of each modulation type. The constellations begin to be blurred due to the increased Gaussian noise.

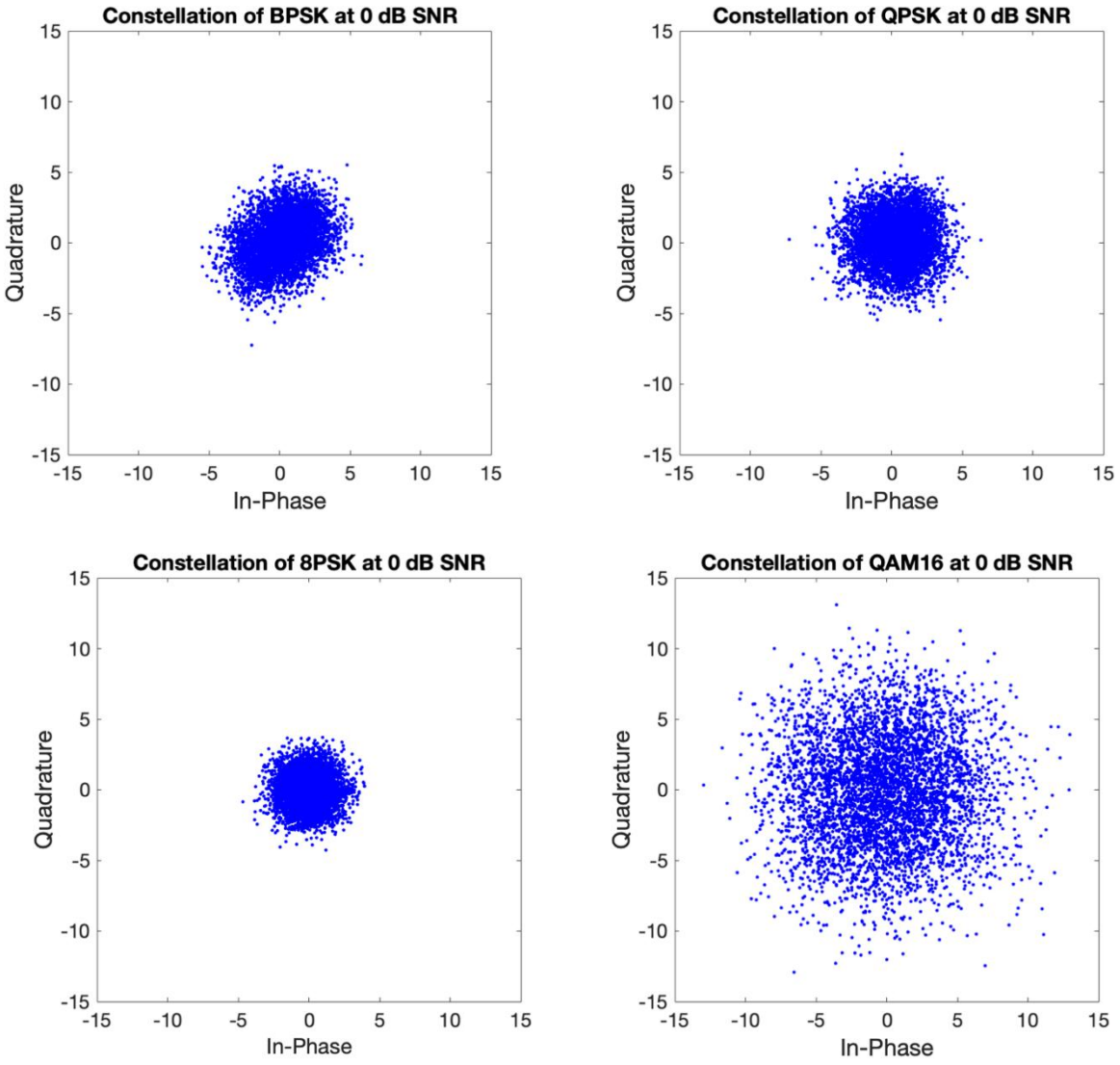

Figure 7 Constellations of BPSK, QPSK, 8PSK and QAM16 at 0 dB SNR

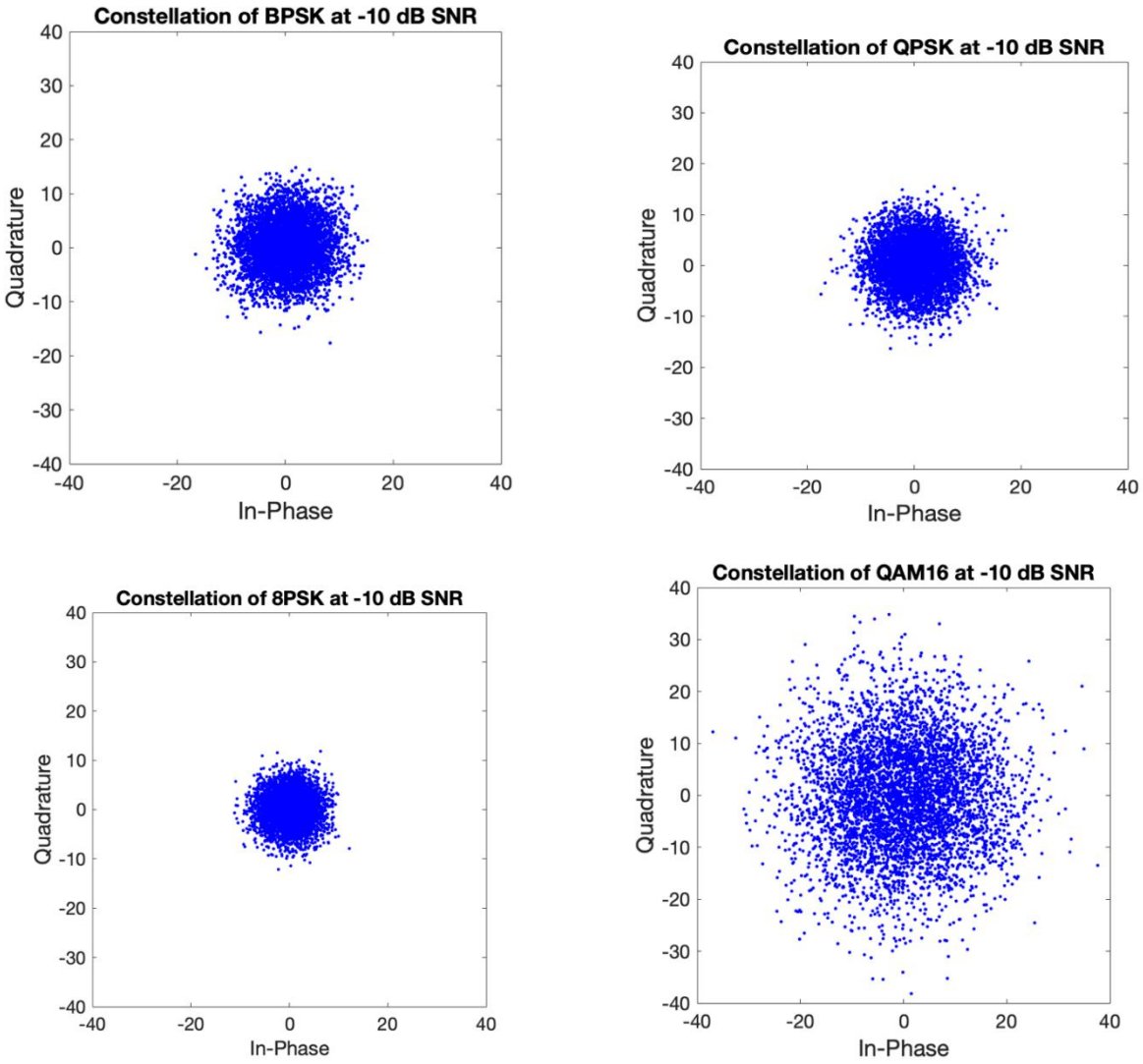

Figure 8 Constellations of BPSK, QPSK, 8PSK and QAM16 at -10 dB SNR

Figure 7 and Figure 8 provide the constellation images at 0 dB and -10 dB SNR, which means plenty of noise is introduced for the situations. Compared to Figure 5 and Figure 6, significant differences cannot be found between the constellation images at lower SNR levels. In this way, a slight difference can still be observed between BPSK and the other modulation types, as shown in Figure 7. The constellation of BPSK is a n oval shape in Figure 7, and the constellations of the other three modulation types are nearly a Gaussian noise. Although the shapes of the rest of the three modulation types look similar, there is still a difference between the amplitudes of the constellations, particularly making QAM16 distinguished from the rest modulation types.

After discussing the differences between the constellation images at the same SNR level, the difference across the different SNR levels should also be considered. All the constellation images are plotted into a complex plane, yet each of them has its own characteristics. It can easily be distinguished with eyesight at higher SNR levels, as shown in Figure 5 and Figure 6, and the constellations are not clear enough for observation with the induced Gaussian noise, as shown in Figure 7 and Figure 8. Although the constellation shapes of the modulation types look similar at the low SNR area, the scale of the amplitudes of the constellations differs from different SNR levels, which can be found in the figures with different scales of Quadrature and In-Phase.

From the examples of generated simulation data above, the physical characteristics of the four modulation types from different modulation types can be seen, although some of them are not easily recognisable to the eyes. Consequently, the constellation images are suitable for the DL inspired by image classification. The constellation images are collected with 50 samples per symbol and from -10 dB to 20 dB SNR by step of 1. After the MATLAB simulation, the practical signals should also be considered. The system, consisting of transmitter and receiver, is built up to simulate the digital modulated signals in practice.

3.3.2 Lab Collected Data

The simulation data collected from MATLAB can be employed as references and contrasts for this section to find the difference and further analysis. In this section, the system is built to simulate the practical situation.

This system is built with a transmitter, receiver and cables. The signal generator, Agilent E4437B, is employed as the transmitter. The receiver is the SDR Ettus E310, which is connected to the laptop. The signals are collected and plotted by MATLAB after receiving them from the SNR. All the equipment is connected with cables. The PN15 sequence is utilised as the baseband RF signal. The symbol rate was 100 ksps and the sample rate was 2 MHz.

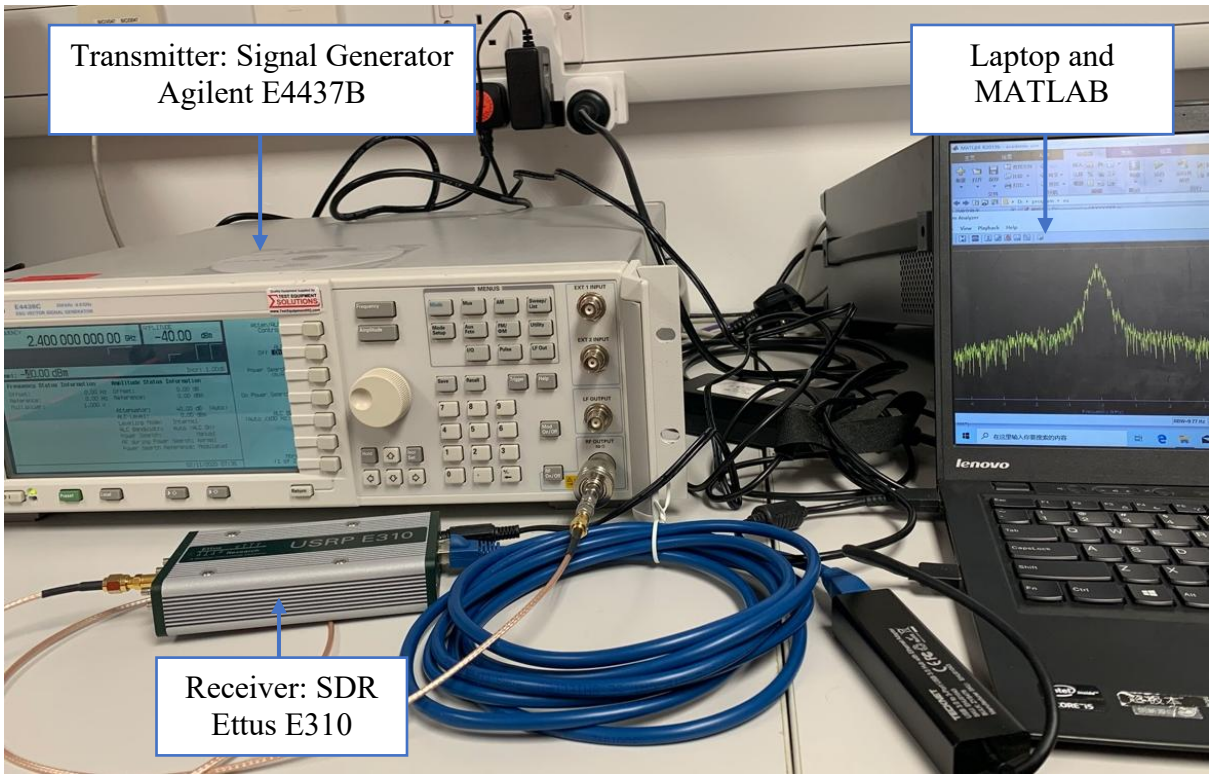

Figure 9 Photograph of the lab transmission system

Figure 9 shows the connection of the hardware system. The specific types of equipment are labelled in the photograph for instruction. The different modulated signals are simulated by setting the signal generator. The modulated signals are transmitted through the cable and received by the SDR which has the receiving function. To read the data collected by SDR, MATLAB is a platform to connect the SDR and plot the signals in the time domain, frequency domain and constellation images. The data is saved to be analysed in the following section.

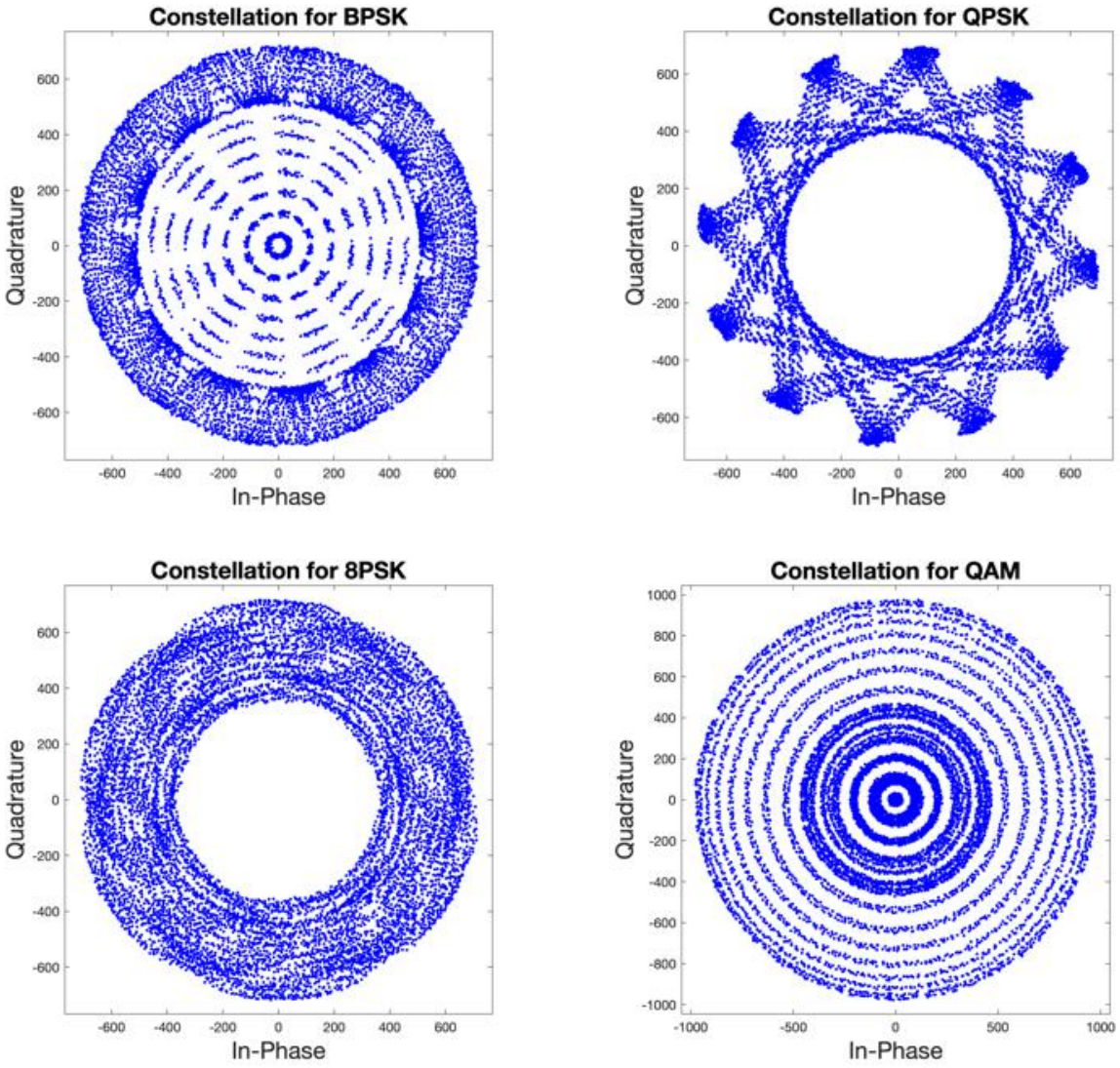

Figure 10 Constellations of BPSK, QPSK, 8PSK and QAM16 with raw data

The raw data collected from the signal generator is shown in Figure 10. When the number of sample dots increases, it is hard to distinguish the constellation images without phase and frequency lock in the system. The sample dots rotate all the time which cannot be ignored because all the constellations look like annuli in the image with enormous sample dots. For the examples shown in Figure 10, the constellation images can still be distinguished. Once the AMC with CI is involved in a dynamic transmission system, the unprocessed received data cannot be observed and classified by the algorithm. In this situation, dividing the data into small groups is reasonable for the AMC in the next step.

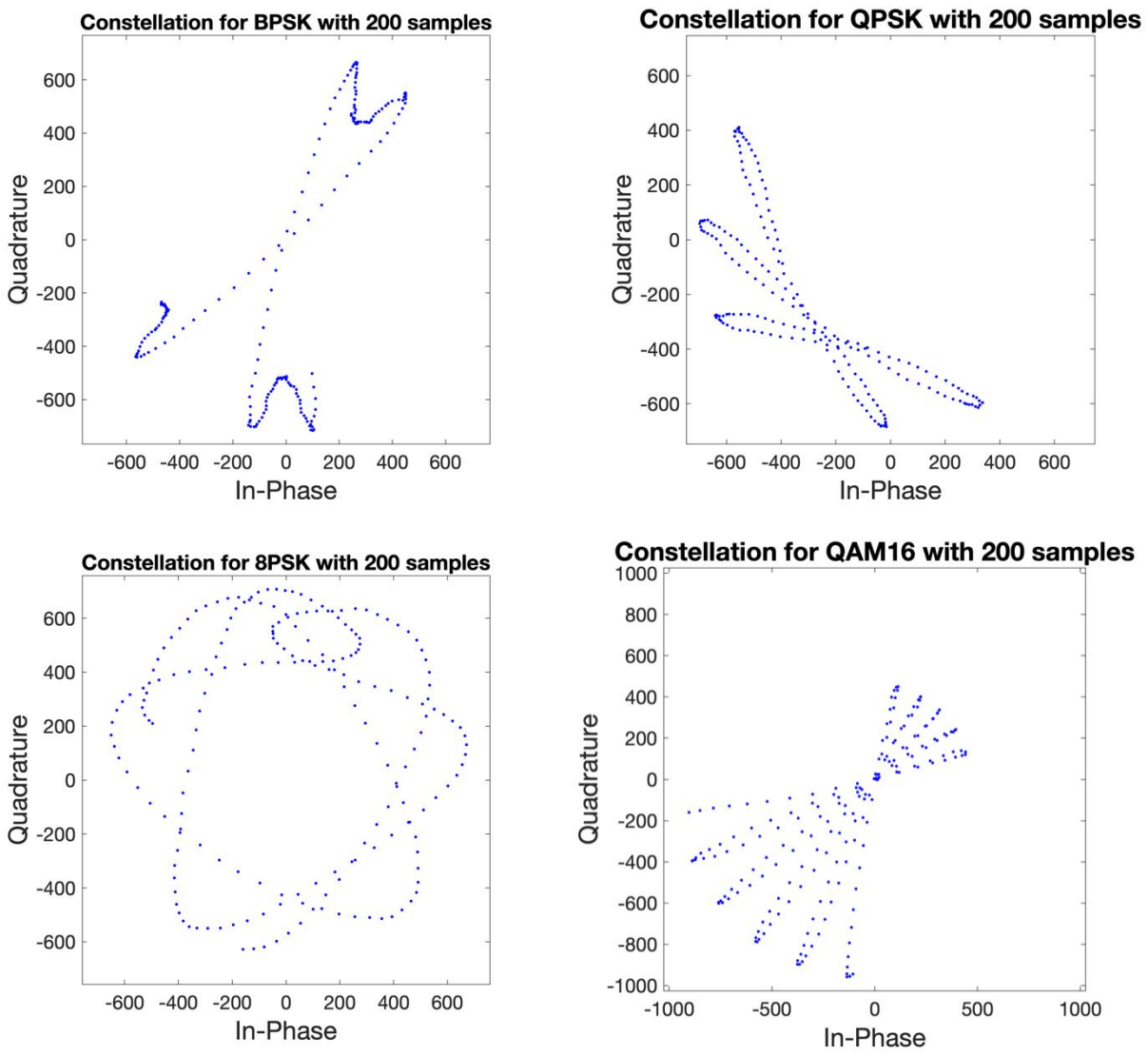

Figure 11 Constellations of BPSK, QPSK, 8PSK and QAM16 with 200 samples

Figure 11 indicates the images of the first 200 samples of the received data as small groups, which is clear to observe the distribution of the sample dots of each modulation type.

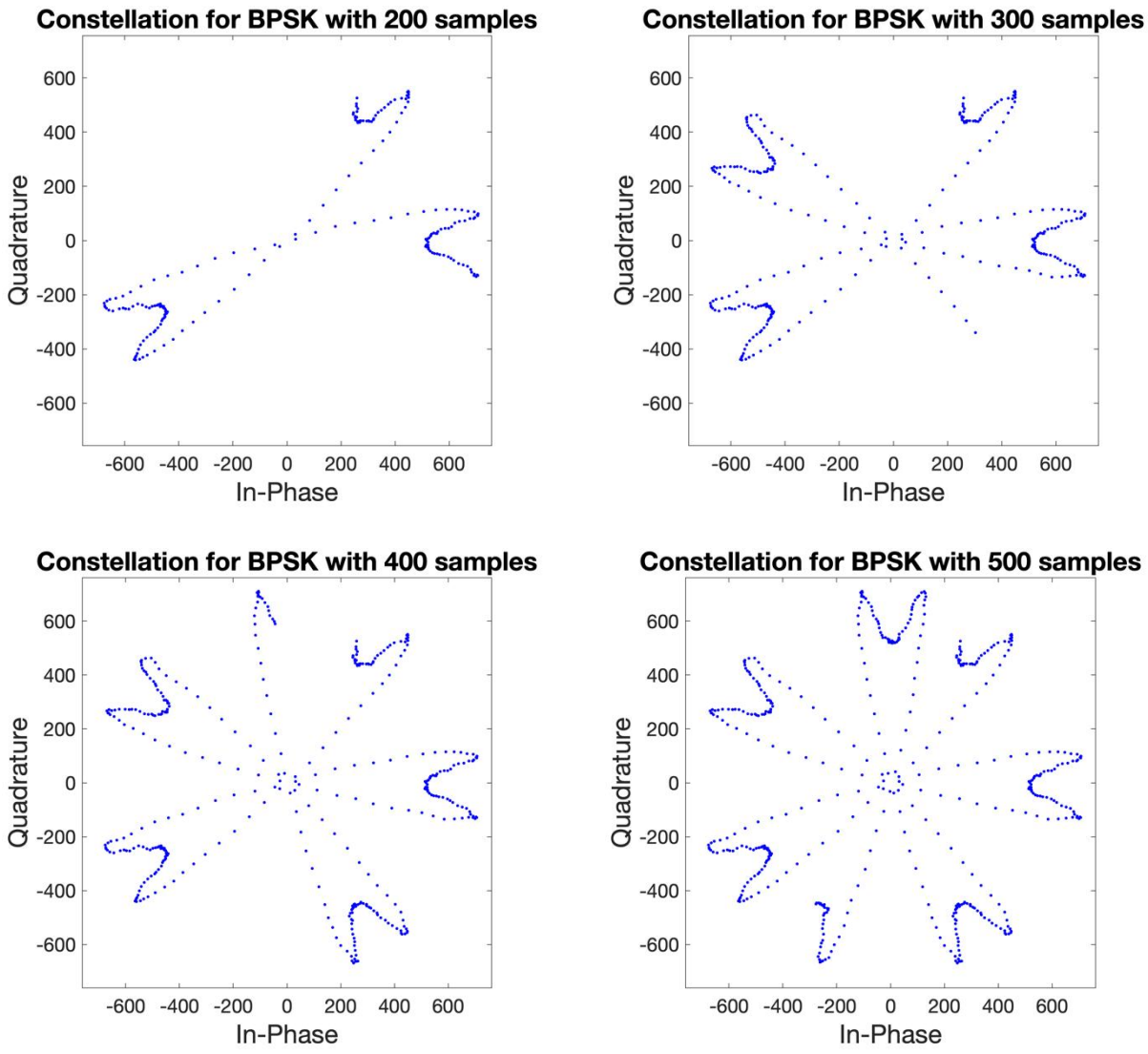

Figure 12 Constellations of BPSK, QPSK, 8PSK and QAM16 with different samples

After observing the first group of 200 samples, the small groups are also built into 300, 400 and 500 samples as one group and plotted into constellation images. As shown in Figure 12, the examples of constellation images of BPSK with 200, 300, 400 and 500 samples. It also provides the progress of the rotation from the system without phase and frequency lock.

In this scenario, the small groups provide clear constellation images for the AMC with CI. If there are too fewer sample dots in the constellation, the characteristics of the modulation types cannot be found. The dataset consists of the constellation images of each modulation type with 200, 300, 400 and 500 samples. There are 2000 images for the algorithm with 70 %

of the images utilised for training, 20 % of images for the validation process and the remaining 10 % used for testing: proportions as used by others [52].

3.4 Deep Learning Structures

In this section, the Deep Learning models are introduced. These models include one CNN model and three pretrained Transfer Learning models. The dataset for the DL is the constellation images collected from section 3.2. Both MATLAB simulated data and lab-collected data are tested with the DL models introduced in this section.

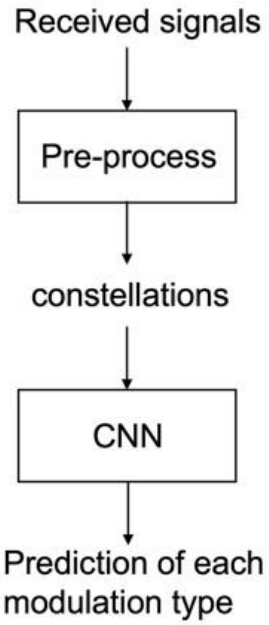

Figure 13 System structure of AMC with CI

Figure 13 indicates the system graph of AMC with CI. The raw data is collected and processed to generate the constellation images with the proper number of data samples. After collecting sufficient data, they are fed to the CNN as the training dataset and the testing dataset. After that, the CNN will provide the prediction of modulation types and the accuracy overall. The specific CNN structures are introduced in the following sections.

The first structure is the one which CNN developed from the Iris model. At the beginning stage of developing a CNN model for image classification, the Iris Model is a classical model to be considered and started with. The Iris dataset is a classic dataset used in machine learning and consists of 150 samples of iris flowers with four features each: i.e. sepal length, sepal width, petal length and petal width. The goal is to classify the flowers into one of three species (setosa, versicolor or virginica) based on their features. This CNN model developed from the Iris model is not pretrained, which is used as a contrast to the CNNs in Transfer Learning in the next section.

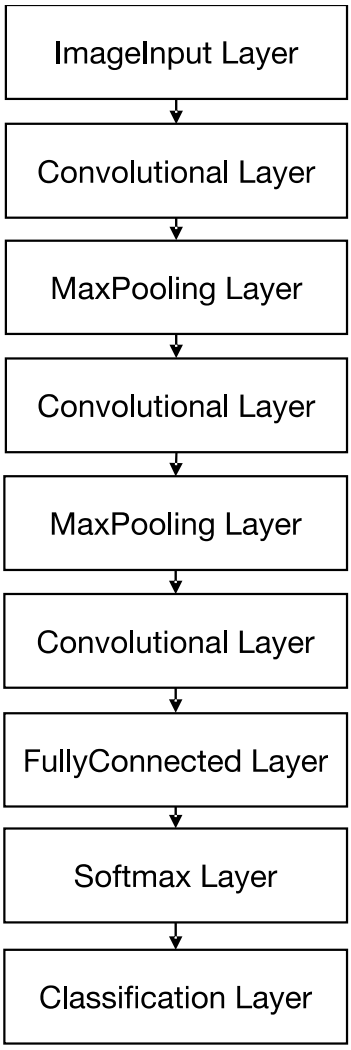

Figure 14 Structure of CNN

This model is created as a development from the Iris recognition case. The main structure is shown in Figure 14. The model is created by classifying the Iris images first, then revising the

parameters, whilst keep the same model structures to classify the constellation images. The convolutional layers are followed by the batch normalisation layers and ReLu layers in the system. Two max-pooling layers are set between the other three convolutional blocks, which can down-sample the input data and reduce the risk of overfit. The convolutional layers can capture the physical features of the images by the filters, such as the profile and grayscale of the images. In this way, the convolutional layer is significant in being able to influence the classification of the images. The batch normalisation layers can normalise the input channel. The ReLu layers calculate the threshold for the elements [53]. Fully connected layers are used in the final layers of a neural network to make predictions based on the learned features of the preceding layers. The Softmax function maps the outputs of the previous layer to a probability distribution over multiple class. The resulting output can be interpreted as the predicted probability of each class.

Transfer learning is a subfield of machine learning that aims to leverage knowledge learnt from one task to another related task. The main idea behind transfer learning is to use the knowledge learnt from a source task to initialise a model for a target task, which requires much less labelled data to achieve a good performance. This approach has been shown to be particularly effective in computer vision, natural language processing and other areas where there is a shortage of labelled data. With their outstanding performance, three Transfer Learning model are introduced in this work.

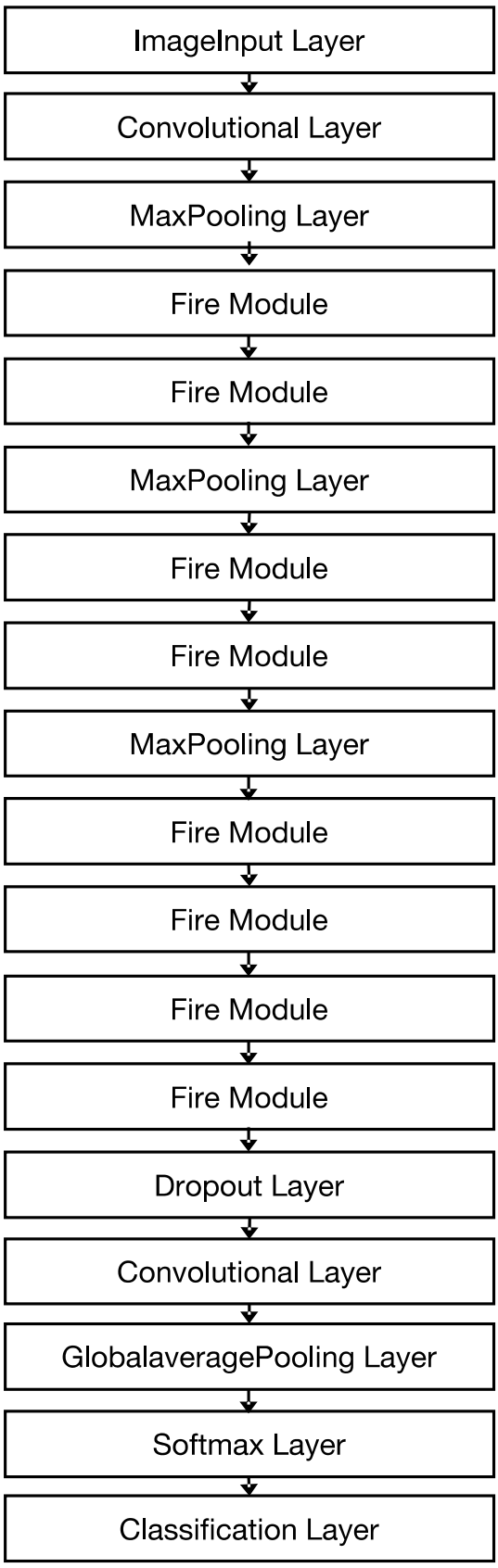

Figure 15 Structure of SqueezeNet

SqueezeNet is a small deep neural network architecture designed for efficient computation on low-power devices like smartphones and laptops. The main structure is shown in Figure 15. The size of each input image is 227-by-227 pixels [54]. This network has millions of parameters, making it one of the smallest deep neural networks, which is 50 times smaller than AlexNet with equivalent accuracy. SqueezeNet has input layers, convolutional layers, fire modules, pooling layers, dropout layers and output layers. The dropout layer is used for regularisation to prevent overfitting and the pooling layer can reduce the spatial dimensions and computational cost.

The main building block of SqueezeNet is the Fire module, which aims to reduce the number of parameters and computation required for deep neural networks. It consists of a squeeze layer, which reduces the number of feature maps by using 1x1 convolutions, followed by an expand layer, which increases the number of feature maps using 1x1 and 3x3 convolutions. The squeeze layer compresses the spatial dimensions of the input whilst maintaining its rich information. In the meantime, the expand layer restores the spatial information and increases the depth of the network. The Fire module is designed to improve the accuracy and efficiency of SqueezeNet by reducing the number of parameters and computation required, whilst still retaining the ability to learn complex features from the input data. The Fire module repeats multiple times in this network, which helps to build a deep, lightweight architecture capable of achieving good performance.

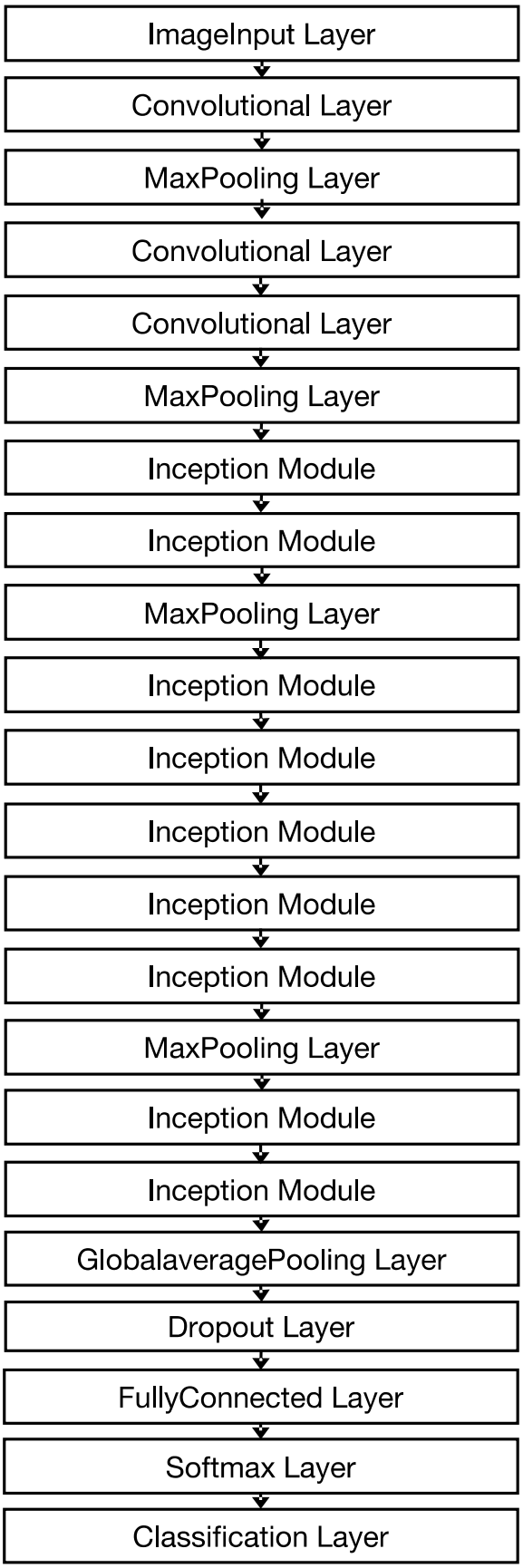

Figure 16 Structure of GoogleNet

GoogleNet, also known as Inception-v1, is a deep convolutional neural network architecture that was introduced and pretrained to classify the images into 1000 categories and 365 places. The input image size is 224-by-224 pixels [55]. The main structure is shown in Figure 16. GoogleNet consists of multiple Inception modules, which aims to capture both the spatial and channel-wise information in the input data. Each Inception module consists of several parallel branches, each with a different filter size, such as 1x1, 3x3 and 5x5, as well as pooling layers. The outputs from each branch are concatenated, producing a combined feature representation that captures information at different scales and in different ways. This allows the network to learn a more diverse range of features, improving its ability to represent the input data and make accurate predictions.

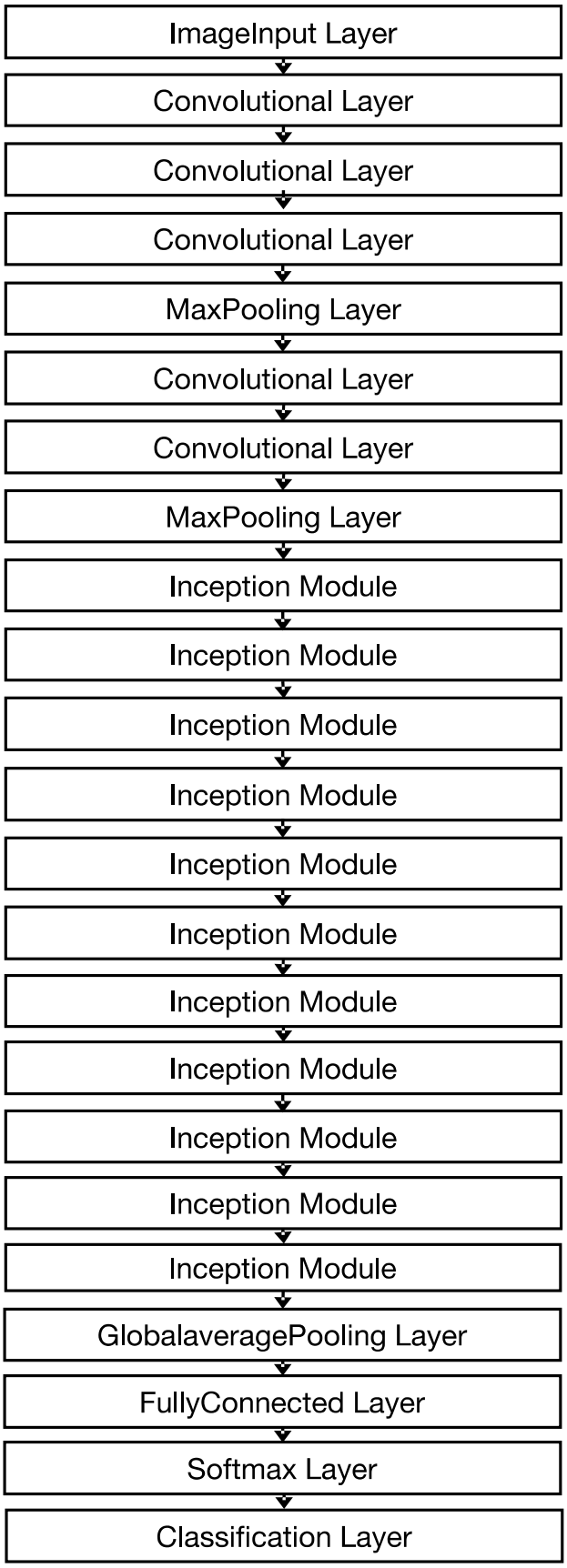

Figure 17 Structure of Inception-v3

Inception-v3 is the updated version of the Inception network architecture, first introduced in 2014, which increases the accuracy and efficiency of the network. The Inception-v3 has 48 layers and was trained by over a million images to classify into 1000 categories [56]. The input size is 299-by-299 pixels. Inception-v3 also includes more complex and efficient Inception modules, which allow the network to learn features at multiple scales and in multiple ways [55]. Inception-v3 uses batch normalisation and rectified linear unit (ReLU) activations, which are not used in GoogleNet, to improve the convergence of the network during training. In this way, Inception-v3 represents a significant improvement.

Overall, the size of the images need to be modified before feeding to the models, in order to fit the input size criteria. The final learning layers are modified, to provide only 4 outputs, corresponding to each of the modulation types. In our experiments, 70 % of images are used as training and the rest are used as validation. Images are rotated in -90 to 90 degree steps (representing constellation phase errors) and the images are rescaled from 1 to 1.5 randomly (representing amplitude variations), which can help to improve the amount of training data and avoid overfitting [43]. Each DL model uses 10 times the iterative experiments. During these experiments, the models are trained to adjust the new dataset by getting feedback from the experiment results. The novelty of this part is the application of the transfer learning, which avoids the need to adjust the parameters and details of the AI models.

3.5 Hybrid Model

During the testing process of the CNNs in session 3.4, the prediction is not robust enough at low SNR levels. At the beginning of the AMC with CI experiments, the system cannot always distinguish the modulation types at low SNR levels. Figure 18 indicates an example that one of the classifications of GoogleNet detecting QAM16.

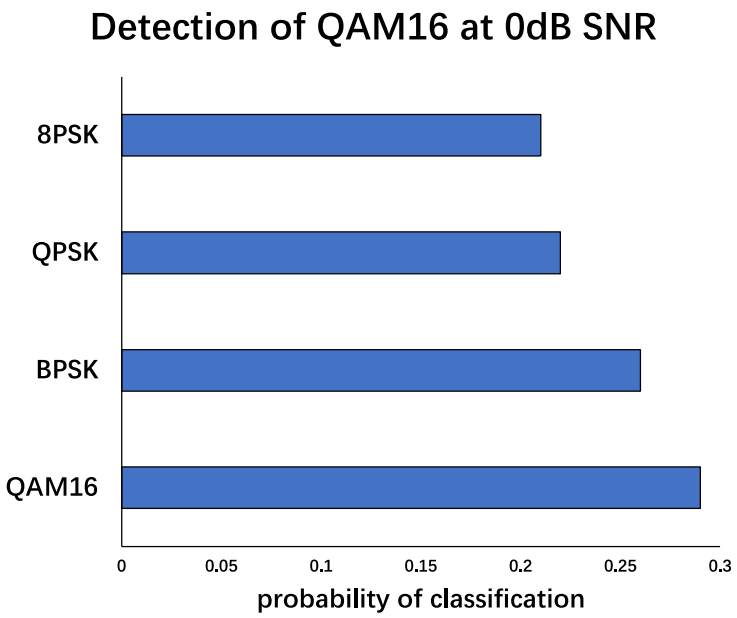

Figure 18 Detection of QAM16 at 0 dB SNR

As shown in Figure 18, the probabilities of the system prediction of QAM16 are quite similar, especially for the predicted results which are QAM16 and BPSK. That means that there is still a risk to detect the QAM16 as BPSK by any chance. To avoid this situation and improve the accuracy of the prediction at low SNR levels, the statistical features of the modulated signals are induced. In this situation, the hybrid model is provided as an application of the statistical features based on previous CNN models.

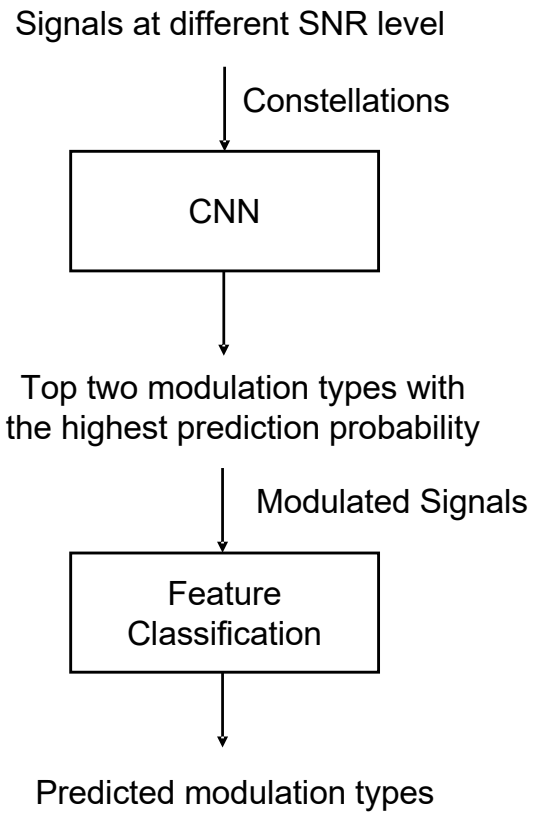

Figure 19 System structure of Hybrid model

Figure 19 provides the system structure of the Hybrid model. As shown in Figure 19, DL is utilised at first, and the statistical features of the signals are applied to the second process for the classification.

The decision tree algorithm is involved in the second process. The Hybrid model is an intermediate model, the statistical features are introduced in Chapter 4. The statistical features are captured and compared to classify the modulation types. The calculated values of the statistical features are introduced in Chapter 4. Based on the traditional Machine learning method, the features which can obviously help to distinguish the modulation types are chosen to help classify them are discussed later in this thesis.

3.6 Results

After all the experiments of AMC with CI and the last developed Hybrid model, the results are analysed in this section. In Figure 20, the results are shown from the four CNN models. The CNN which was developed using the Iris case performs worse than other traditional DL methods. This is likely due to the structures and coefficients of this CNN variant potentially being very sensitive and thus will significantly influence the classification system.

The other three models are also forms of CNN, although they have more complicated structures, and they are pre-trained by millions of generic images. Although the images applied for pretraining are not the constellation of modulated signals, they can also help the models classify the images by modifying the coefficient iteratively and repeatedly.

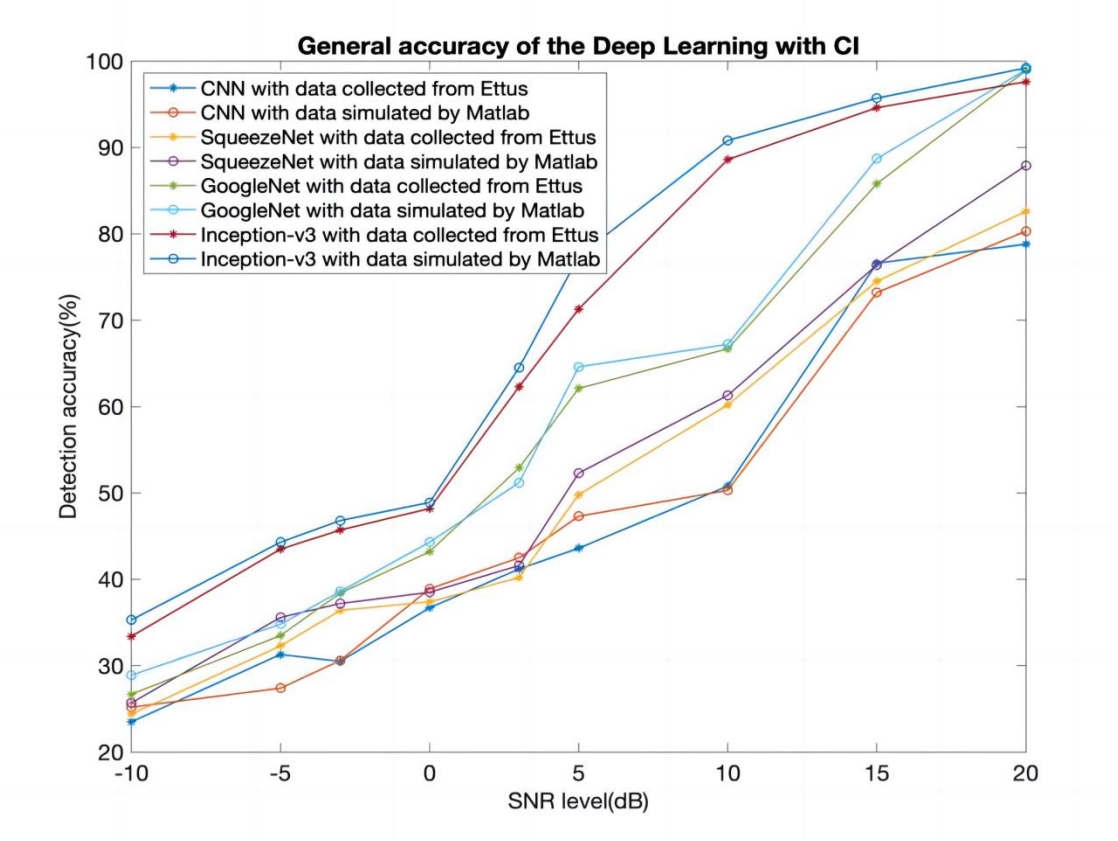

Figure 20 General accuracy of the AMC with CI

Figure 20 shows the general accuracy of each DL model at different SNR levels. The general accuracy means the probability of correct classification which can be defined as:

$$Probability\ of\ correct\ classification = \frac{Number\ of\ correctly\ classified\ results}{Total\ number\ of\ classified\ results}$$

The data are also collected in two ways: simulation in MATLAB and lab signals from the Ettus. For the low SNR area, both sources of the data have significant noise. That is why the accuracies of both are quite similar and low. From Figure 20, it is obvious that the Inception-v3 shows the best performance over the whole detection range when compared to the CNN, SqueezeNet and GoogleNet. With the updated depth and complexity of the network, Inception-v3 has a significant increase of accuracy, especially around 10 dB SNR.

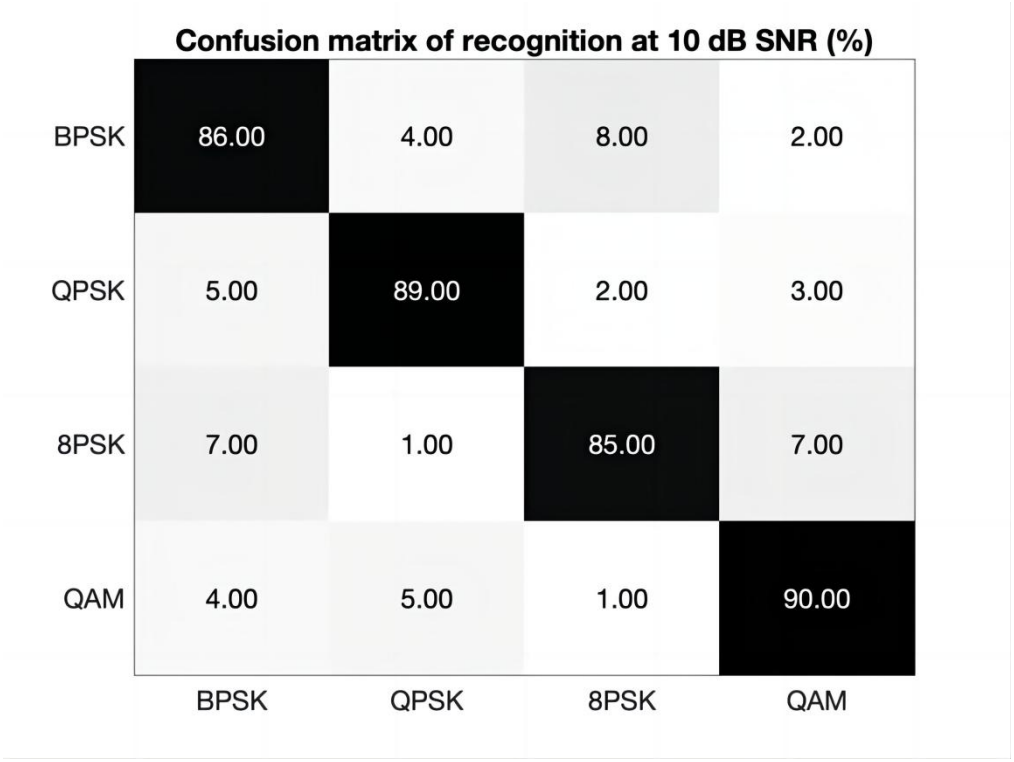

Figure 21 Detection of AMC with CI at 10 dB SNR

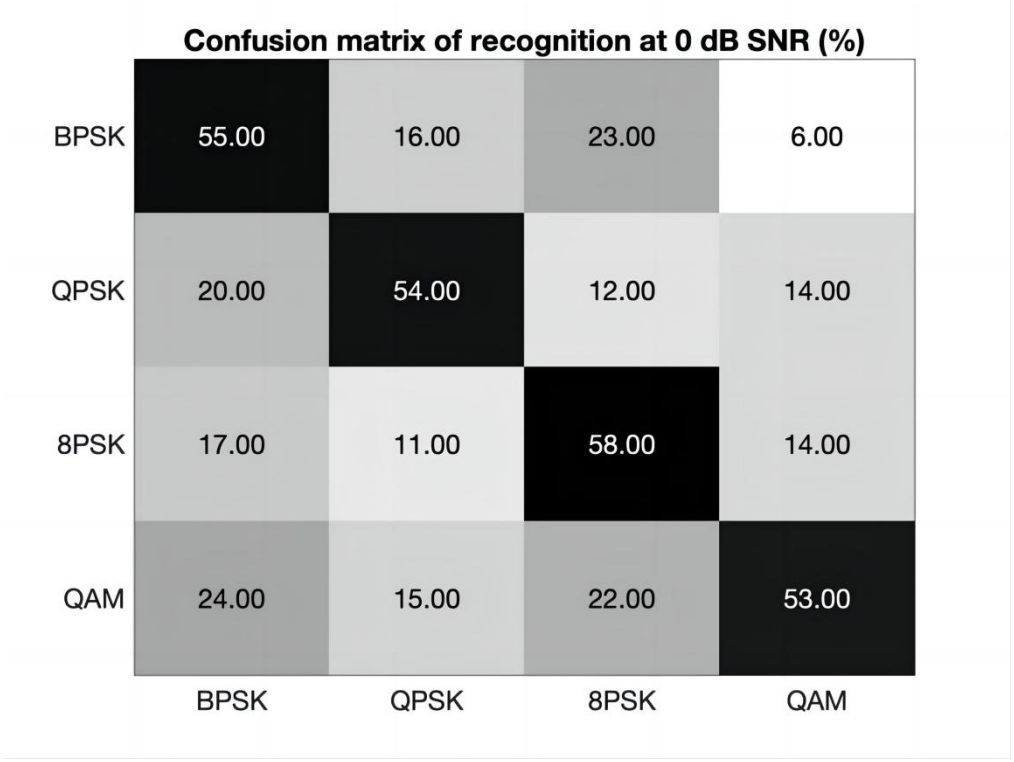

Figure 22 Detection of AMC with CI at 0 dB SNR

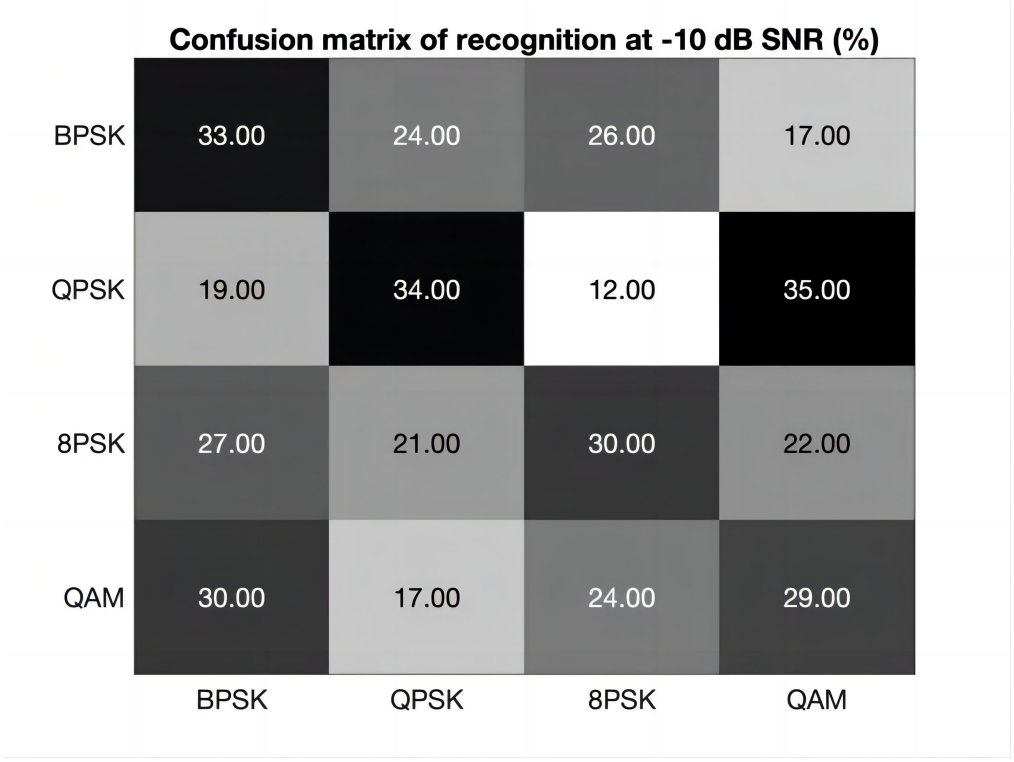

Figure 23 Detection of AMC with CI at -10 dB SNR

Figure 21, Figure 22 and Figure 23 show examples of the classification results from AMC with CI at 10, 0 and -10 dB SNR. Based on the results provided in Figure 20, the confusion matrices are collected by the results of the Inception-v3 model. They also indicate the probability of when the AMC model output the classification results. At 10 dB SNR, the classification is valid according to Figure 21. In general, the random guess detection rate would therefore be 25% (since there are four possible modulation types). This model also provides accuracy slightly higher than a random guess at -10 dB SNR, which cannot help in the receiving system. The simulated data is used as a reference in the previous experiments to choose the best Neural Network structure, so results utilise the data collected from Ettus SDR, representing real world signals. From Figure 21, Figure 22 and Figure 23, the details of each prediction can also be found.

According to the table in the previous work [48], the accuracy of this study is significantly improved for two reasons. Firstly, the dataset is expanded, which includes all the SNR levels to provide better training for the networks. After that, the CNN models run on 10 occasions for the iterative experiment, which also makes the models adjust the parameters for the AMC system.

Table 2 Detection accuracy of AMC with CI and Hybrid Model

SNR Levels (dB)	Accuracy of AMC with CI	Accuracy of Hybrid Model
-10	34.7 %	57.3 %
-5	44.3 %	62.1 %
0	51.4 %	67.7 %
5	85.6 %	88.3 %
10	89.0 %	95.1 %
20	98.2 %	98.7 %

Table 3 Comparison of AMC Techniques

Model name	Detection accuracy
Maximum likelihood [28]	Less than 80% at 10 dB
Log-likelihood functional [29]	Less than 55% at -10 dB
Ph&D-GLRT and ADMP [31]	Near 90% at 6 dB
High order cumulants and SVM [33]	50 % at 0 dB
CNN [39]	20% at -10 dB
AMC with CI	34.7% at -10 dB
Hybrid model	57.3% at -10 dB

After the testing of AMC with CI, the Hybrid model is employed. The results and comparison with AMC with CI are indicated in Table 2. The Hybrid model shows the improvement compared to the results from the AMC with CI. When the SNR level is over 0 dB, the increase is slight. At the low SNR level, the Hybrid model performs its advantages with improvements over 10%. According to these results, attention should be given to the statistical features to refine the AMC technique.

The comparison with existing studies is indicated in Table 3. The first four AMC techniques use the traditional method, and the overall limitation is the low accuracy especially at low SNRs. The Ph&D-GLRT and ADMP show the good performance at 6 dB, although the limitation is that the classification is only between the specific pairs such as QAM16 and 16PSK. The high order cumulants and SVM provides the idea of high order cumulants, which can be used in the later studies. The advantage of CNN model is its efficiency, as it uses less time than the SVM model. However, the accuracy of CNN model should be improved. Compared to these models, there are several contributions: first of all, the accuracy is improved, and the detection areas are wider. Secondly, compared to the CNN model, this study has a good use of transfer learning, which does not require complex progress of adjusting parameters and structures of the networks.

3.7 Summary

In this chapter, AMC with CI is introduced based on image classification. This section makes good use of the original constellation images. The geometric characteristics are involved by the CNNs. The signals simulated from MATLAB and collected in the lab are both tested. Due to the thermal noise and the absence of the phase and frequency lock, the signals collected in the lab have a worse detected accuracy. According to the results shown in section 3.4, the Inception-v3 contributes the best performance overall, which achieves a highest accuracy of 34.7% at -10 dB SNR and 98.2% at 20 dB SNR.

After that, to provide better classification results in the low SNR area, the Hybrid model is developed based on the CNN models. The Hybrid models increase the accuracy significantly. Especially at a low SNR area, it achieves over 10% improvements of accuracy. This method makes use of the statistical features of the modulated signals. The main principle of this technique is to classify the signals by their statistical features after the process of AMC with CI. The Hybrid model improves the prediction accuracy in some way, yet this method also relies on the previous CNN, shows more complexity and it takes a longer time to process. Consequently, the statistical features should be given more attention for the modulation classification.

Chapter 4 AMC with GRF

This chapter proposes a new algorithm, AMC with Graphic Representation of Features (GRF), which presents the statistical features as spider graphs for DL. Modulation types can be detected in a dynamic way without phase lock and frequency lock. The concepts are tested and verified using simulations and RF data using a lab Software Defined Radio (SDR).

4.1 Introduction

To achieve the overall objective, improve the accuracy of AMC, AMC of GRF is indicated. As the sequence of the models is developed from Chapter 3, which takes advantages of image classification and develops the accuracy by additional statistical feature classification at the last step. Attention should be also paid to the value of statistical features of the modulated signals. AMC with GRF is proposed in this chapter as a result of the combination of advantages from statistical features and image classification based on DL.

The statistical algorithm from existing studies requires some calculation of the different features [28] [33] [39]. Although the classification results are not outstanding, these studies still give an insight with the statistical features. The AMC technique with AI models have some completive results [39], in which the results are not as good as SVM, although they take less running time. The CNN model involved into Automatic Cognitive Radio Waveform Recognition [44] also provide an innovative solution, which is also using image classification. However, this model needs a pre-process of the waveform and different features to detect different waveforms. To take both advantage of, and to develop the AMC with CI from chapter 3, AMC with GRF is indicated.

To involve the image classification technology and the advantages of the statistical features, GRF is proposed in this chapter. After analysing the statistical features of the four kinds of

modulation types, twelve features are selected to help build the spider graphs. The spider graphs, which are the training and testing data used for the GRF, are shown in detail below. Both signal data collected from Ettus and simulated from MATLAB are processed and the spider graphs are generated for the Neural Networks.

As previously stated, DL with CI and the hybrid model already provide the methods to develop the AMC. However, the AMC with CI does not perform well enough at the low SNR area. To explore the low SNR area, the GRF method is developed, inspired by the hybrid model which also involves the statistical features. To employ both advantages from graphic characteristics and statistical features, this chapter mainly indicates the new method, DL with GRF. The main contribution of this technique is that is represents the statistical features of modulation types graphically, utilised as the image classification dataset. With the GRF technique, the overall classification accuracy reaches 58 % for 0 dB SNR and 86 % at 10 dB SNR, compared to a random guess accuracy of 25 %. The details of the technique are described in the following sections.

This chapter is organised as follows: in section 4.2, the statistical features involved in GRF methods are introduced. There are 19 original features in total describing the characteristics of the modulated signals. All of them are calculated and compared to be chosen as the essential conditions classifying the modulation types. In section 4.3, the GRF method is indicated, and it is utilised with deep learning as a new technique of AMC. In section 4.4, according to the analysis of GRF and the AMC models, the results are shown and discussed. The results from DL with GRF are also compared to the results from Chapter 3.

4.2 Statistical Features for GRF

In this section, the statistical features of the modulated signals are introduced and analysed from -10 dB SNR to 20 dB SNR. These features can describe the physical characteristics of the signals; some of them can be used for the classification, which are contributed for GRF. The procedure of choosing the effective features is also indicated.

4.2.1 Statistical Features

The main purpose of the GRF method is to build the dataset of the spider graphs which can represent the characteristics of modulated signals and help to distinguish the modulation types from different SNR levels, so the 19 features prepared to be involved in GRF are introduced as follows:

The signal power ratio of in-phase and quadrature part, β, is extracted by (11).

$$\beta = \frac{\sum_n a_Q^2[i]}{\sum_n a_I^2[i]} \tag{11}$$

where the range of n is from 1 to N, where N is the number of the samples, i is the i-th sample.

The standard deviation of the direct instantaneous phase, σ_{dp}, is extracted by (12).

$$\sigma_{dp} = \sqrt{\frac{1}{N}\left(\sum_{i=1}^{N} \varphi_{NL}^2[i]\right) - \left(\frac{1}{N}\sum_{i=1}^{N} \varphi_{NL}[i]\right)^2} \tag{12}$$

$\varphi_{NL}[i]$ is the instantaneous phase which is defined by $\varphi_{NL}[i] = \tan^{-1}\frac{a_Q[i]}{a_I[i]}$.

The standard deviation of the signal instantaneous normalised amplitude, σ_{aa}, is extracted by (13), and where a_{cn} is defined as the normalised-centred instantaneous amplitude by (14).

$$\sigma_{aa} = \sqrt{\frac{1}{N}\left(\sum_{i=1}^{N} a_{cn}^2[i]\right) - \left(\frac{1}{N}\sum_{i=1}^{N} |a_{cn}[i]|\right)^2} \tag{13}$$

$$a_{cn}[i] = \frac{a[i]}{E(a[i])} - 1 \tag{14}$$

Normalisation is required to compensate the Channel gain [57].

The standard deviation of the signal normalised amplitude of signal, σ_v, is extracted by (15) and (16) [42].

$$\sigma_v = \sqrt{\frac{1}{N}\left(\sum_{i=1}^{N} a_v^2[i]\right) - \left(\frac{1}{N}\sum_{i=1}^{N} |a_v[i]|\right)^2} \tag{15}$$

$$a_v[i] = \sqrt{\frac{a[i]}{var(a[i])}} - 1 \tag{16}$$

The standard deviation can describe the statistical dispersion, with the above three types of standard deviation results utilised for describing the signals in the main characteristics of phase and amplitude [58]. As FSK is not considered in this work, the standard deviation of the frequency is not required here.

The Mixed order moment of signals, v_{20}, is extracted by (17).

$$v_{20} = \frac{M_{42}(a)}{M_{21}^2(a)} = \frac{E(|a[i]|^4)}{E(|a[i]|^2)} \tag{17}$$

The Mixed order moment is defined by the fourth order moment M_{42} and second order moment, $M_{21,}$ of the signal. This feature employs the Joint Power Estimation and Modulation Classification (JPEMC) algorithm [59], which is associated with the power of signal and noise. This feature can represent the received power.

The mean value of the signal samples, X, is extracted by (18).

$$X = \frac{1}{N}\sum_{n=1}^{N} |a[i]| \tag{18}$$

The mean value aims to describe the amplitude of the signals without normalisation.

The normalised square root of the signal, X_2, is extracted by (19).

$$X_2 = \frac{\sqrt{\sum_{n=1}^{N} |a[i]|}}{N} \tag{19}$$

The normalised square root of signal can describe the amplitude scale of the signals.

The maximum value of power spectral density (PSD) is defined as (*20*).

$$\gamma_{max} = \frac{1}{N} max|DFT(a_{cn}[i])|^2 \tag{20}$$

$a_{cn}[i]$ is given by (14), and the Parameter γ_{max} relates to the power spectrum of the normalised instantaneous signals' amplitude in the frequency domain, using the Discrete Fourier Transform (DFT). As mentioned in [57], this key feature is used to discriminate between FSK and PSK, the analysis of this feature is still worthy to see if it can contribute to classifying other kinds of modulation type in this work.

The Cumulants of signals are extracted by (21) to (27).

$$C_{20} = E[a^2[i]] \tag{21}$$

$$C_{21} = E[|a[i]|^2] \tag{22}$$

$$C_{40} = M_{41} - 3M_{20}^2 \tag{23}$$

$$C_{41} = M_{41} - 3M_{20}M_{21} \tag{24}$$

$$C_{42} = M_{42} - |M_{20}|^2 - 2M_{21}^2 \tag{25}$$

$$C_{63} = M_{63} - 6M_{20}M_{40} - 9M_{42}M_{21} + 18M_{20}^2M_{21} + 12M_{21}^3 \tag{26}$$

$$C_{80} = M_{80} - 35M_{40}^2 - 28M_{60}M_{20} + 420M_{40} - 630M_{20}^4 \tag{27}$$

$M_{p+q,p}$ could be defined by $E[a[i]^p a[i]^{*q}]$. Cumulants and moments are widely used in a variety of classification techniques, especially the high-order cumulants, which can reduce the influence of AWGN [59]. Cumulants are the coefficients of the Maclaurin Series of the generating function. They are proposed to represent the moments and the moments can measure functions quantitively [35]. When the higher order cumulants of the received signals are calculated, the effect of the Gaussian noise is removed and the signals are independent [36].

The Kurtosis of signals, *K*, is extracted by (28).

$$K = \left|\frac{E[(a-E[a])^4]}{E[(a-E[a])^2]^2}\right| \tag{28}$$

Kurtosis is a measurement of outlier-prone distribution, which describe the steepness or flatness of the distribution of signals physically. According to the formula of moments and Kurtosis, it can be found that the Kurtosis is also a high order statistic by involving the fourth order moments [60].

The Skewness of signals, *S*, is extracted by (29).

$$S = \left| \frac{E[(a - E[a])^3]}{E[(a - E[a])^2]^{3/2}} \right| \tag{29}$$

Skewness can describe the position of the tapering side of the distribution by indicating the asymmetry of the data according to the mean value. Similar to the Kurtosis, Skewness is a high order statistic by employing the third moment. Both the Kurtosis and Skewness are used to measure the shape of the signal's distribution, which helps to distinguish the modulation type.

The Ratio of peak-to-rms, *PR*, is extracted by (30).

$$PR = \frac{max|a|^2}{\frac{1}{N}\sum_{i=1}^{N}(a[i])^2} \tag{30}$$

PR indicates how the maximum absolute value relates to the RMS value of the sampled signals.

The Ratio of peak-to-average of the signal, *PA*, is extracted by (31).

$$PA = \frac{max|a|}{\frac{1}{N}\sum_{i=1}^{N} a[i]} \tag{31}$$

PA describes the comparison between the maximum absolute value to the mean value of the signals. The two impulsive features, *PA* and *PR* both require the maximum absolute value, measuring the relation between the impulse and the signals. They can describe the shapes of different signals in other aspects.

All the features are analysed under different conditions in the following section. Based on the performance, the effective and robust features are chosen working into the GRF system.

4.2.2 Analysis of Features

Following all the statistical features presented in the last section, this section provides the detailed analysis of each feature. The features are tested and calculated at different SNR levels. After the calculation and comparison, some of the features are selected to contribute to the building of the GRF technique.

First of all, each feature is calculated by the formulas provided from the last section. To make the feature solid, each feature is tested 500 times for each modulation at the same SNR level by generating 500 times different modulated data. For example, the mesh graphs of the feature Kurtosis are presented in Figure 24, Figure 25, Figure 26, and Figure 27.

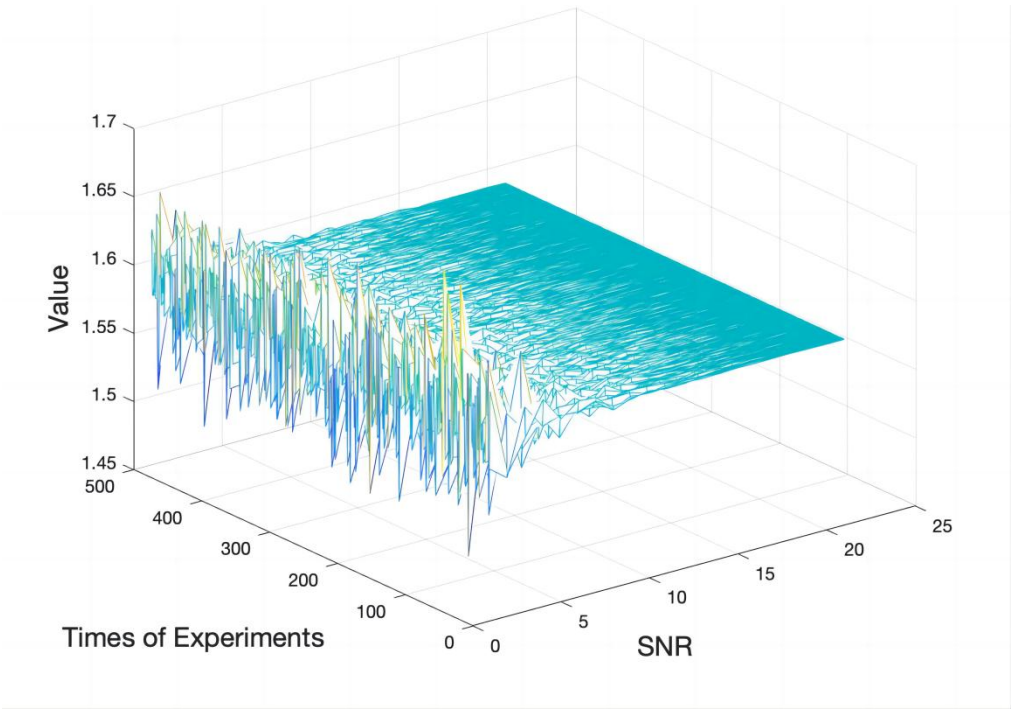

Figure 24 Kurtosis of BPSK

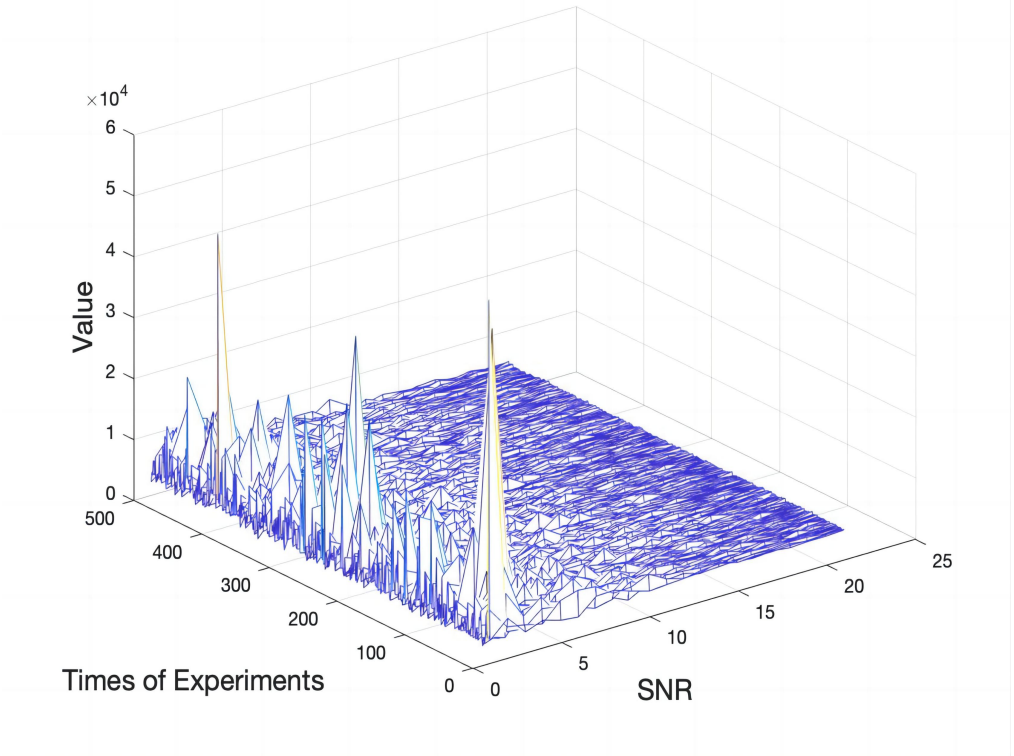

Figure 25 Kurtosis of QPSK

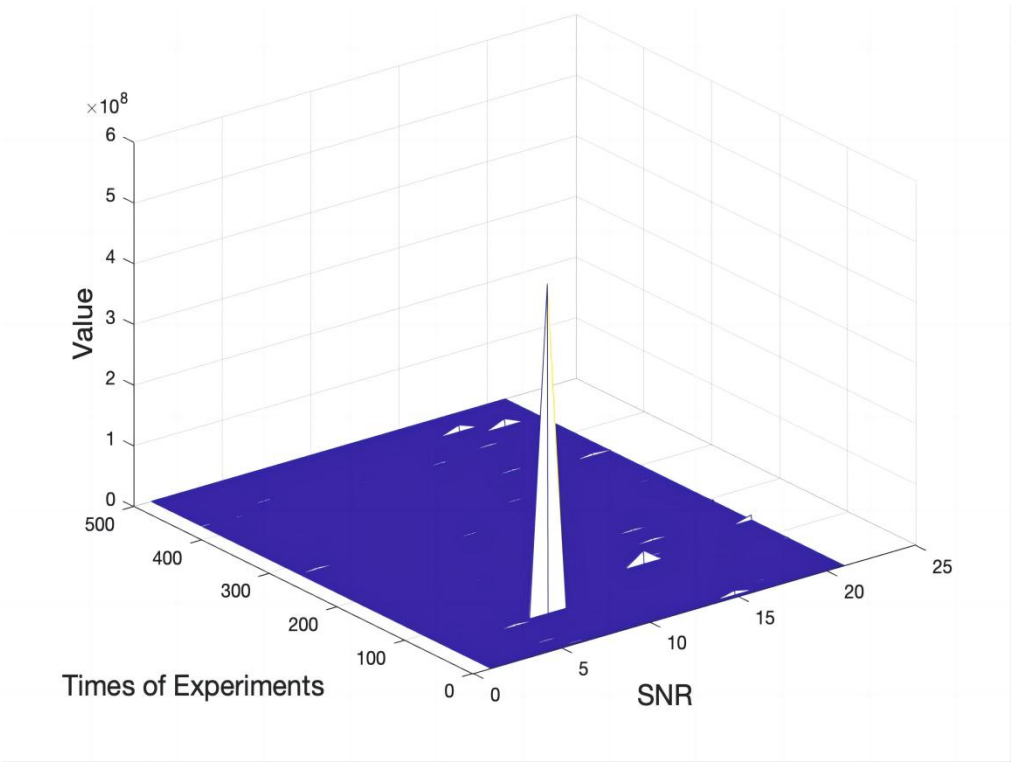

Figure 26 Kurtosis of 8PSK

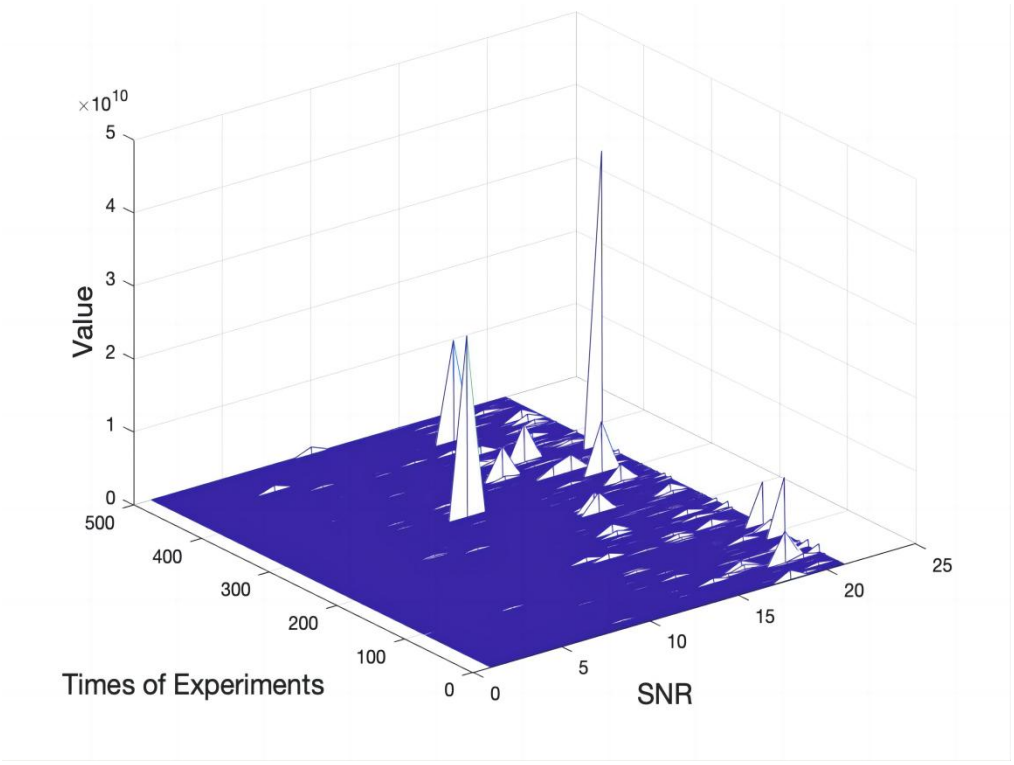

Figure 27 Kurtosis of QAM16

As seen in Figure 24, Figure 25, Figure 26 and Figure 27, Kurtosis of BPSK, QPSK, 8PSK, and QAM 16 is plotted as an example in four mesh graphs. In each graph, the x-axis is labelled with SNR levels, the y-axis is labelled with the number of experiments, and the z-axis is labelled with the value of the specific feature. The graphs are observed at the same SNR level. If the value of the feature fluctuates across the experiment times, the mean value will be employed for the following comparison. If there are several obvious spikes that show a significant difference in magnitude at the same SNR level, the value will be calculated by applying a threshold and ignoring the spike values.

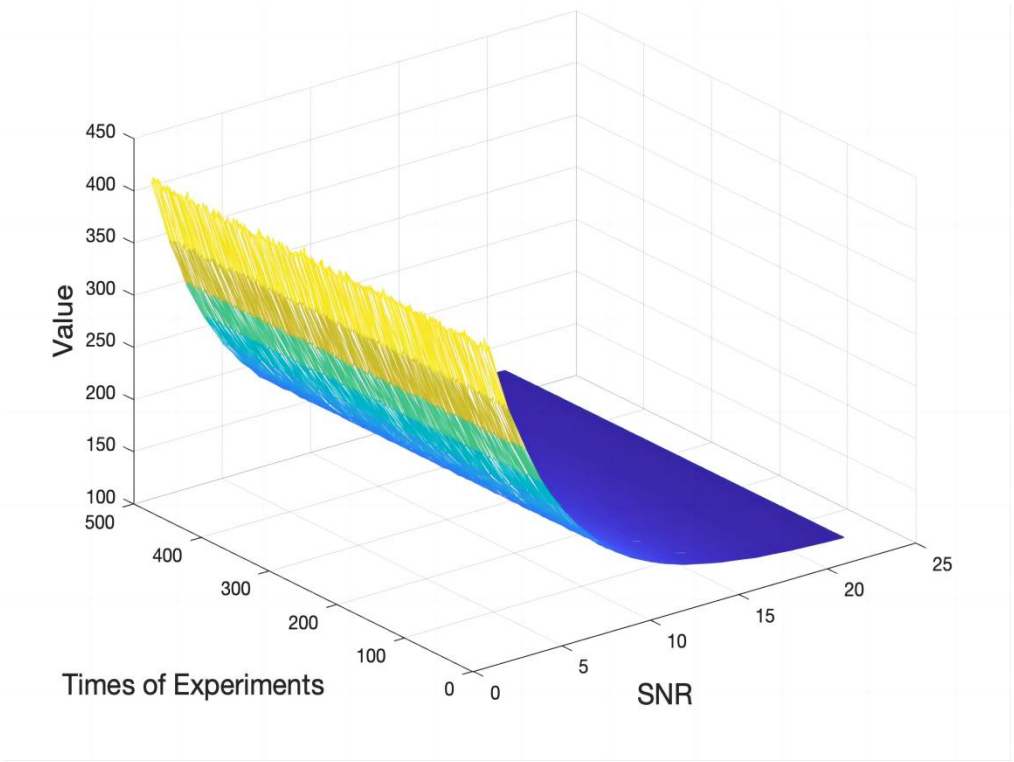

Figure 28 C_{63} of BPSK

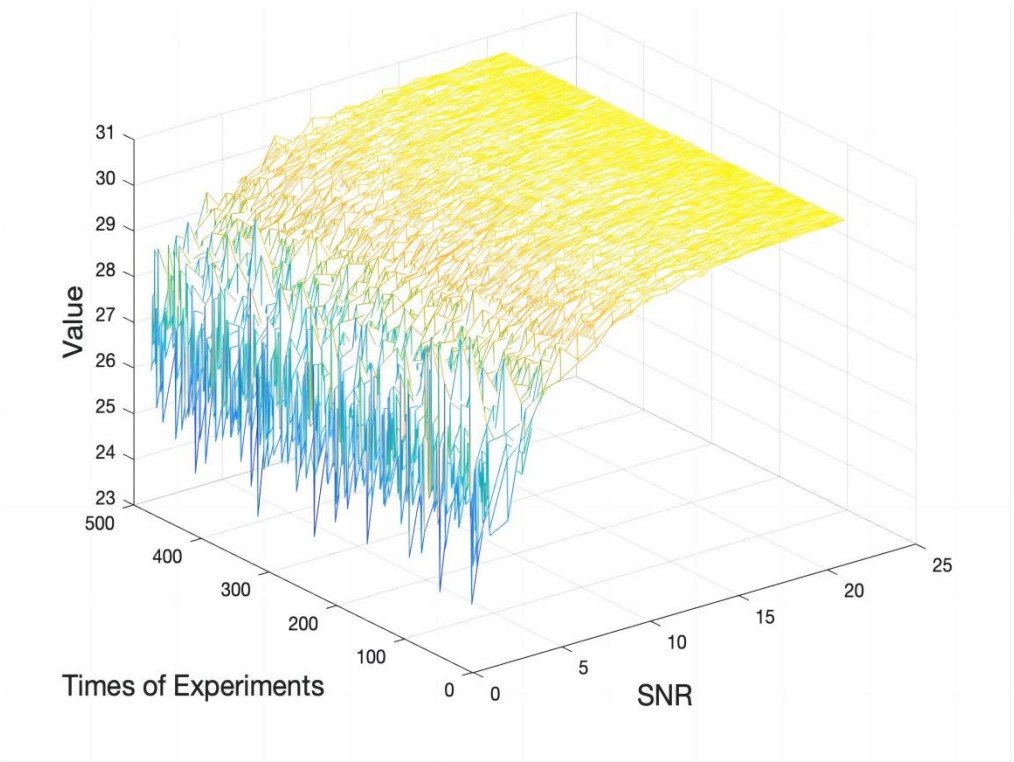

Figure 29 C_{63} of QPSK

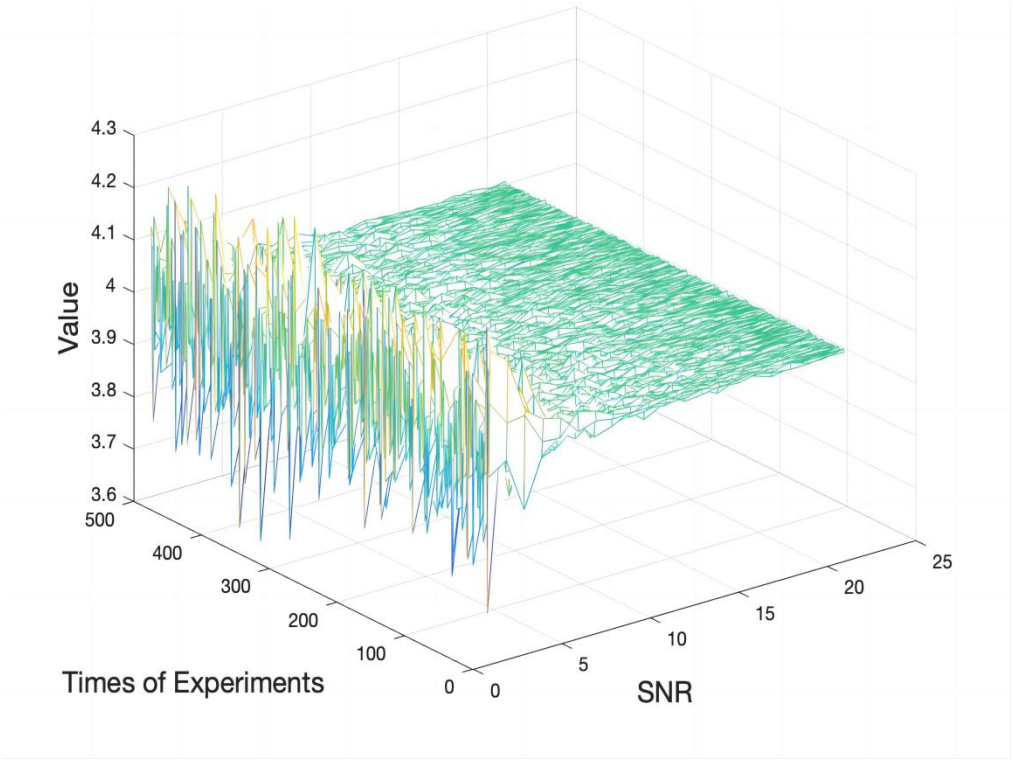

Figure 30 C_{63} of 8PSK

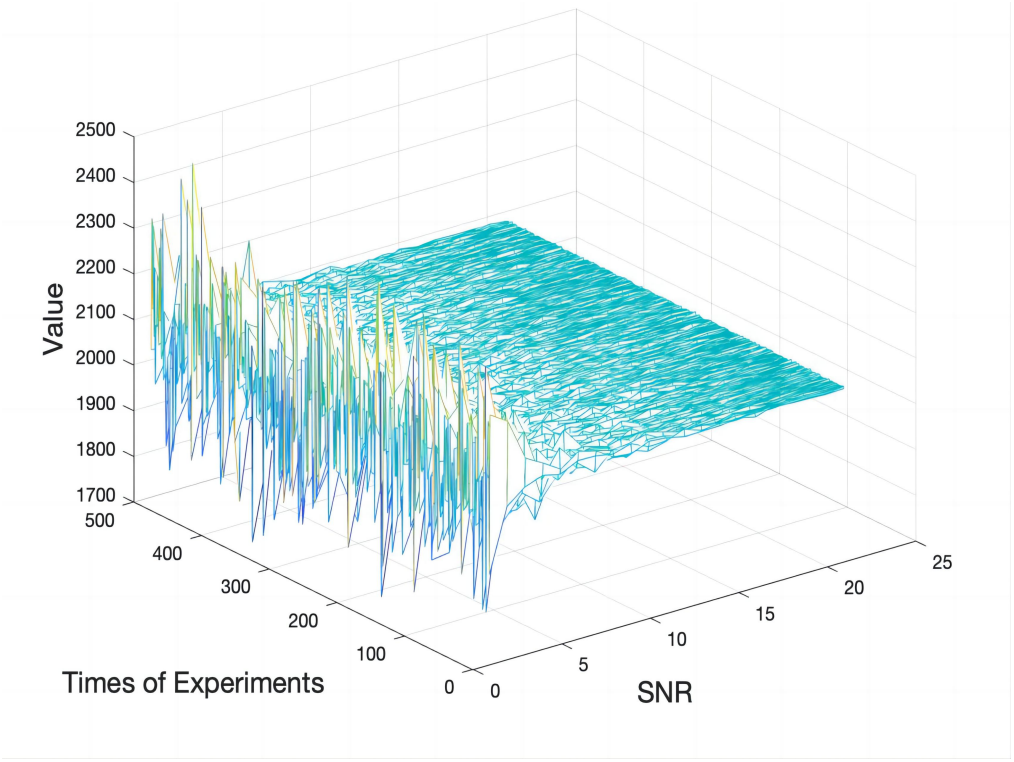

Figure 31 C_{63} of BPSK

Figure 28, Figure 29, Figure 30 and Figure 31 present the C_{63} of the four different modulation types over 500 experiments at various SNR levels. The values from different modulation types generally differ, making it easy to distinguish between the four modulation types. However, it is not convenient to analyse and observe all nineteen features simultaneously. Bar graphs have been introduced to facilitate the analysis of all the features at the same time during the comparison session. As the values shown in the Figure 32 are in a different magnitude, to sketch them into the same visualisable bar graph, some of the features need to be taken in logarithmic form.

After processing the data properly, the features mentioned before are all indicated in the bar graph for the next comparison session.

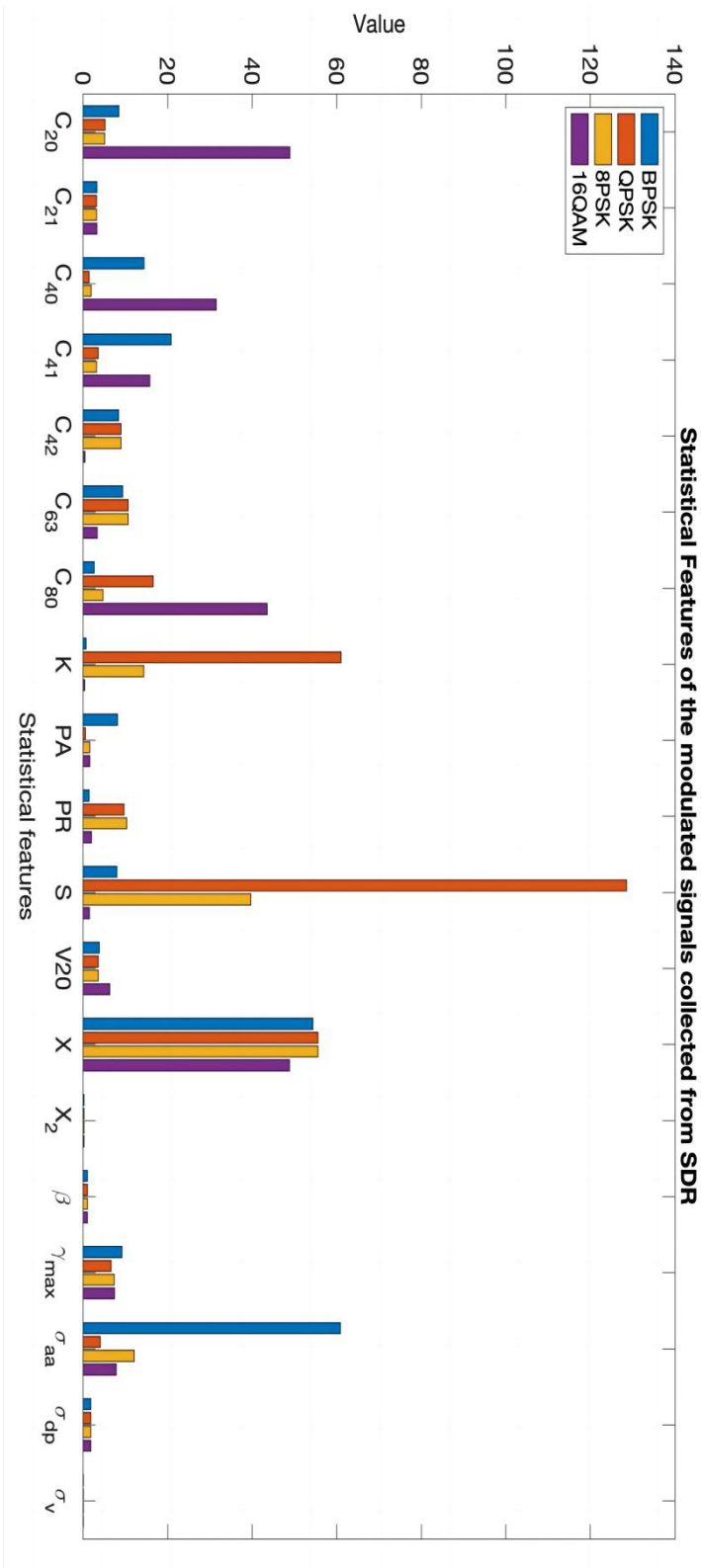

Figure 32 Features of the tested modulated signals at 10 dB SNR

Figure 32 shows the comparison of the statistical features between four kinds of modulated signals at 10 dB SNR. The values presented in Figure 32 are calculated by the formulas in section 4.2.1 and processed if required. All the features are calculated with the four kinds of modulated signals. The calculated values are gathered in Figure 32. Each feature shows four different values labelled by the different modulation types, which means that each modulation has specific value of the statistical feature. The values of some features are similar, whilst some are not. As shown in Figure 32, it is obvious that the values of β, σ_{dp}, σ_v, v_{20}, X, X_2 and C_{21} from the four modulation types are close. They cannot help to classify the four modulation types; these features remain constant around fixed values. The rest of the features are obvious enough to build up the GRF in the following sessions.

4.3 GRF

With the analysis of the features provided from previous section, the selected features are calculated and build up to the GRF technique. GRF is a method of representing the features into spider graphs and be utilised as the data for Deep Learning. The system structure of Deep Learning with GRF is shown in Figure 33.

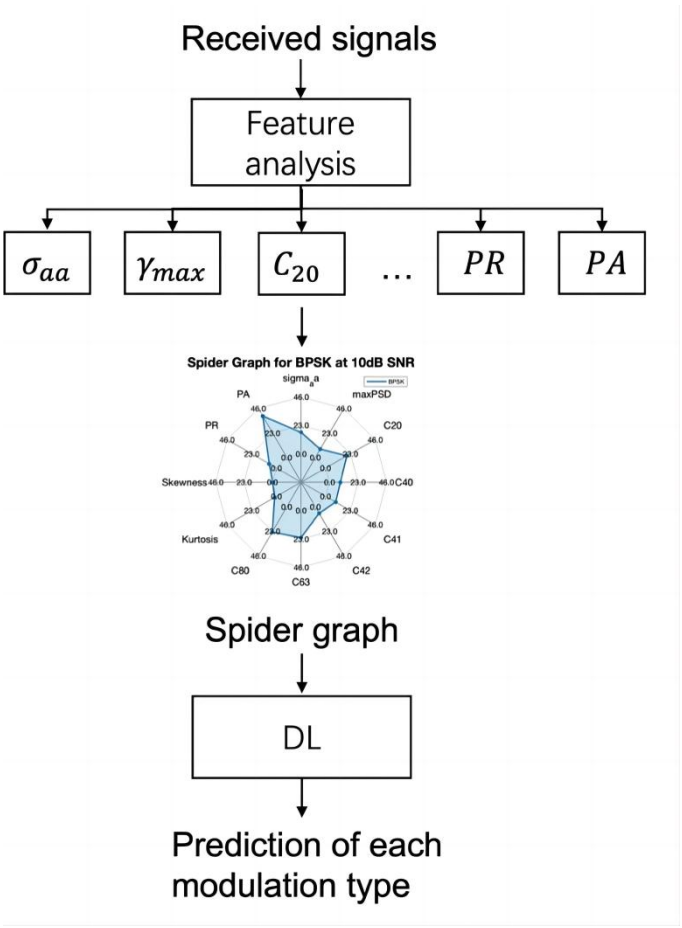

Figure 33 Structure of Deep Learning with GRF

GRF is a novel method for graphically representing statistical characteristics. In this method, data can be calculated from the dynamic receiving system without the need for phase and frequency locking, and characteristics are consistently displayed. By utilising image data with GRF, pretrained Deep Learning networks, along with existing advanced image classifiers, can efficiently classify modulations. A crucial aspect of this AMC system is the extraction of features into spider graphs, which represent all the relevant graphical features simultaneously. There are four sets of spider graphs at -10 dB, 0 dB, 10 dB, and 20 dB SNR, which are shown as examples for four modulation types below.

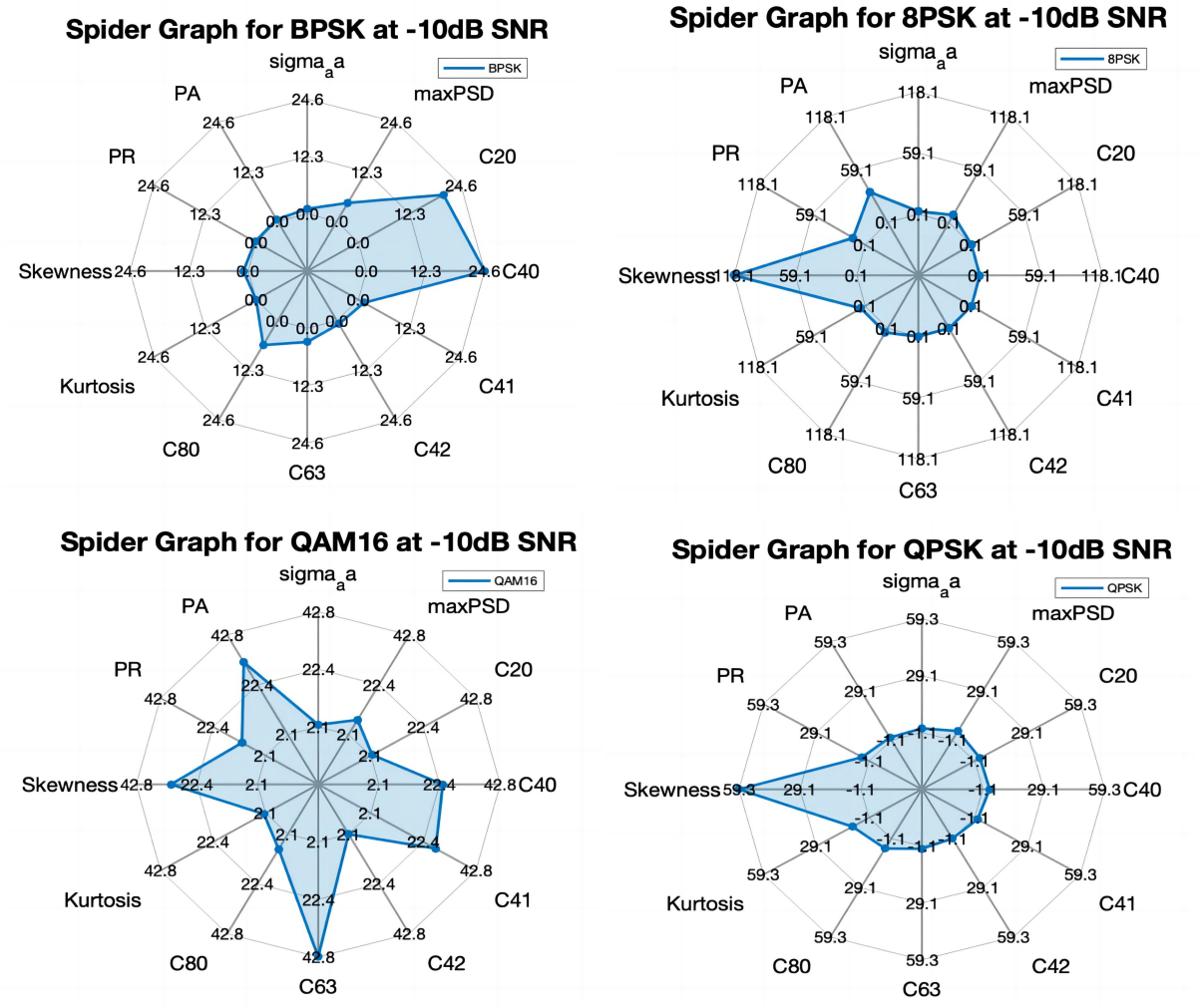

Figure 34 Spider Graphs of BPSK, QPSK, 8PSK and QAM16 at -10 dB SNR

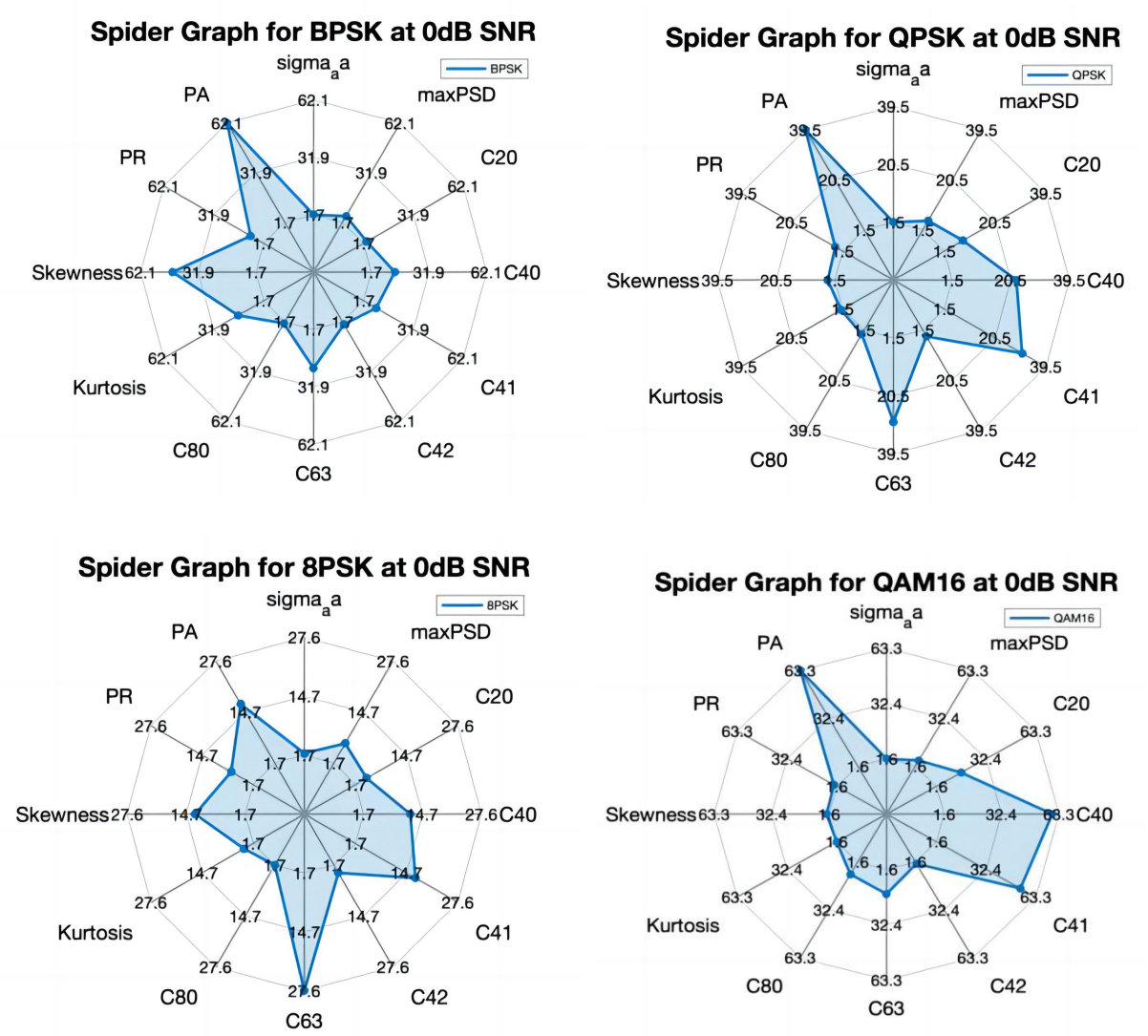

Figure 35 Spider Graphs of BPSK, QPSK, 8PSK and QAM16 at 0 dB SNR

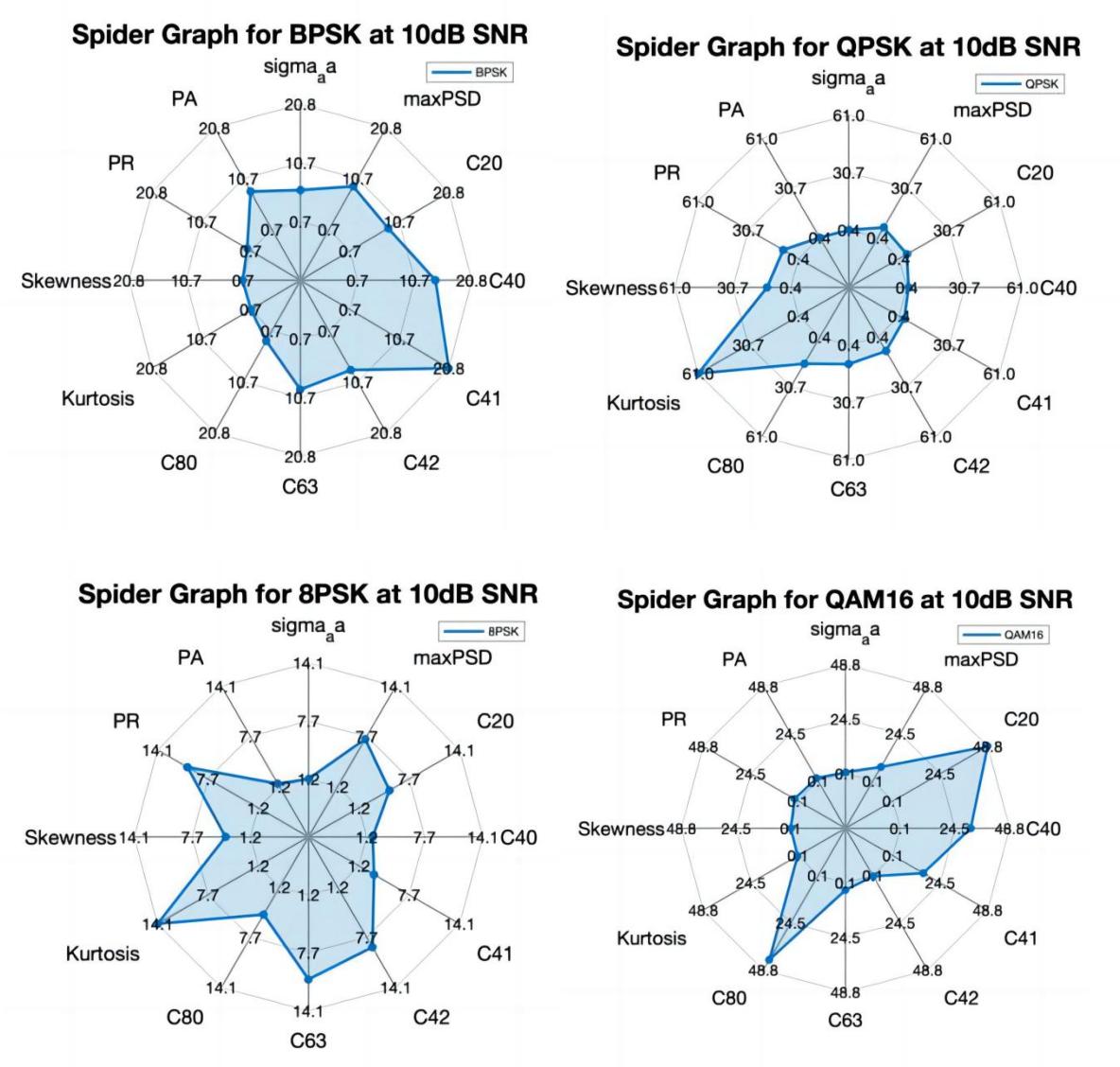

Figure 36 Spider Graphs of BPSK, QPSK, 8PSK and QAM16 at 10 dB SNR

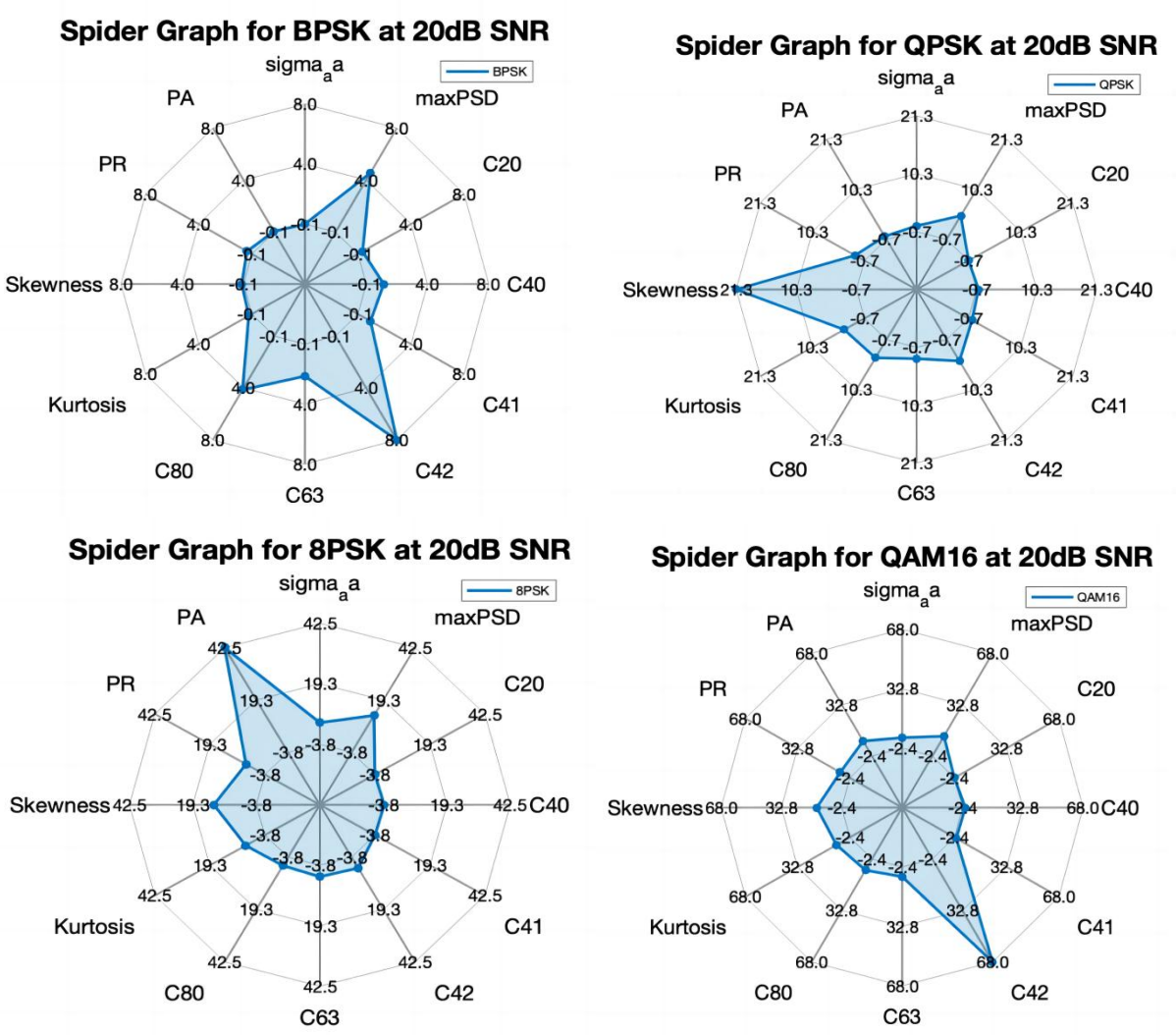

Figure 37 Spider Graphs of BPSK, QPSK, 8PSK and QAM16 at 20 dB SNR

Figure 34, Figure 35, Figure 36 and Figure 37 explain the application of statistical features in the spider graphs. Building on the previous sections, twelve statistical features of the modulated signals have been chosen as the components of the spider graphs. These selected features serve as the axes of the graph, allowing each modulation type to display its specific values on the graphs. In cases where the values vary significantly in magnitude, an appropriate logarithmic function is applied. The spider graphs consolidate the statistical features into a unified visual representation. Consequently, different data groups generate distinct spider graphs at varying SNR levels. As seen in Figure 34, Figure 35, Figure 36 and Figure 37, at different SNR levels, each modulated signal shows the different form of

representation. These graphs can be utilised as the data for the GRF systems. After collecting the graphs, all the image forms are used for Neural Network based on image classification.

4.4 Results

In this section, the results of AMC with GRF are proposed from -10 dB to 20 dB SNR. The data simulated by MATLAB and the data collected from Ettus are both tested by the four CNN models.

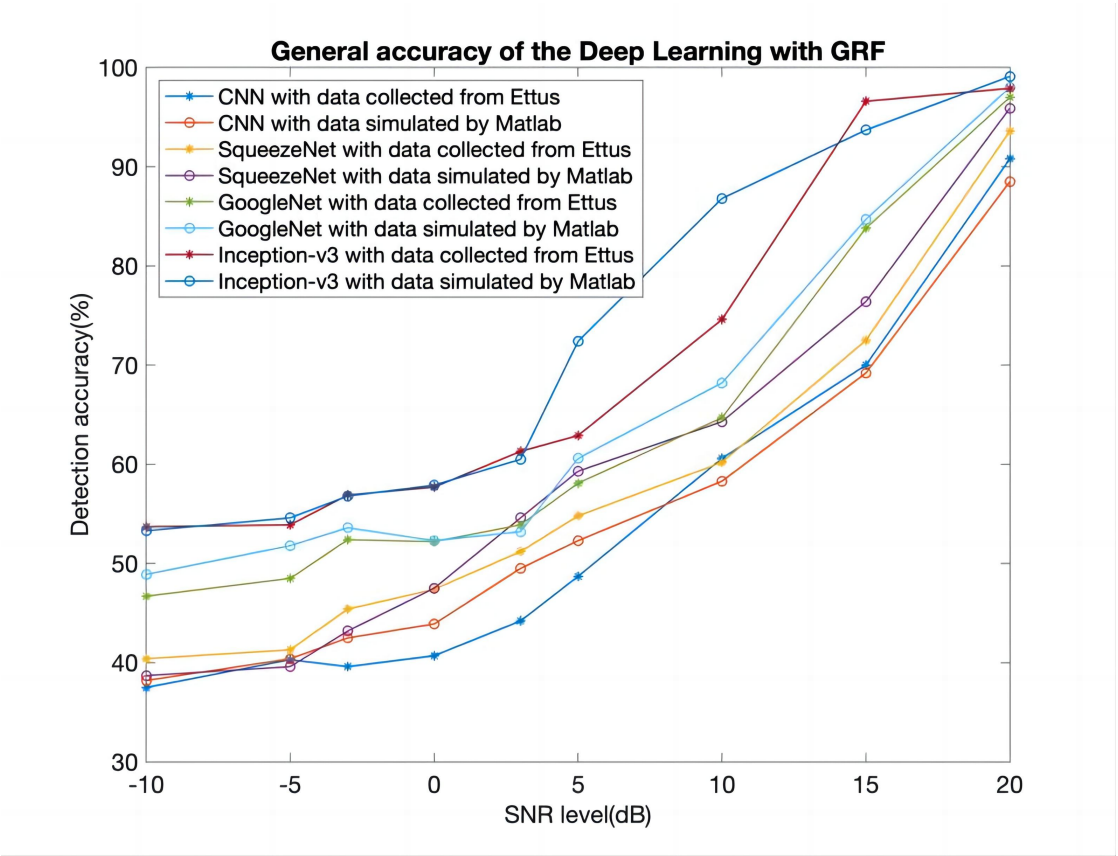

Figure 38 General accuracy of AMC with GRF over different SNR levels (all modulation types)

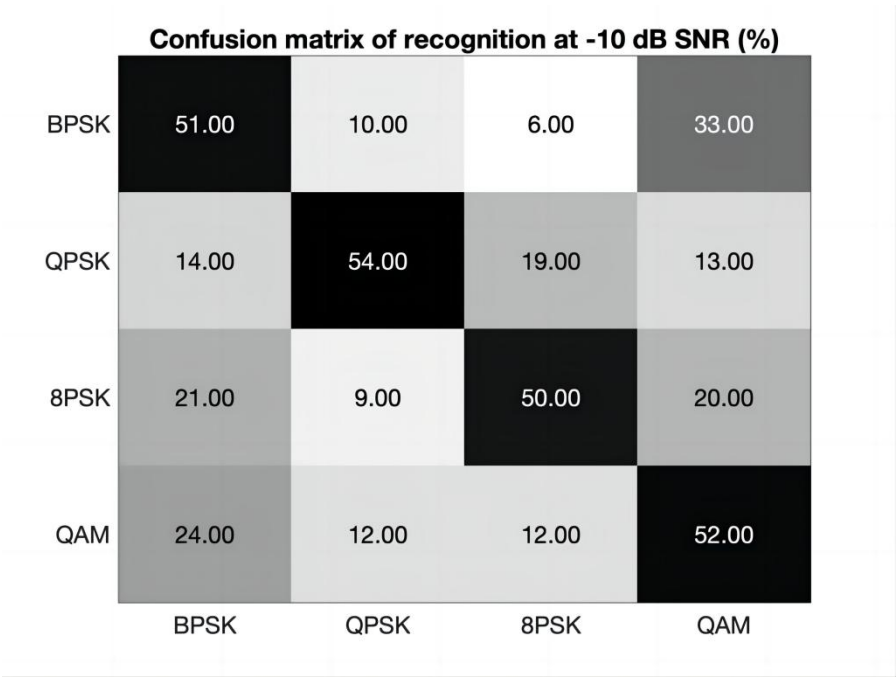

Figure 39 Detection of AMC with GRF (Lab data) at -10 dB SNR

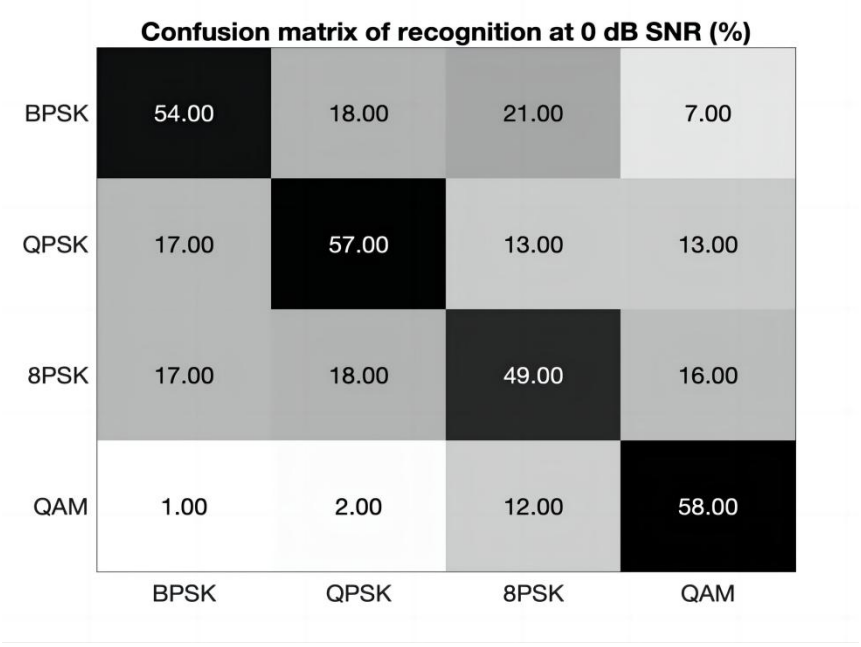

Figure 40 Detection of AMC with GRF (Lab data) at 0 dB SNR

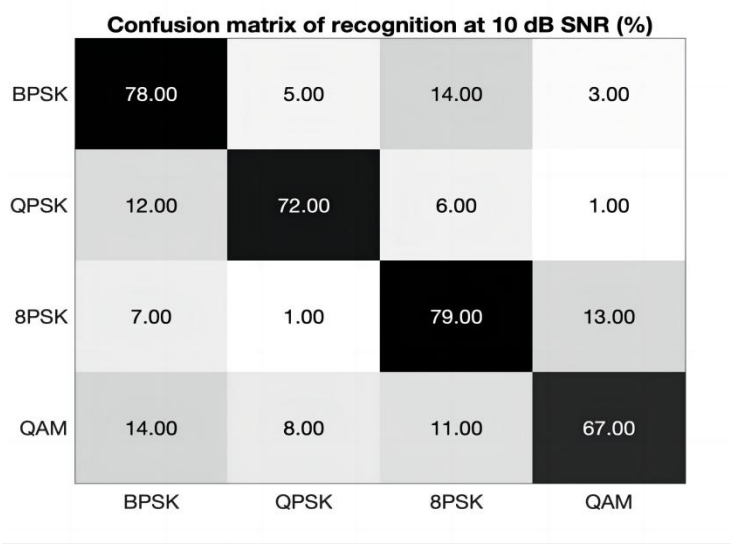

Figure 41 Detection of AMC with GRF (Lab data) at 10 dB SNR

Figure 38 shows the general results of GRF with different Neural Network structures. Two kinds of training data are collected and employed in the same network and the results are compared: 1) from MATLAB simulation; and 2) the SDR platform in the lab. At low SNR levels, both measurement and simulation produce similar accuracy. Compared to the probability of random guess (25 %), the detection accuracy is significantly better for the AMC with GRF approach. The Inception-v3 model also shows the best ability of classification.

The accuracy was improved (especially at low SNR which reaches over 50 % with Inception-v3 model) by training with the whole SNR range of data. The Detection results of the four kinds of modulation types at -10 dB, 0 dB and 10 dB SNR are shown in Figure 39, Figure 40 and Figure 41. The data to be utilised is collected from Ettus SDR, representing real-world signals in Figure 39, Figure 40 and Figure 41. The model of AMC with GRF is based on the inception-v3.

Compared to the results in Chapter 3, when the SNR is more than 10 dB, the detection accuracy of constellation-based classification achieves close to 100 %. However, from Figure 38, the detection accuracy of DL with GRF is not as good as the CI model at high SNR level. After comparison, the detection accuracy of CI classification increases from around 35 % at -10 dB SNR to 50 % at 0 dB SNR. However, the detection of accuracy of DL with GRF

increases with 52 % at -10 dB SNR to 58 % at 0 dB SNR. DL with GRF has shown its advantages for low SNR usage cases. Hence, to improve the classification accuracy in low SNR, the GRF classification can work as a supplement to CI recognition.

Table 4 Detection accuracy of DL with GRF

Model name	Detection accuracy
DL with CI	65.1 %
DL with GRF	69.3 %

Table 5 Comparison of detection accuracy at 0 dB SNR

Model name	Detection accuracy
SVM [33]	50%
Binary Hierarchical polynomial classifier [37]	56 %
DL with GRF	58.6 %

Table 6 Comparison of AMC Techniques

Model name	Detection accuracy
Maximum likelihood [28]	Less than 80% at 10 dB
Log-likelihood functional [29]	Less than 55% at -10 dB
Ph&D-GLRT and ADMP [31]	Near 90% at 6 dB
High order cumulants and SVM [33]	50 % at 0 dB
CNN [39]	20% at -10 dB
AMC with CI	34.7% at -10 dB
AMC with GRF	53.7% at -10 dB

Table 4 shows the detection accuracy of different systems over the whole tested SNR range. From this, it can be found that the DL system with GRF has the highest accuracy at 69.3 %. From Figure 38, the Inception-v3 model with constellations can achieve near 100 % for more than 10 dB SNR and this model provides the best results in the high SNR area. The DL method with the GRF performs well in general results, especially for the low SNR.

Table 6 compares the defects in the results between different AMC techniques. AMC with GRF shows the advancement compared to the other models. In comparison with the traditional AMC techniques, AMC with GRF takes the advantage of statistical features like these and provides a better accuracy. Compared to the normal CNN models, this model has the advantage of the intelligence and image classification. The application of transfer learning eliminates the steps of adjusting parameters and structures of AI models. Compared to the AMC with CI in Chapter 3, it improves the accuracy in a similar running time.

4.5 Summary

In this chapter, different classification models based on DL are applied to modulation recognition in the dynamic receiving system without phase and frequency lock. With the inspiration of the Hybrid model, the AMC with GRF has a better performance at the low SNR area compared to AMC with CI especially without frequency and phase lock. At -10 dB SNR, the AMC with GRF improves the accuracy of 19 % to the AMC with CI. At 0 dB SNR, the AMC with GRF improves the accuracy of 8 % to the AMC with CI. The models of AMC with GRF use the same Neural Network as Chapter 3.

These methods are all based on image classification, but with different datasets: CI from Chapter 3 and GRF in this chapter. The AMC with GRF system has an efficient use of statistical features, requiring only twelve features yet to achieve 69.3 % detection accuracy overall (and significantly better at lower SNR, as discussed above) with the random guess accuracy of the system being 25 %. The AMC systems employed transfer learning networks to detect the constellation dataset directly which reduces the mathematical complexity. For low SNR levels, the GRF provides the superior accuracy.

Chapter 5 AMC in mmW

As a rapidly evolving technology, automatic Modulation Classification (AMC) is employed in SDR structures, especially in 5G and 6G technology. Deep Learning (DL) can provide innovative and efficient technology for modulation classification, especially for systems working at low SNR levels. According to the outstanding results from Chapter 4, a dynamic AMC system for the Millimetre wave (mmW) band is introduced and tested, which is not reliant on the received signal phase lock and frequency lock. AMC with GRF employs four CNNs to compare the results of modulation classification for different received SNR levels and different mmW bands. The RF modulation is generated by a lab signal generator, sent through antennas and then captured by an RF signal analyser. The results of the system at 28 GHz and 70 GHz are analysed.

5.1 Introduction

With the evolution of digital communication systems, improvements to radio spectrum usage efficiency are becoming increasingly important. In this scenario, the modulation classification performs a significant role and can be widely used in a range of applications, including a software defined radio system, and radar and military communications. There is a high demand for RF bands. In the crowded spectrum situation, the AMC technology can respond to the requirements, optimising signal detection and subsequent demodulation when multiple complex / unknown signals are to be handled, or for cognitive radio primary-user detection. Radio spectrum is a valuable resource, and AMC is method of identifying the users off the spectrum as well as the unused spectrum. This chapter works on the mmW band, which has shown a high demand in the current communication society.

The introduction of mmW in 5G is a revolution for wireless communication. The 5G New Radio standards have allocated large amounts of the spectrum in the mmW band, enabling

high data rate transmission and low latency communication. The mmW technology is identified as a key enabler for 5G networks, providing the high-speed and high-capacity connectivity to support a wide range of applications [61]. With the ongoing development of 6G technology, mmW is also expected to perform a critical role in the future of wireless communication. The requirements for 6G are expected to be even more demanding than 5G, with the need for even higher data rates, lower latency and improved network efficiency [62]. The vast bandwidth and high data rate potential are well-positioned to support the demanding requirements of 6G networks. In this way, exploring and evaluating the AMC in mmW is a demanding objective for 6G communications, which is rare in previous studies.

This chapter concentrates on AMC in mmW with the GRF algorithm. In scenarios with low SNR, the power of the desired signal is comparable to the power of the noise. In such conditions, the signal's characteristics become indistinct and can closely resemble noise. This makes it challenging to differentiate the actual signal from the noise, leading to potential ambiguities in signal analysis. The purpose of this chapter is to develop the accuracy of the classification in the low SNR in mmW band. With the improvement of AI technology, many areas have achieved new progress by this innovative area [5]. Classification of modulation types based on statistical properties of signals is common in classic statistical machine learning approaches [6]. From this, DL working as a subproject of machine learning has advanced to a new level by incorporating the essence of biological information processing systems [7]. In image classification, DL is employed as an efficient technique.

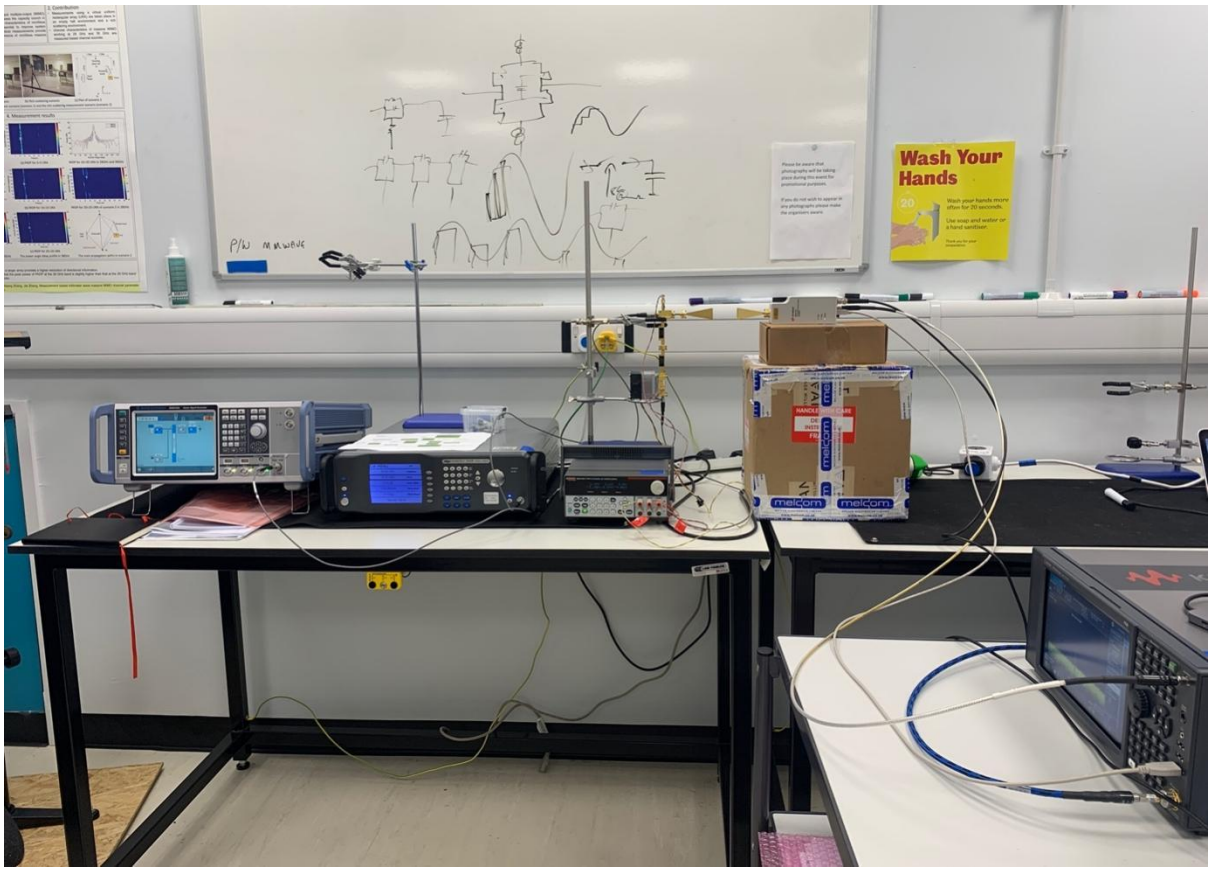

Figure 42 Hardware transmission system for mmW

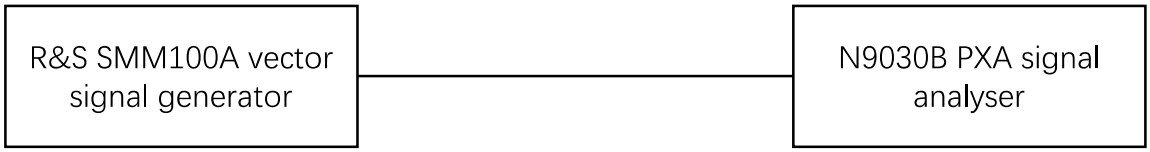

Figure 43 Hardware structure of conducted transmission system in 28 GHz

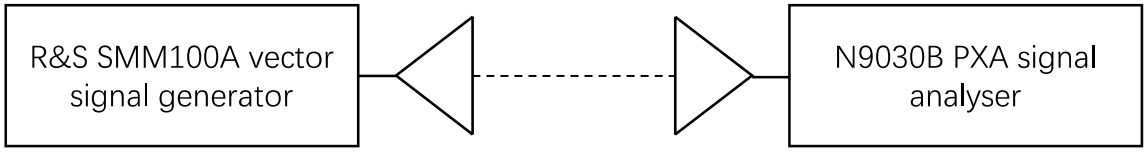

Figure 44 Hardware structure of radiated transmission system in 28 GHz (with 1 m distance)

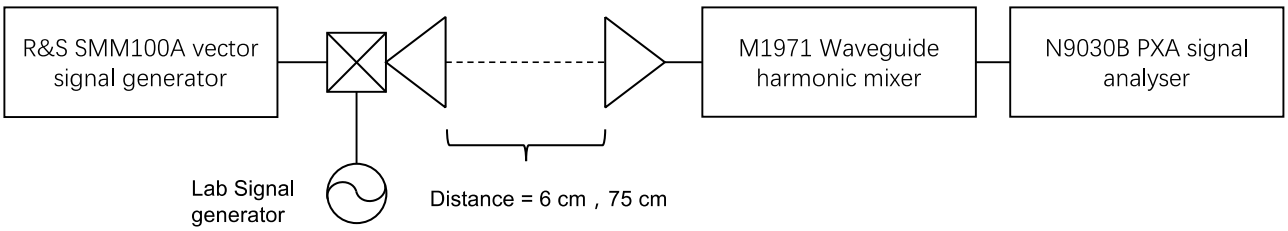

Figure 45 Hardware structure of transmission system in 70 GHz

Figure 42 provides the practical hardware transmission system in the lab. Figure 43 and Figure 44 provide the structures of a conducted system and a radiated system with 1 m distance between the horns in 28 GHz. Figure 45 shows the structures of the transmission system in 70 GHz. Due to the limitation of the hardware, the conducted data cannot be tested in 70 GHz. In this work, the approximate conducted data will be collected when the distance between the horns is 6 cm. The radiated data is collected when the horn is 75 cm away from the other.

Due to the use of complex 70GHz upconverter hardware, the actual TX power of the signal generator used is not an indication of the absolute RX power received at the spectrum analyser, although it will vary directly as the sig gen power is varied. The noise and carrier with no modulation applied are tested as well checking the actual RX power and SNR levels at the receiver. In this case, artificial noise is added to simulate the practical situation and to explore the lower SNR areas.

The innovative contribution of this chapter is the work in mmW and the testing of the signals from the real world. Although the results are not as good as the model at 2 GHz, it still gives the insight for the future studies.

This chapter is organised as follows: in section 5.2, the data collected at 28 GHz is introduced and tested by AMC with GRF. Both conducted data and radiated data are applied to the AMC models. The data is tested from -10 dB to 20 dB SNR. After that, the data collected at 70 GHz is provided and analysed in section 5.3. The results are along the same lines as the results test in section 5.2. Different CNN models are compared within the experiments.

5.2 AMC in 28 GHz

Based on the results and analysis from Chapter 3 and Chapter 4, AMC with GRF is used in this chapter. To start with the analysis of the signals, the constellation images of the modulated signals are introduced to be observed. After that, the statistical features are calculated according to the formulas provided in Chapter 4. The statistical features are compared and chosen as evidence to generate the spider graphs for the GRF technique.

5.2.1 Data in 28 GHz

The constellation graphs in this section help to display the characteristics. However, in this work, only statistical features are used, some of the features also describe the characteristics of the shape of the modulated signals. Figure 46 shows the constellations of conducted data collected from the lab as examples of the four modulation types (BPSK, QPSK, 8PSK, QAM16) at 10 dB SNR at 28 GHz.

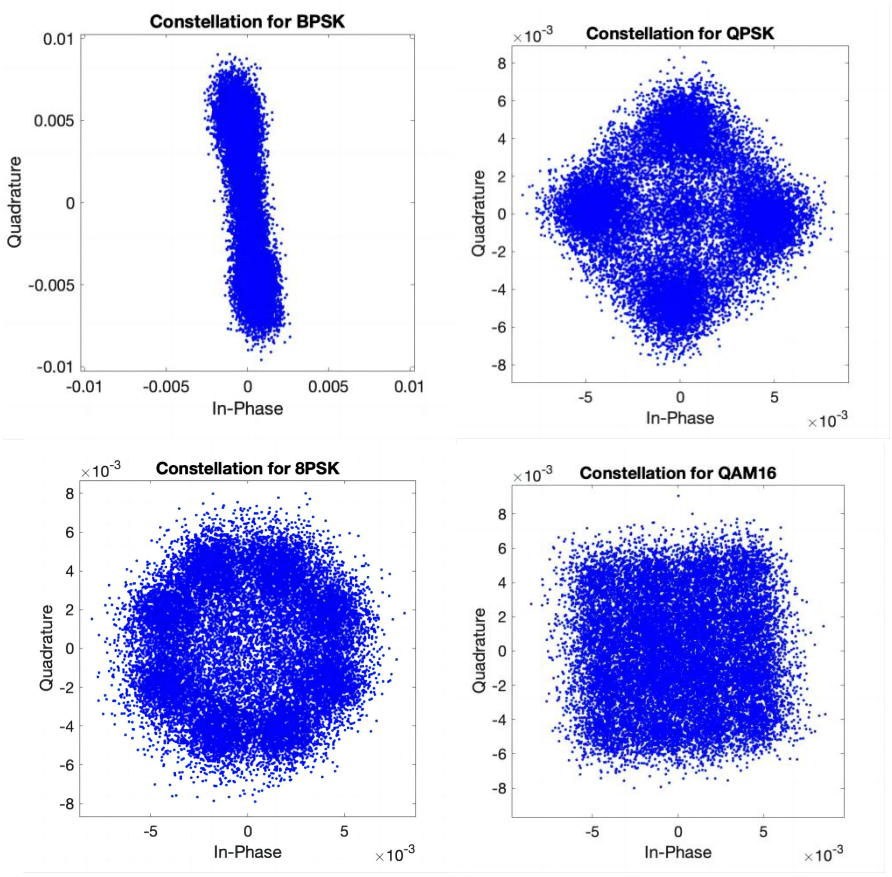

Figure 46 Captured conducted signals in at 10 dB SNR, 28GHz

Figure 46 shows the constellation diagrams of the conducted data. At 10 dB SNR, the underlying constellation types are still identifiable and clear. However, at low SNR levels, it becomes hard to distinguish between the characteristics. The statistical features are thus introduced to the AMC systems.

Based on the features from earlier work in Chapter 4, all the features are calculated for the four modulation types. Figure 47 shows all statistical features of the four modulated signals at the 10 dB SNR level at 28 GHz. The features are represented in one graph, where some of the features are displayed in logarithmic form, such as σ_{aa}, X_2, γ_{max}, which is a clear way to visualise the magnitude of the data differences. According to Figure 47, it is obvious that β, σ_{dp}, σ_v, v_{20}, X, X_2 and C_{21} cannot help to classify the modulations (BPSK, QPSK, 8PSK and QAM16); the difference of the values of these statistical features are insignificant.

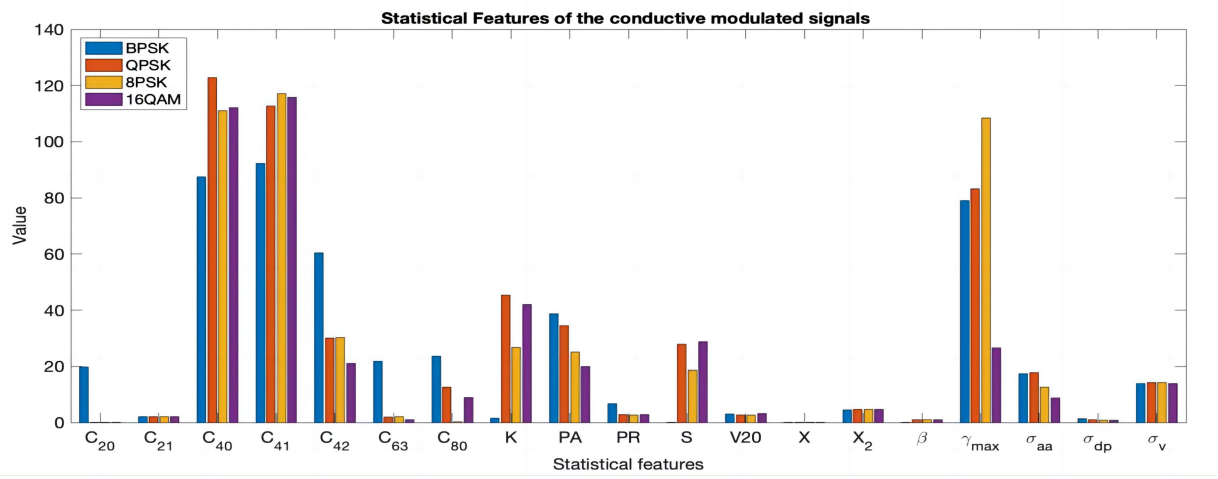

Figure 47 Features of conducted modulated signals at 10 dB SNR, 28 GHz

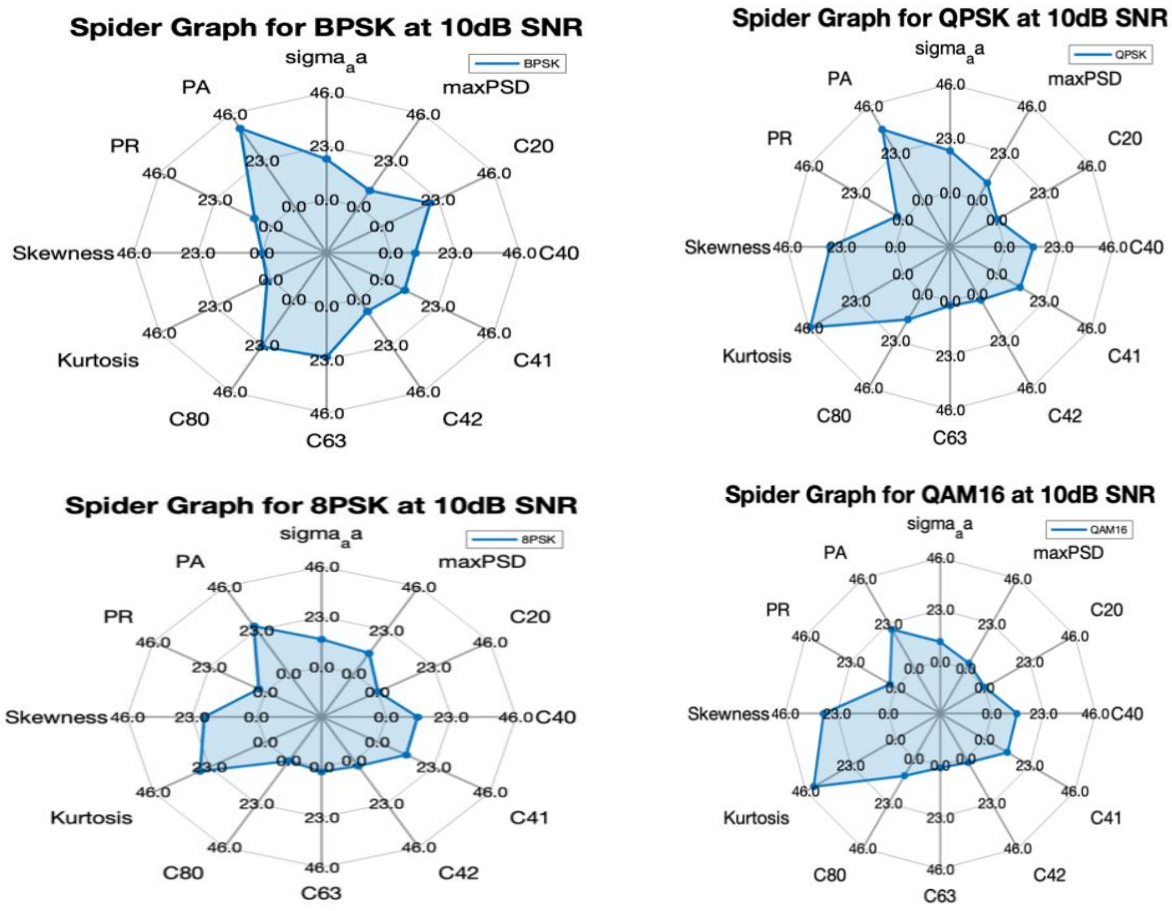

Figure 48 Spider Graphs of conducted modulated signals at 10 dB SNR, 28 GHz

Figure 48 shows the statistical features applied in the spider graph. Based on the previous analysis in Figure 47, the twelve features of the modulated signals are selected. The features are employed as the axes of the spider graph, where each modulation type can then display the values in the graph. The spider graphs turn the statistical features into one representation and represent the collected statistical features in a graphic way. Labelling the value of the features in the same common graph required the use of the log function for some of the features, where appropriate. As seen in Figure 48, each modulated signal shows a different shape of representation. After collecting the graphs, all the graphical representations are used for the Neural Network with image classification.

5.2.2 Results in 28 GHz

This section presents the results from the different classification networks. All the detecting systems are based on the DL technology. The high order cumulants are employed for this system as the second classification process to be trialled. The Kurtosis, Skewness, PR and PA can describe the shape of the signals. The system uses conducted data and radiated data collected by horn antenna. In this work, different DL structures are compared. The conductive data are only used as a training dataset, although both conducted data and radiated data are tested in classification.

In Figure 49, the results are shown from the four CNN models. The CNN developed using the Iris case performs worse than other traditional DL methods. This is likely due to the structures and coefficients of this CNN variant being potentially very sensitive, meaning that it will significantly influence the classification system.

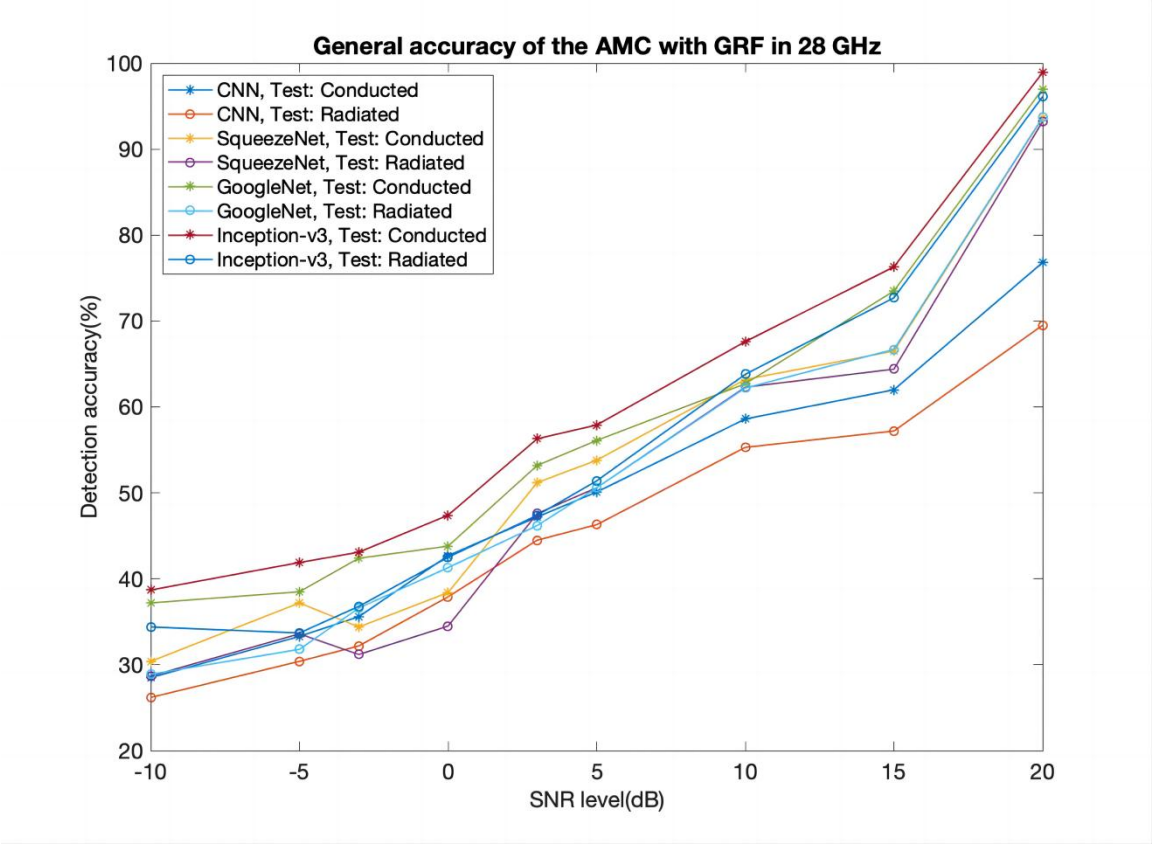

Figure 49 General accuracy of AMC with GRF over SNR levels in 28 GHz (radiated testing at 1m)

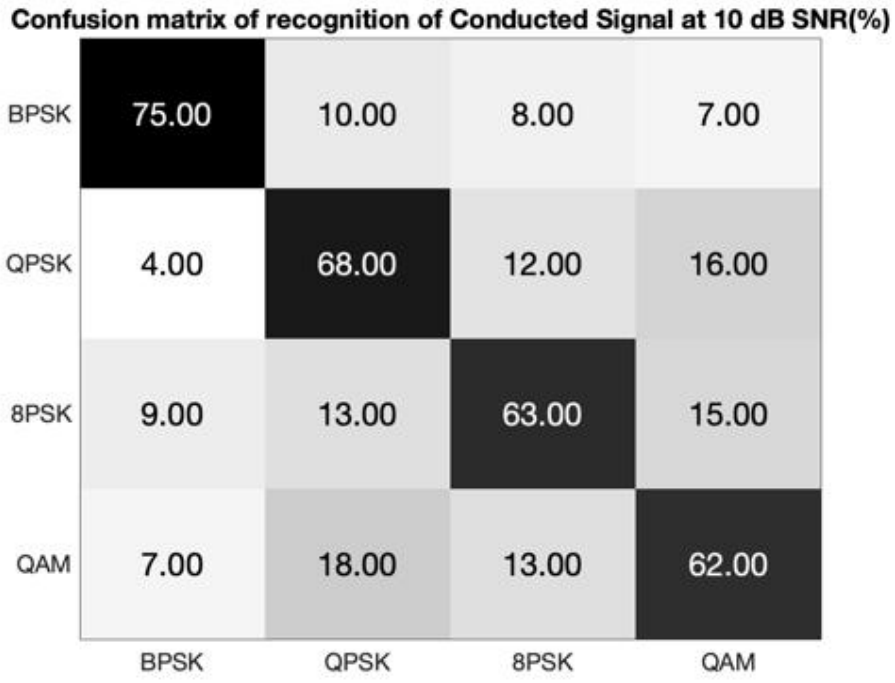

Figure 50 Detection of AMC with GRF at 10 dB SNR in 28 GHz (conducted signals)

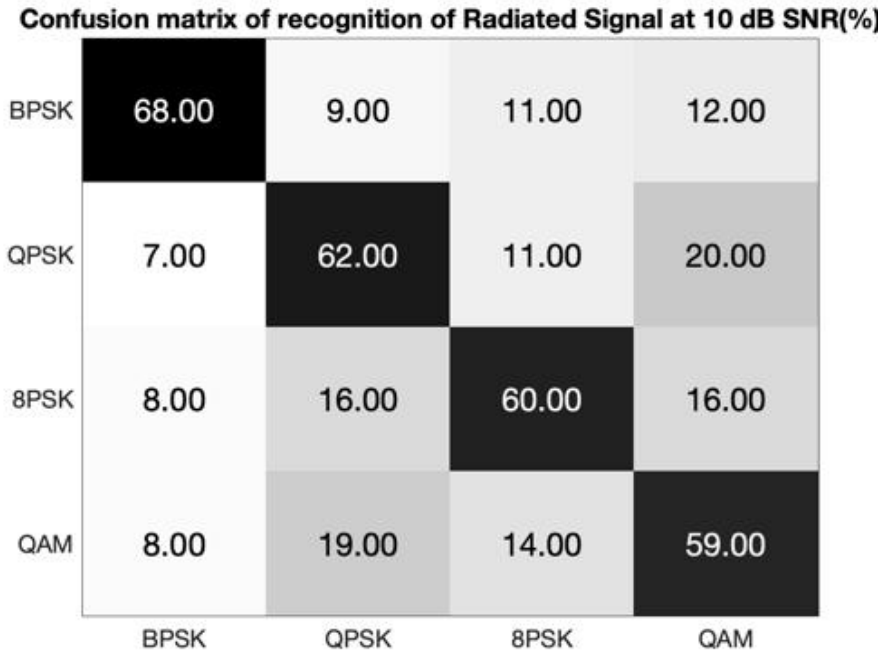

Figure 51 Detection of AMC with GRF at 10 dB SNR in 28 GHz (radiated signals)

Figure 50 and Figure 51 show two confusion matrices of the results at 10 dB SNR by using the Inception-v3 network. In general, the random guess detection rate would be 25 % (since there are four possible modulation types). This model also provides a slightly higher accuracy than the random guess at -10 dB SNR, an SNR level well below what most communication systems would use.

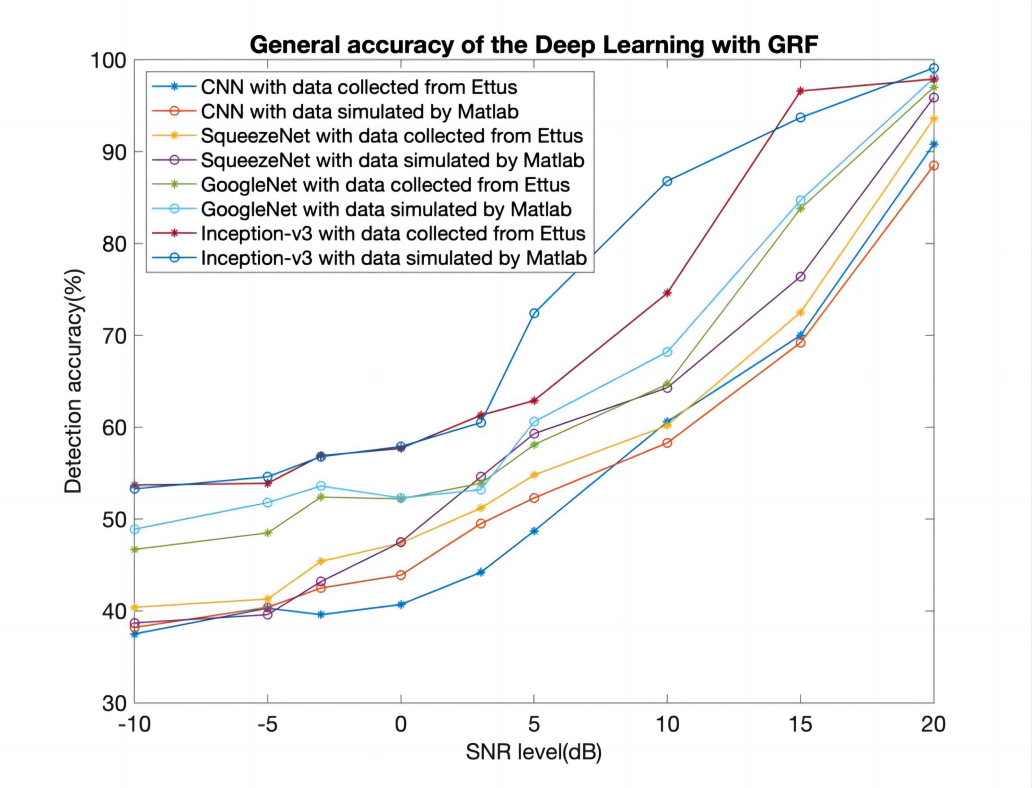

Figure 52 General accuracy of AMC with GRF over different SNR levels at 2 GHz

Figure 52 is provided to compare the detection accuracy for the technique as applied at 2 GHz. In that scenario, the detection accuracy is obtained as in Figure 52 for various SNR levels. From this, the detection accuracy using the system at 28 GHz is slightly worse (circa 10 % worse at -10 dB SNR, though this improves as SNR increases). The possible causes for this difference could be due to propagation effects in the lab and the different RF equipment used.

In this section, the AMC models based on DL, applied to modulation recognition in a dynamic receiving system without phase and frequency lock in mmW band at 28 GHz, are reported. Firstly, conducted and radiated data at 28 GHz is collected and the statistical

features are analysed. After that, an overview of the GRF method is provided for feature representation. The system utilises Inception-v3 to obtain the highest accuracy for the brief comparison between the results at 28 GHz and the previous results at a lower frequency of 2 GHz and discuss possible causes for differences in classification accuracy. Though the 28 GHz modulation classification performance is circa 10 % lower than with the 2 GHz system, it still is capable of a good classification and is significantly better than a random guess probability.

5.3 AMC in 70 GHz

After the experiments of AMC at 28 GHz, the higher frequency area also can be explored. Due to the limitation of the hardware equipment, the modulated signals are collected at fixed power levels with a distance of 6 cm between the horn antennas, which approximately represent the conducted situation. Another group of modulated data is collected at two fixed power levels with a distance of 75 cm between the transmitter and receiver for the radiated data. According to the SNR equation provided in Chapter 1, the signals are labelled and divided with SNR levels. Due to the situation of the lack of collected signals, artificial noise is added to the signal dataset to explore the lower SNR area. In this section, the data collected in 70 GHz are introduced and the results from the AMC with the GRF are proposed.

5.3.1 Data in 70 GHz

The constellation images collected from the lab are provided in this section, although AMC with CI is not used for this chapter, it is still worth observing the characteristics from the constellation graphs. Figure 53 shows the constellations of radiated data collected from the lab as examples of the four modulation types (BPSK, QPSK, 8PSK, QAM16) at 9 dB SNR at 70 GHz.

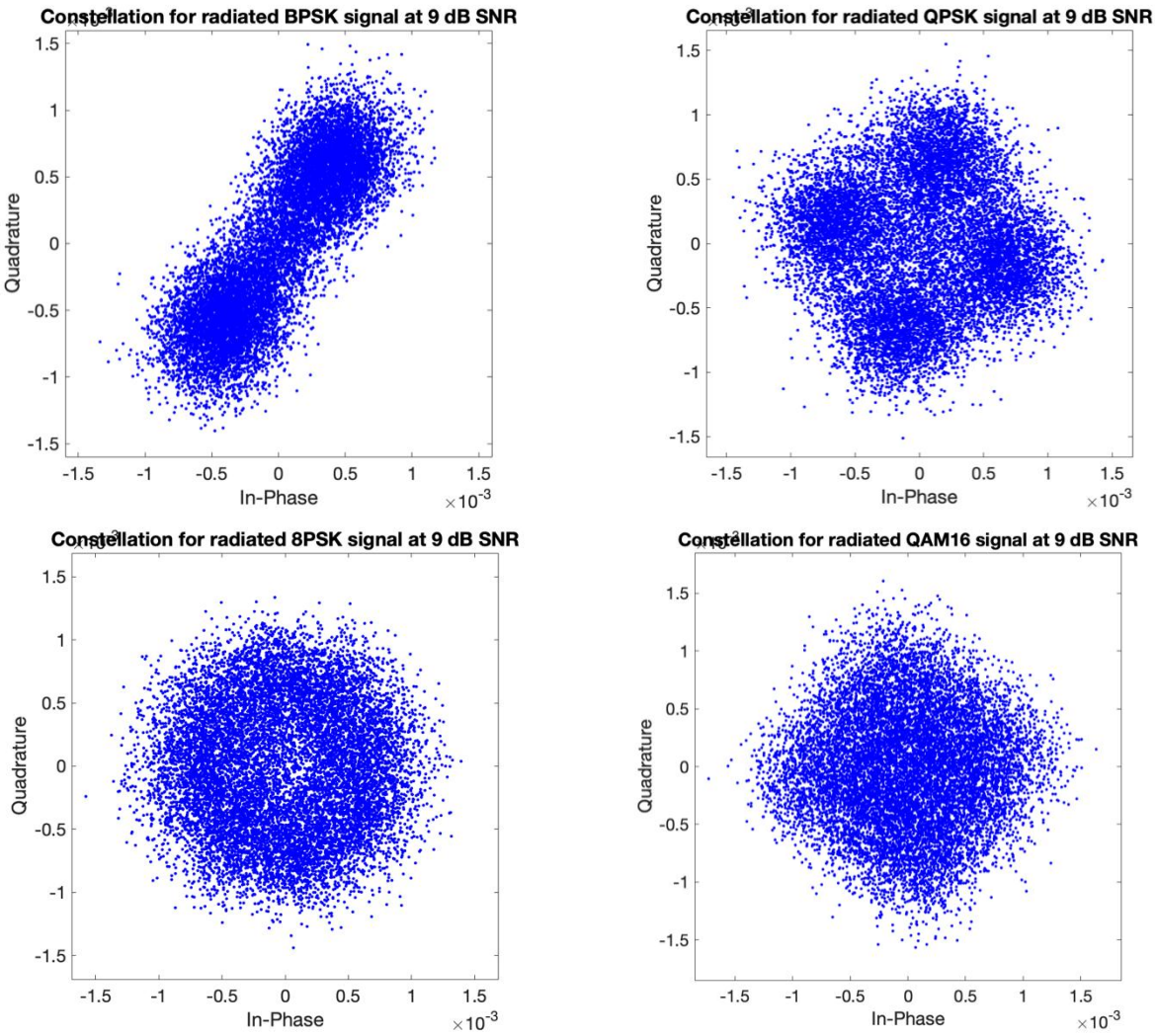

Figure 53 Radiated signals at 9 dB SNR in 70GHz (Radiated testing distance: 6 cm)

Figure 53 provides the constellation images of BPSK, QPSK, 8PSK and QAM16 in a radiated system in 70GHz. The distance between the horns is 6 cm, which is highly like the conducted system. They can still be distinguished from each other through their shape characteristics. After this, the radiated signals with longer radiated testing distance are provided in Figure 54.

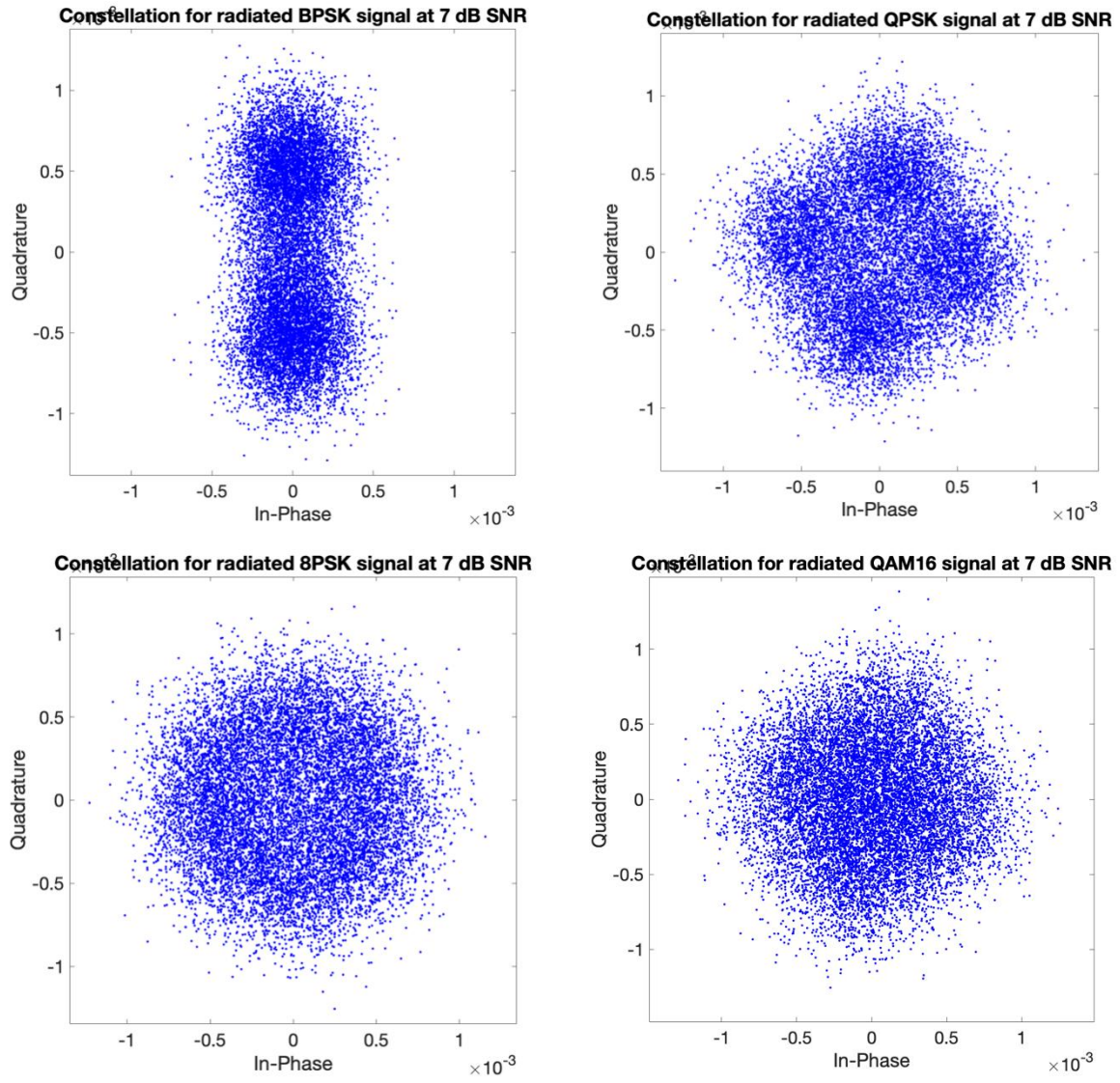

Figure 54 Radiated signals at 7 dB SNR in 70GHz (Radiated testing distance: 75 cm)

As shown in Figure 54, the constellation graphs are collected at 7 dB SNR. The signals are scattered and attenuated through the transmission by air. With the limitation of the equipment, artificial noise is added based on the received signals to explore the lower SNR levels.

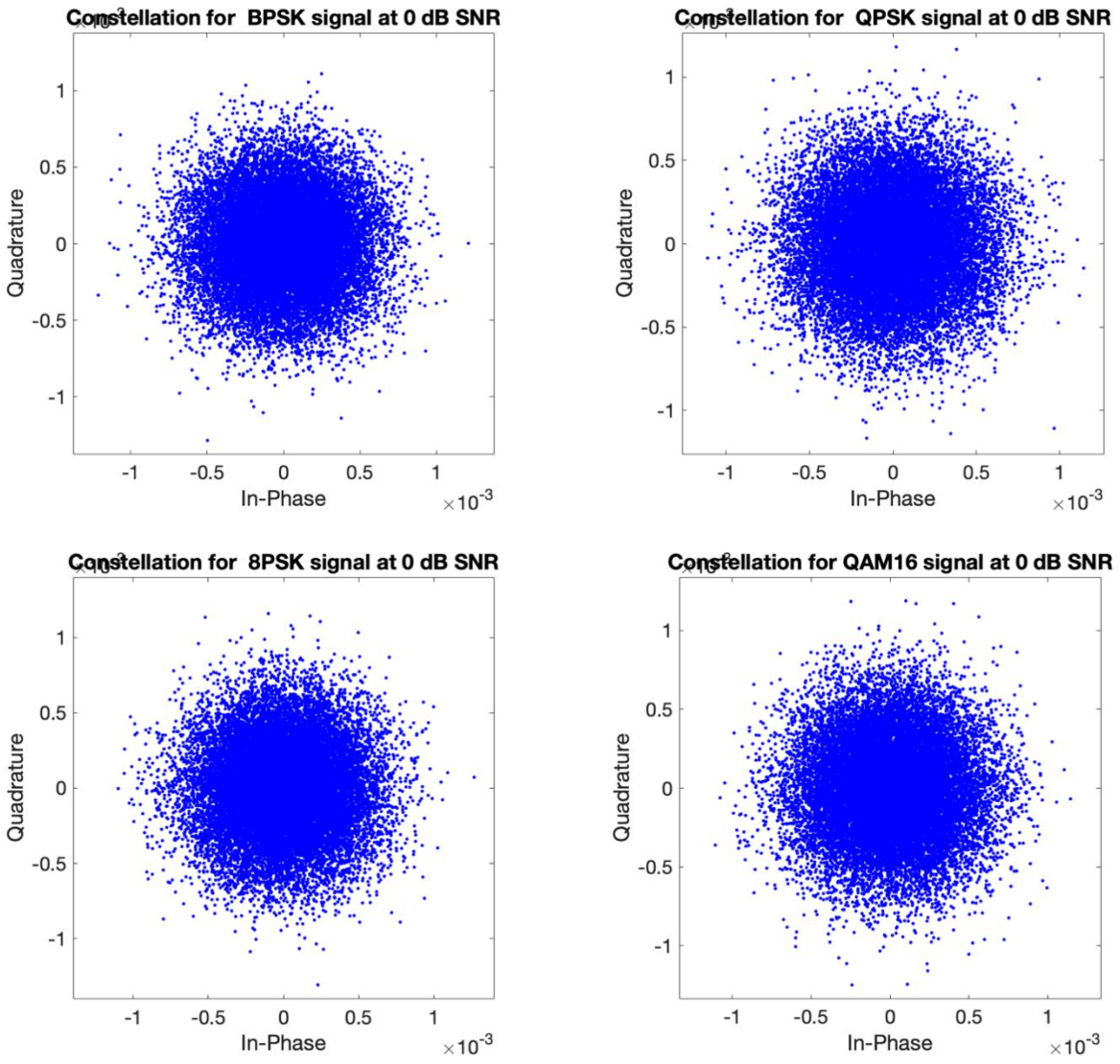

Figure 55 Radiated signals with simulated noise at 0 dB SNR in 70GHz (Radiated testing distance: 6 cm)

Figure 55 provides the examples of constellations with additional simulated noise based on the original received signals. With the simulated noise, the radiated signals with the distance of 6 cm are approximately like the conducted signals at 0 dB SNR, which is difficult to recognise the modulation types by eyes. This also makes it difficult to be classified with the AMC with CI.

After observing the constellation images, the statistical features are analysed for the following AMC with the GRF algorithm. According to the formulas proposed in Chapter 4, the features can be found in Figure 56.

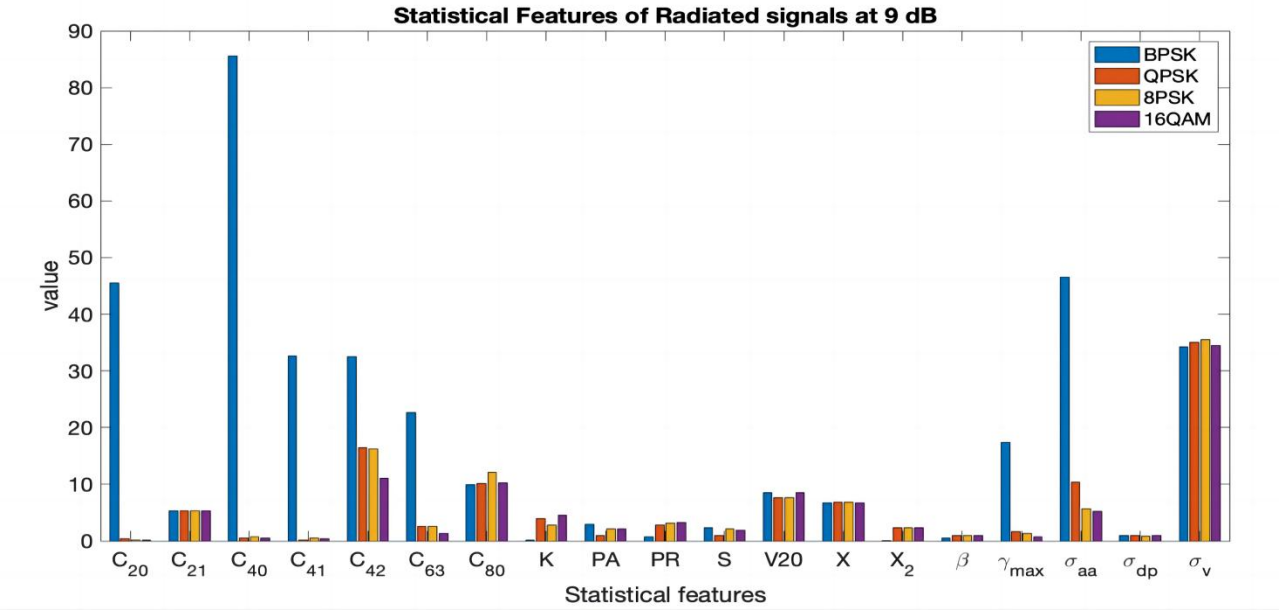

Figure 56 Features of the conducted signals at 9 dB SNR in 70 GHz (Radiated testing distance: 6 cm)

As shown in Figure 56, the statistical features of the aforementioned four modulation types are compared. Figure 56 shows all the statistical features at 9 dB SNR at 70 GHz. The features are represented in one graph to make the values comparison obvious, which are employed for the GRF.

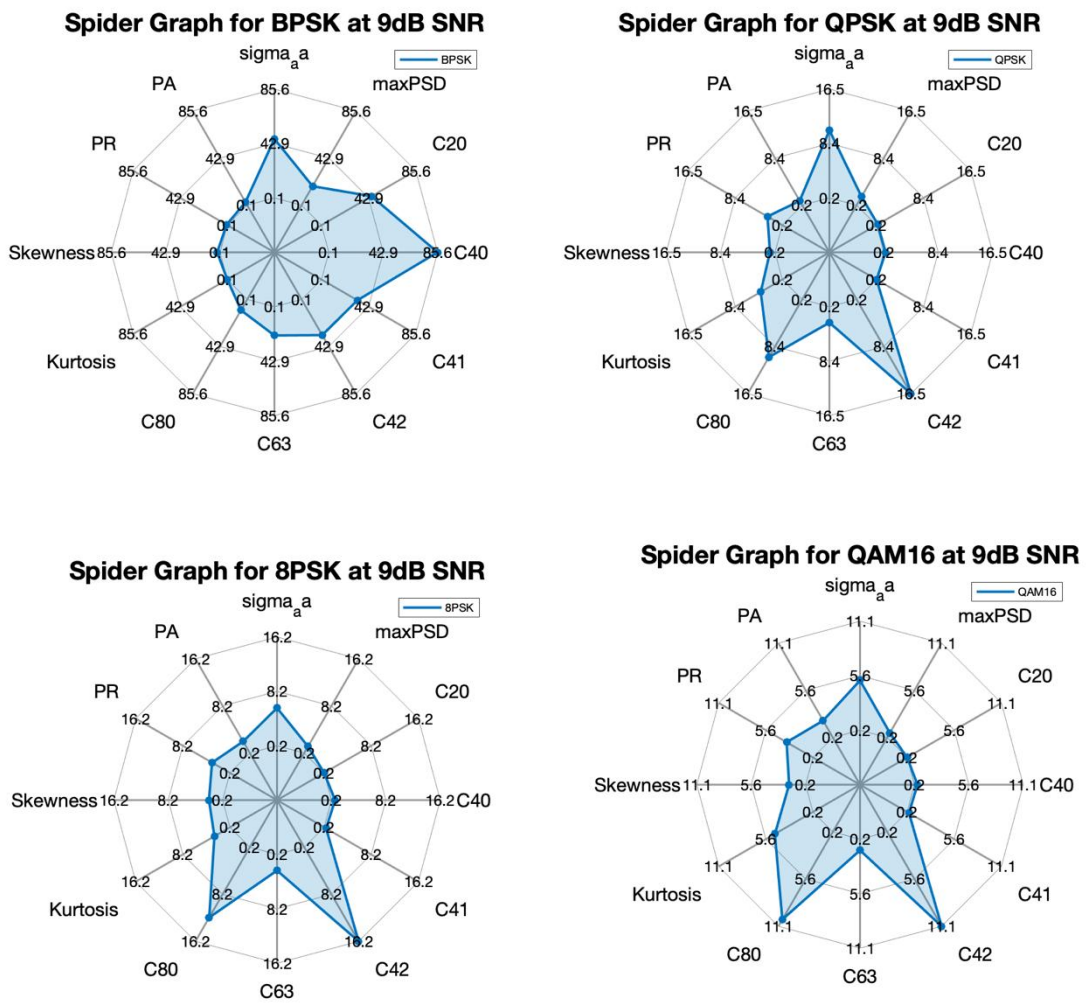

Figure 57 Spider Graphs of Radiated modulated signals at 9 dB SNR in 70 GHz (Radiated testing distance: 6 cm)

After the feature analyses, the spider graphs are built for the GRF algorithm. At the 9 dB SNR level, the BPSK can still be easily classified from the other three modulation types. Although the other three modulation types have similar shapes, their scales are still different. There is still a limitation for the proposed techniques here. The features need to use a log function, or other pre-processing, to make the value fit the graph for imaging, which will influence the classification. After this preprocessing, the distinguishable difference between the modulation types is no longer obvious, which leads to similar spider graphs. In this way, it will influence the classification. Plotting them into the same size graph here limited the shapes of the other three modulation types.

5.3.2 Results in 70 GHz

This section provides the results of the AMC with GRF at 70 GHz. The results from the radiated system (with a testing distance of 6 cm) where the SNR levels are under 9 dB and the results from the radiated system (with testing distance of 75 cm) where the SNR levels are under 7 dB are tested by the received signals with the additional simulated noise. The general classification results are applied below from -10 dB to 20 dB SNR.

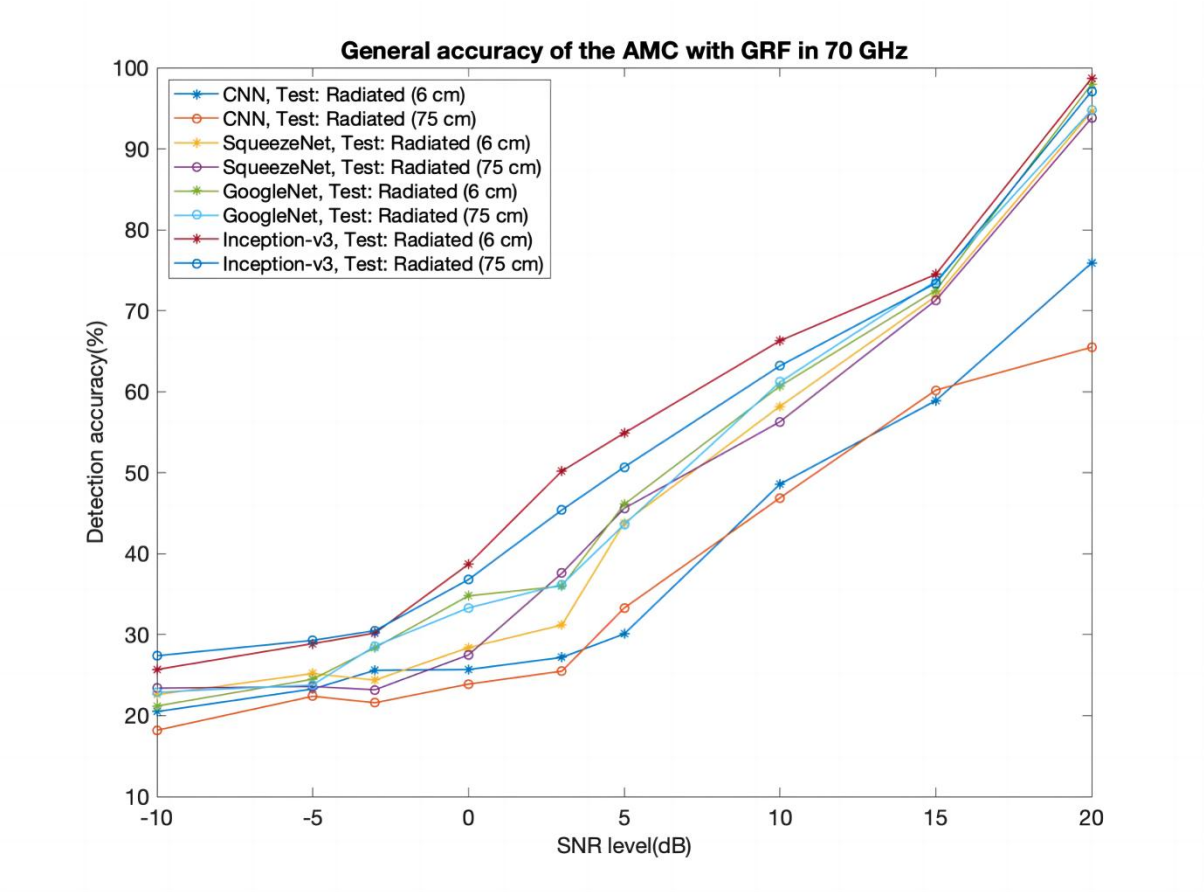

Figure 58 General accuracy of AMC with GRF over different SNR levels in 70 GHz

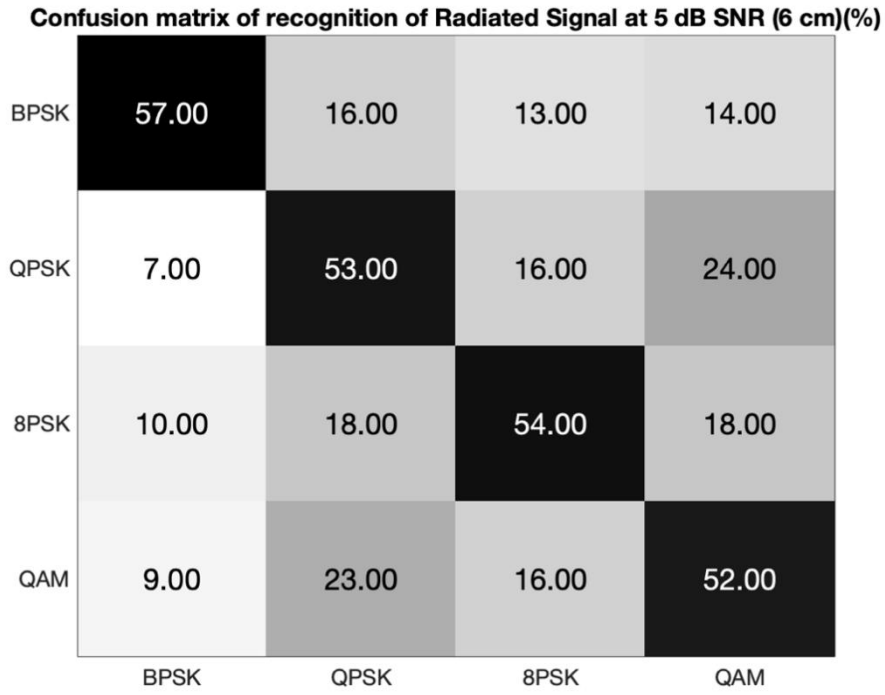

Figure 59 Detection of AMC with GRF at 5 dB SNR in 70 GHz (Radiated signals with 6 cm)

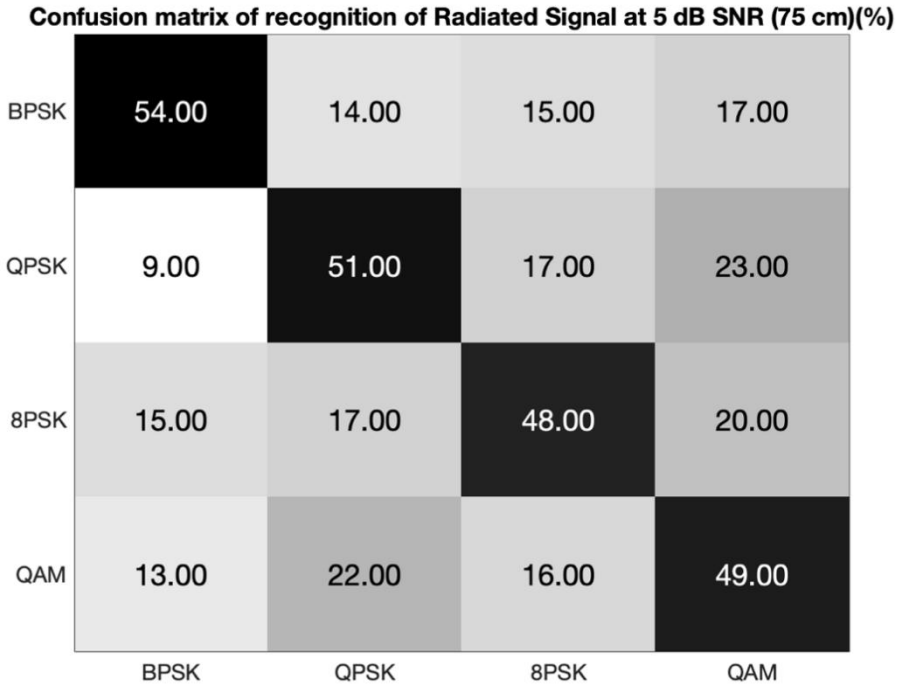

Figure 60 Detection of AMC with GRF at 5 dB SNR in 70 GHz (Radiated signals with 75 cm)

Figure 58 shows the general classification results with different CNN from -10 dB to 20 dB SNR. Figure 59 and Figure 60 provide examples of confusion matrix of the detection radiated signals with testing distances of 6 cm and 75 cm, respectively, at 5 dB SNR in 70 GHz. Each of the radiated data is tested and analysed, although all the CNN provides similar accuracy of classification at high SNR scenarios. The Inception-v3 proposes the best performance compared to the other three CNN models, with a significant accuracy of around 28 % at -10 dB SNR. Although he results are not as robust as in previous experiments, they are still higher than 25 %.

5.4 Summary

This chapter focuses on the AMC algorithm applied to the mmW band. For the higher frequency, the signals are neither clear nor distinguishable enough. For the 28 GHz, the best result of the accuracy performs well at a high SNR level. When the SNR level goes under 0dB SNR, the best accuracy is 38 % at -10 dB SNR which is still above the random guess of 25 %.

For the 70 GHz band, the signals are hard to capture the distinguishable features, the accuracy of detection is around 40 % at 0 dB SNR, which is only slightly less than the accuracy in 28 GHz. At the same time, the accuracy is 28 % at -10 dB, which is still slightly higher than the random guess. Overall, the results provide worthy evidence for the investigation of AMC with GRF in mmW.

The performance of the AMC with GRF from both mmW bands are significant as providing valuable results. The systems are useful for the further research and the future 6G development.

Chapter 6 Conclusion and Recommendation

6.1 Conclusion

This study focuses on developing AMC technology and starts with the observation of the characteristics of the digital modulation types. With the inspiration of the image classification by DL, the AMC with CI is proposed based on the constellation graphs of the signals. Different CNNs are introduced, tested and compared for this model. To develop the practical application, the datasets are simulated by MATLAB and the signals collected by the hardware in the lab also become involved in the AMC system. After developing the AMC with CI, according to the comparison of the constellation images, the signals at low SNR levels are blurred and hard to be classified by both eyes and DL. This model indicates that only the application of the constellation graphs is not robust for AMC.

After that, the Hybrid model is developed as a transition, which adds the process of statistical features judgement at the end. The statistical features are induced to the new model, which is AMC with GRF. To combine the intelligence of the image classification and the characteristics of the statistical features, the spider graphs are employed to represent the GRF algorithm and used for the DL. In the scenarios with high SNR, AMC with CI has better results after running the experiments several times, and the AMC with GRF provides a new efficient way for the classification at lower SNR levels. Overall, the AMC with GRF shows better performance.

Table 7 Comparison of AMC models (Accuracy-Acc)

SNR Levels	Acc of AMC with CI	Acc of Hybrid Model	Acc of AMC with GRF
-10	34.7 %	57.3 %	53.7 %
-5	44.3 %	62.1 %	55.2 %
0	51.4 %	67.7 %	60.2 %
5	85.6 %	88.3 %	74.6 %
10	89.0 %	95.1 %	82.4 %
20	98.2 %	98.7 %	97.6 %

The best results based on Inception-v3 networks in the 2 GHz spectrum are shown in Table 7, where the accuracy of AMC with CI, Hybrid model and AMC with GRF are compared. At 20 dB SNR, the three models all achieve the highest accuracy at near 100 %. At 10 dB SNR, the AMC with CI (89.0 %) and Hybrid model (95.1%) perform better than the AMC with GRF (82.4%). At the low SNR area, the accuracies of AMC with GRF and Hybrid models are outstanding.

With the SNR level decreasing, the accuracies decrease gradually. The accuracy of AMC with CI decreases by 63.5 % and the accuracy of AMC with GRF decreases by 43.9 %. The accuracy of Hybrid model decreases by 41.4 %, which is close to the results of AMC with GRF. The Hybrid model has the highest accuracy, but it is much more complex than the AMC with CI and AMC with GRF. With the system structure proposed in Chapter 3, the Hybrid model has two parts. The first part is AMC with CI; the second part is the analysis of the statistical features , which relies on the previous results from AMC with CI. The AMC with GRF is more efficient and has a similar accuracy, whilst also taking advantage of statistical features and graphic features from the modulated signals.

Table 8 Comparison of the AMC Techniques

Model name	Detection accuracy
Maximum likelihood [28]	Less than 80% at 10 dB
Log-likelihood functional [29]	Less than 55% at -10 dB
Ph&D-GLRT and ADMP [31]	Near 90% at 6 dB
High order cumulants and SVM [33]	50 % at 0 dB
CNN [39]	20% at -10 dB
AMC with CI	34.7% at -10 dB
Hybrid model	57.3% at -10 dB
AMC with GRF	53.7% at -10 dB

The models indicated in this study are compared to the existing work in Table 8. The existing studies have the limitation on the detection accuracy, which is required to be improved in academic research and 6G communications to provide a robust communication system. The normal CNN provides a novel solution in AMC with less running time, but the detection results can be improved. In this work, AMC with CI is indicated acquiring the use of transfer learning, which can provide less running time like CNN and also eliminate the complex progress of building neural networks. Based on the AMC with CI, the hybrid model is provided with adding the decision tress algorithm after the AMC with CI to improve the detection. But the two stage of the model takes a much longer time with different features choosing process. The hybrid model works as an intermediate model from AMC with CI to AMC with GRF, which provides the idea of image classification and the use of statistical features. However, the results of AMC with GRF shown in Table 8 are not better than the hybrid model, yet the running time is less than the hybrid model and similar to the AMC with CI. In this way, AMC with GRF gives the insight for the future studies.

Table 9 Comparison of AMC with GRF in different bands

SNR Levels	Acc of AMC with GRF in 2 GHz	Acc of AMC with GRF in 28 GHz	Acc of AMC with GRF in 70 GHz
-10	53.7 %	37.8 %	28.3 %
-5	55.2 %	42.2 %	30.1 %
0	60.2 %	47.6 %	38.5 %
5	74.6 %	57.3 %	53.6 %
10	82.4 %	66.7 %	63.4 %
20	97.6 %	97.8 %	97.5%

In this work, the three AMC algorithms are developed and compared in 2 GHz. With the superb results of AMC with GRF, signals at the mmW area are considered. Table 9 provides AMC with GRF model working in different bands. Whilst the classification results in 28 GHz are not as good as the signals in 2 GHz, the accuracies of classification at -10 dB, -5 dB, 0 dB and 5 dB SNR are still over 25 %, which are higher than a random guess. The signals at 70 GHz are more challenging, the accuracy at -5 dB and 0 dB SNR is still more than 25 %. The mmW system needs to be improved for the low SNR level to provide a better classification. In this way, more attention should also be paid to the signals in mmW. The factors which cause this difference of accuracy in different bands should also considered for further research.

Overall, this study makes good use of DL with AMC. There are four key contributions of this work. For the first contribution, the assessment of TL is made. The good usage of the TL reduces the complexity of calculation and improves the accuracy of modulation classification. Secondly, this study develops and assesses the innovative method named Graphic Representation of Features (GRF) to indicate the statistical features of modulation types, represented graphically and used as image classification data. This method takes the advantage of both statistical characterisation and image classification. For the third

contribution, the combination of the simulated data and the lab-collected data is compared in this work. Additionally, there is a simulated supplement for the hardware limited situation. The final contribution is the overall assessment of generic DL image classifiers as applied to communications AMC usage.

6.2 Recommendation for Future Studies

Based on the analysis and the conclusions in previous chapters, the recommendations for future studies are focused on the AMC in the practical model, which includes indoor propagation and the real channel. At the same time, different features of the modulation should be explored to help develop the AMC model.

6.2.1 Indoor Propagation Models

In indoor environments, the propagation of radio signals can be affected by several factors, such as walls, furniture and other obstructions [66]. These factors can cause fading, multipath and interference, making modulation classification more challenging. To address these challenges, the indoor propagation model should be considered when designing AMC algorithms. The propagation model can provide information about the expected behaviour of radio signals in the indoor environment and can be used to design AMC algorithms that are robust against the effects of indoor propagation [67].

Conducted signals and radiated signals are collected in Chapter 5, as the purpose of the application of the AMC model is involved in the real world. The indoor propagation model will be the next step for the research. The reflection will also be considered to help distinguish the modulation types, which employs the statistical features. The constellation images will be considered again based on previous chapters, and the received signals with overlapping and interference from other signals should also be analysed.

6.2.2 AMC within the Real Channel

To develop the practical applications of AMC, the signal model should also be established within the real channel which is more complicated than the simulation or the lab-built simple transmission system [68], [69]. With the addition of the artificial noise at 70 GHz in Chapter 5, detecting the legally acquired signals in the mmW band from the practical system will be the promising areas of future research.

At the same time, the AMC models based on DL should also be considered when implementing at the hardware level, which is a further step for the application of AMC based on DL in the future. It is important to conduct systematic experiments and simulations to validate the performance of the proposed AMC algorithms and techniques. The results of these studies can then be compared with the state-of-the-art AMC methods and used to guide the development of future AMC technologies.

The integration of AMC with other communication technologies in 6G, such as massive MIMO and mmW communication. This can help to improve the overall performance of these systems and enable new applications and services especially in the mobile phone industry.

6.2.3 Improvement in 70 GHz

According to the results in Chapter 5, the signals in 70 GHz band make it hard to capture the distinguishable features; BPSK is easier to be classified compared to the other three modulation types. There is still a potential area to develop the AMC technique and improve the detection performance. At the same time, the system should be small and efficient, which can be installed to the mobile equipment and benefit the next generation of wireless networks. For future research, the AMC system should be considered at a hardware level, and thus have practical application experiments.

References

[1] Z. Zhu and A. K. Nandi, *Automatic Modulation Classification : Principles, Algorithms and Applications*, 1st ed. John Wiley & Sons, 2015.

[2] D. H. Al-Nuaimi, I. A. Hashim, I. S. Z. Abidin, L. B. Salman, and N. A. M. Isa, "Performance of feature-based techniques for automatic digital modulation recognition and classification-a review," *Electron.*, vol. 8, no. 12, 2019, doi: 10.3390/electronics8121407.

[3] G. Manisha and M. Nikhil, "A Review on Automatic Signal Classification Techniques for Software Defined Radios," in *Proceedings of IEEE International Conference on Signal Processing, Computing and Control*, 2019, vol. 2019-Oct, pp. 281–286, doi: 10.1109/ISPCC48220.2019.8988509.

[4] Q. Zheng, P. Zhao, Y. Li, H. Wang, and Y. Yang, "Spectrum interference-based two-level data augmentation method in deep learning for automatic modulation classification," *Neural Comput. Appl.*, vol. 33, no. 13, pp. 7723–7745, 2021, doi: 10.1007/s00521-020-05514-1.

[5] M. Zaerin and B. Seyfe, "Multiuser modulation classification based on cumulants in additive white gaussian noise channel," *IET Signal Process.*, vol. 6, no. 9, pp. 815–823, 2012, doi: 10.1049/iet-spr.2011.0357.

[6] P. Triantaris, E. Tsimbalo, W. H. Chin, and D. Gunduz, "Automatic Modulation Classification in the Presence of Interference," in *2019 European Conference on Networks and Communications, EuCNC 2019*, 2019, pp. 549–553, doi: 10.1109/EuCNC.2019.8802004.

[7] P. Yang, Y. Xiao, M. Xiao, and S. Li, “6G Wireless Communications: Vision and Potential Techniques,” *IEEE Netw.*, vol. 33, no. 4, pp. 70–75, 2019, doi: 10.1109/MNET.2019.1800418.

[8] K. David and H. Berndt, “6G Vision and Requirements,” *IEEE Veh. Technol. Mag.*, vol. 13, no. July, pp. 72–80, 2018, doi: 10.1109/MVT.2018.2848498.

[9] E. Muscinelli, S. S. Shinde, and D. Tarchi, “Overview of Distributed Machine Learning Techniques for 6G Networks,” *Algorithms*, vol. 15, no. 6, 2022, doi: 10.3390/a15060210.

[10] F. Tariq, M. R. A. Khandaker, K. K. Wong, M. A. Imran, M. Bennis, and M. Debbah, “A Speculative Study on 6G,” *IEEE Wirel. Commun.*, vol. 27, no. 4, pp. 118–125, 2020, doi: 10.1109/MWC.001.1900488.

[11] W. Saad, M. Bennis, and M. Chen, “A Vision of 6G Wireless Systems: Applications, Trends, Technologies, and Open Research Problems,” *IEEE Netw.*, vol. 34, no. 3, pp. 134–142, 2020, doi: 10.1109/MNET.001.1900287.

[12] G. Wikström *et al.*, “6G – Connecting a cyber-physical world,” *Ericsson White Paper*, 2022. https://www.ericsson.com/4927de/assets/local/reports-papers/white-papers/6g--connecting-a-cyber-physical-world.pdf.

[13] S. Ali *et al.*, “6G White Paper on Machine Learning in Wireless Communication Networks,” 2020, doi: 10.48550/arxiv.2004.13875.

[14] M. Chen, U. Challita, W. Saad, C. Yin, and M. Debbah, “Artificial Neural Networks-Based Machine Learning for Wireless Networks: A Tutorial,” *IEEE Commun. Surv. Tutorials*, vol. 21, no. 4, pp. 3039–3071, 2019, doi: 10.1109/COMST.2019.2926625.

[15] E. Nachmani, Y. Be’ery, and D. Burshtein, “Learning to decode linear codes using deep learning,” in *54th Annual Allerton Conference on Communication, Control, and Computing, Allerton 2016*, 2017, pp. 341–346, doi: 10.1109/ALLERTON.2016.7852251.

[16] A. Askri and G. R. Ben Othman, “DNN assisted Sphere Decoder,” *IEEE Int. Symp. Inf. Theory - Proc.*, vol. 2019-July, pp. 1172–1176, 2019, doi: 10.1109/ISIT.2019.8849786.

[17] D. Gunduz, P. De Kerret, N. D. Sidiropoulos, D. Gesbert, C. R. Murthy, and M. Van Der Schaar, “Machine Learning in the Air,” *IEEE J. Sel. Areas Commun.*, vol. 37, no. 10, pp. 2184–2199, 2019, doi: 10.1109/JSAC.2019.2933969.

[18] C. De Lima *et al.*, “Convergent communication, sensing and localization in 6g systems: An overview of technologies, opportunities and challenges,” *IEEE Access*, vol. 9, pp. 26902–26925, 2021, doi: 10.1109/ACCESS.2021.3053486.

[19] H. Ye, G. Y. Li, and B. H. Juang, “Power of Deep Learning for Channel Estimation and Signal Detection in OFDM Systems,” *IEEE Wirel. Commun. Lett.*, vol. 7, no. 1, pp. 114–117, 2018, doi: 10.1109/LWC.2017.2757490.

[20] M. Chen, O. Semiari, W. Saad, X. Liu, and C. Yin, “Federated Echo State Learning for Minimizing Breaks in Presence in Wireless Virtual Reality Networks,” *IEEE Trans. Wirel. Commun.*, vol. 19, no. 1, pp. 177–191, 2020, doi: 10.1109/TWC.2019.2942929.

[21] C. Hoymann *et al.*, “LTE release 14 outlook,” *IEEE Commun. Mag.*, vol. 54, no. 6, pp. 44–49, 2016, doi: 10.1109/MCOM.2016.7497765.

[22] S. Ali, A. Ferdowsi, W. Saad, N. Rajatheva, and J. Haapola, “Sleeping Multi-Armed Bandit Learning for Fast Uplink Grant Allocation in Machine Type Communications,” in *2018 IEEE Globecom Workshops (GC Wkshps)*, 2018, pp. 1–6, doi: 10.1109/GLOCOMW.2018.8644350.

[23] J. Lam and R. Abbas, “Machine Learning based Anomaly Detection for 5G Networks,” pp. 1–12, 2020, doi: DOI: 10.48550/arxiv.2003.03474.

[24] H. Shiri, J. Park, and M. Bennis, “Remote UAV Online Path Planning via Neural Network-Based Opportunistic Control,” *IEEE Wirel. Commun. Lett.*, vol. 9, no. 6, pp. 861–865, 2020, doi: 10.1109/LWC.2020.2973624.

[25] H. Shiri, J. Park, and M. Bennis, “Communication-Efficient Massive UAV Online Path Control: Federated Learning Meets Mean-Field Game Theory,” 2020, doi: 10.1109/TCOMM.2020.3017281.

[26] S. D. Amuru, C. Tekin, M. Van Der Schaar, and R. M. Buehrer, “Jamming Bandits - A Novel Learning Method for Optimal Jamming,” *IEEE Trans. Wirel. Commun.*, vol. 15, no. 4, pp. 2792–2808, 2015, doi: 10.1109/TWC.2015.2510643.

[27] T. Erpek, Y. E. Sagduyu, and Y. Shi, “Deep learning for launching and mitigating wireless jamming attacks,” *IEEE Trans. Cogn. Commun. Netw.*, vol. 5, no. 1, pp. 2–14, 2018, doi: 10.1109/TCCN.2018.2884910.

[28] J. A. Sills, “Maximum-likelihood modulation classification for PSK/QAM,” in *MILCOM 1999. IEEE Military Communications. Conference Proceedings (Cat. No.99CH36341)*, 1999, pp. 217–220.

[29] A. Polydoros and K. Kim, “On the Detection and Classification of Quadrature Digital Modulations in Broad-Band Noise,” *IEEE Trans. Commun.*, vol. 38, no. 8, pp. 1199–1211, 1990, doi: 10.1109/26.58753.

[30] A. General and L. Framework, “A GENERAL MAXIMUM LIKELIHOOD FRAMEWORK FOR MODULATION CLASSIFICATION,” *Techniques*, pp. 65–68, 1998.

[31] P. Panagiotou, “Likelihood ratio tests for Modulation Classification,” *Proc. - IEEE Mil. Commun. Conf. MILCOM*, vol. 2, no. C, pp. 670–674, 2000, doi: 10.1109/milcom.2000.904013.

[32] J. E. Whelchel, D. L. McNeill, R. D. Hughes, and M. M. Loos, “Signal understanding: An artificial intelligence approach to modulation classification,” in *IEEE International Workshop on Tools for Artificial Intelligence*, 1989, pp. 231–236, doi: 10.1142/9789814354707_0021.

[33] H. Gang, L. Jiandong, and L. Donghua, “Study of modulation recognition based on HOCs and SVM,” in *2004 IEEE 59th Vehicular Technology Conference*, 2004, vol. 2, pp. 898–902, doi: 10.1109/vetecs.2004.1388960.

[34] M. R. Mirarab and M. A. Sobhani, “Robust modulation classification for PSK/QAM/ASK using higher-order cumulants,” *2007 6th Int. Conf. Information, Commun. Signal Process. ICICS*, no. 1, 2007, doi: 10.1109/ICICS.2007.4449591.

[35] C. M. Spooner, “On the utility of sixth-order cyclic cumulants for RF signal classification,” in *Conference Record of the Asilomar Conference on Signals, Systems and Computers*, 2001, vol. 1, pp. 890–897, doi: 10.1109/ACSSC.2001.987051.

[36] O. A. Dobre, Y. Bar-Ness, and W. Su, “Higher-order cyclic cumulants for high order modulation classification,” in *IEEE Military Communications Conference*, 2003, vol. 1, pp. 112–117, doi: 10.1109/milcom.2003.1290087.

[37] A. Abdelmutalab, K. Assaleh, and M. El-Tarhuni, “Automatic modulation classification based on high order cumulants and hierarchical polynomial classifiers,” *Phys. Commun.*, vol. 21, pp. 10–18, 2016, doi: 10.1016/j.phycom.2016.08.001.

[38] S. Riyaz, K. Sankhe, S. Ioannidis, and K. Chowdhury, “Deep Learning Convolutional Neural Networks for Radio Identification,” *IEEE Commun. Mag.*, vol. 56, no. 9, pp. 146–152, 2018, doi: 10.1109/MCOM.2018.1800153.

[39] T. J. O’Shea, J. Corgan, and T. C. Clancy, “Convolutional radio modulation recognition networks,” *Commun. Comput. Inf. Sci.*, vol. 629, pp. 213–226, 2016, doi: 10.1007/978-3-319-44188-7_16.

[40] M. Kulin, T. Kazaz, I. Moerman, and E. De Poorter, “End-to-End Learning from Spectrum Data: A Deep Learning Approach for Wireless Signal Identification in Spectrum Monitoring Applications,” *IEEE Access*, vol. 6, pp. 18484–18501, 2018, doi: 10.1109/ACCESS.2018.2818794.

[41] T. J. O’Shea, T. Roy, and T. C. Clancy, “Over-the-Air Deep Learning Based Radio Signal Classification,” *IEEE J. Sel. Top. Signal Process.*, vol. 12, no. 1, pp. 168–179, 2018, doi: 10.1109/JSTSP.2018.2797022.

[42] B. Kim, J. Kim, H. Chae, D. Yoon, and J. W. Choi, “Deep neural network-based automatic modulation classification technique,” in *2016 International Conference on*

Information and Communication Technology Convergence, ICTC 2016, 2016, pp. 579–582, doi: 10.1109/ICTC.2016.7763537.

[43] S. Peng, H. Jiang, H. Wang, H. Alwageed, and Y. D. Yao, "Modulation classification using convolutional Neural Network based deep learning model," in *2017 26th Wireless and Optical Communication Conference (WOCC)*, 2017, pp. 1–5, doi: 10.1109/WOCC.2017.7929000.

[44] M. Zhang, M. Diao, and L. Guo, "Convolutional Neural Networks for Automatic Cognitive Radio Waveform Recognition," *IEEE Access*, vol. 5, pp. 11074–11082, 2017, doi: 10.1109/ACCESS.2017.2716191.

[45] A. Krizhevsky, I. Sutskever, and G. E. Hinton, "ImageNet classification with deep convolutional neural networks," *Commun. ACM*, vol. 60, no. 6, pp. 84–90, 2017, doi: 10.1145/3065386.

[46] K. Simonyan and A. Zisserman, "Very deep convolutional networks for large-scale image recognition," in *3rd International Conference on Learning Representations, ICLR 2015 - Conference Track Proceedings*, 2015, pp. 1–14.

[47] S. T. Krishna and H. K. Kalluri, "Deep learning and transfer learning approaches for image classification," *Int. J. Recent Technol. Eng.*, vol. 7, no. 5, pp. 427–432, 2019.

[48] Y. Sun and E. Ball, "Automatic modulation classification based on machine learning," in *2021 International Symposium on Automation, Mechanical and Design Engineering: SAMDE 2021*, Dec. 2021, pp. 53–67, doi: 10.1007/978-3-031-09909-0_5.

[49] Y. Sun and E. Ball, "Automatic modulation classification using techniques from image classification," *IET Commun.*, vol. 16, no. 11, pp. 1303–1314, Jan. 2022, doi: 10.1049/cmu2.12335.

[50] K. Z. Chen and A. Q. Hu, "MPSK demodulation algorithm based on pattern recognition," in *2008 International Conference on Neural Networks and Signal Processing*, 2008, pp. 182–186, doi: 10.1109/ICNNSP.2008.4590336.

[51] J. R. Pierce, “Physical Sources of Noise,” *Proc. IRE*, vol. 44, no. 5, pp. 601–608, 1956, doi: 10.1109/JRPROC.1956.275123.

[52] T. O’Shea and J. Hoydis, “An Introduction to Deep Learning for the Physical Layer,” *IEEE Trans. Cogn. Commun. Netw.*, vol. 3, no. 4, pp. 563–575, 2017, doi: 10.1109/TCCN.2017.2758370.

[53] R. M. Alsina-Pages, M. Hervas, X. Vilasis-Cardona, and M. Vinyoles-Serra, “QPSK demodulation using cellular neural networks,” in *2014 14th International Workshop on Cellular Nanoscale Networks and their Applications (CNNA)*, 2014, pp. 1–2, doi: 10.1109/CNNA.2014.6888622.

[54] F. N. Iandola, S. Han, M. W. Moskewicz, K. Ashraf, W. J. Dally, and K. Keutzer, “SqueezeNet: AlexNet-level accuracy with 50x fewer parameters and <0.5MB model size,” 2016, [Online]. Available: http://arxiv.org/abs/1602.07360.

[55] C. Szegedy *et al.*, “Going deeper with convolutions,” in *2015 IEEE Conference on Computer Vision and Pattern Recognition (CVPR)*, 2015, pp. 1–9, doi: 10.1109/CVPR.2015.7298594.

[56] C. Szegedy, V. Vanhoucke, S. Ioffe, J. Shlens, and Z. Wojna, “Rethinking the Inception Architecture for Computer Vision,” in *2016 IEEE Conference on Computer Vision and Pattern Recognition (CVPR)*, 2016, pp. 2818–2826, doi: 10.1109/CVPR.2016.308.

[57] E. E. Azzouz and A. K. Nandi, “Automatic identification of digital modulation types,” *Signal Processing*, vol. 47, no. 1, pp. 55–69, 1995, doi: 10.1016/0165-1684(95)00099-2.

[58] S. Rajendran, W. Meert, D. Giustiniano, V. Lenders, and S. Pollin, “Deep Learning Models for Wireless Signal Classification With Distributed Low-Cost Spectrum Sensors,” *IEEE Trans. Cogn. Commun. Netw.*, vol. 4, no. 3, pp. 433–445, 2018, doi: 10.1109/tccn.2018.2835460.

[59] N. An, B. Li, and M. Huang, “Modulation classification of higher order MQAM signals using mixed-order moments and fisher criterion,” in *2010 The 2nd*

International Conference on Computer and Automation Engineering, ICCAE 2010, 2010, vol. 3, pp. 150–153, doi: 10.1109/ICCAE.2010.5451214.

[60] J. Lee, B. Kim, J. Kim, D. Yoon, and J. W. Choi, "Deep neural network-based blind modulation classification for fading channels," in *2017 International Conference on Information and Communication Technology Convergence (ICTC)*, 2017, pp. 551–554, doi: 10.1109/ICTC.2017.8191038.

[61] H. Sarieddeen, M. S. Alouini, and T. Y. Al-Naffouri, "An Overview of Signal Processing Techniques for Terahertz Communications," *Proc. IEEE*, vol. 109, no. 10, pp. 1628–1665, 2021, doi: 10.1109/JPROC.2021.3100811.

[62] Z. Zhang *et al.*, "6G Wireless Networks: Vision, Requirements, Architecture, and Key Technologies," *IEEE Veh. Technol. Mag.*, vol. 14, no. 3, pp. 28–41, 2019, doi: 10.1109/MVT.2019.2921208.

[63] N. E. West and T. O'Shea, "Deep architectures for modulation recognition," in *2017 IEEE International Symposium on Dynamic Spectrum Access Networks (DySPAN)*, 2017, pp. 1–6, doi: 10.1109/DySPAN.2017.7920754.

[64] J. Kim, B. Lee, H. Lee, Y. Kim, and J. Lee, "Deep Learning-Assisted Multi-Dimensional Modulation and Resource Mapping for Advanced OFDM Systems," in *2018 IEEE Globecom Workshops (GC Wkshps)*, 2019, pp. 1–6, doi: 10.1109/GLOCOMW.2018.8644281.

[65] J. Schmidhuber, "Deep Learning in neural networks: An overview," *Neural Networks*, vol. 61, pp. 85–117, 2015, doi: 10.1016/j.neunet.2014.09.003.

[66] G. R. MacCartney, T. S. Rappaport, S. Sun, and S. Deng, "Indoor office wideband millimeter-wave propagation measurements and channel models at 28 and 73 GHz for Ultra-Dense 5G Wireless Networks," *IEEE Access*, vol. 3, pp. 2388–2424, 2015, doi: 10.1109/ACCESS.2015.2486778.

[67] P. Zhang, J. Li, H. Wang, H. Wang, and W. Hong, "Indoor Small-Scale Spatiotemporal Propagation Characteristics at Multiple Millimeter-Wave Bands,"

IEEE Antennas Wirel. Propag. Lett., vol. 17, no. 12, pp. 2250–2254, 2018, doi: 10.1109/LAWP.2018.2872051.

[68] Y. Xing, T. S. Rappaport, and A. Ghosh, “Millimeter Wave and Sub-THz Indoor Radio Propagation Channel Measurements, Models, and Comparisons in an Office Environment,” *IEEE Commun. Lett.*, vol. 25, no. 10, pp. 3151–3155, 2021, doi: 10.1109/LCOMM.2021.3088264.

[69] E. Rajo-iglesias *et al.*, “Millimeter-Wave Propagation: Characterization and modeling toward fifth-generation systems,” *IEEE Antennas Propag. Mag.*, vol. 58, no. 6, pp. 115–127, 2016, doi: 10.1109/MAP.2016.2609815.